AD-A230 529

MICROMECHANICAL MODELING OF THE
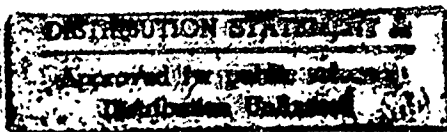FIBER/MATRIX INTERFACE REGION IN A
METAL MATRIX COMPOSITE

THESIS

David D Robertson
Captain, USAF

AFIT/GAE/ENY/90D-22

DEPARTMENT OF THE AIR FORCE

AIR UNIVERSITY

AIR FORCE INSTITUTE OF TECHNOLOGY

Wright-Patterson Air Force Base, Ohio

91 1 3 185

AFIT/GAE/ENY/90D-22

MICROMECHANICAL MODELING OF THE

FIBER/MATRIX INTERFACE REGION IN A

METAL MATRIX COMPOSITE

THESIS

David D. Robertson
Captain, USAF

AFIT/GAE/ENY/90D-22

DTIC
ELECTE
JAN 0 7 1991
S B D

AFIT/GAE/ENY/90D-22

MICROMECHANICAL MODELING OF THE FIBER/MATRIX INTERFACE REGION IN A METAL MATRIX COMPOSITE

THESIS

Presented to the Faculty of the School of Engineering

of the Air Force Institute of Technology

Air University

In Partial Fulfillment of the

Requirements for the Degree of

Master of Science in Aeronautical Engineering

David D. Robertson

Captain, USAF

December 1990

Acknowledgements

I express my deepest thanks to Dr. Shankar Mall for his calm patience and expertise in guiding me through this effort. His many insightful suggestions and enlightenments were invaluable and provided the necessary catalyst to keep me on the right path in spite of my unwary attempts to the contrary. In addition, I express my appreciation to Mr. Ted Fecke and the Turbine Engine Division of Wright Research and Development Center for their interest in sponsoring this thesis.

Furthermore, I would like to thank Captain Howard Gans for his extensive instruction in MSC/NASTRAN and SDRC-IDEAS and for the use of an excellent computer system. Also, I am indebted to Dr. Anthony Palazotto to whom I owe my initial understanding of the finite element method. Likewise, I express my gratitude to all the users of lincoln who exhibited great patience as I devoured memory and processing time, and thank you Randy Aldridge, a friend of mine and employee of Apple Computers Inc., for helping me obtain a first class home computer at a fraction of the cost. No doubt, I would still be trying to write this if I owned an IBM.

Finally, I reserve my most grateful applause for my wife, Diane. Her understanding and hard work have been an inspiration and made this episode in our life a pleasant one, and may God bless two small children with a Daddy who was forced to refuse many invitations to play with them.

Table of Contents

List of Figures

vii

List of Tables

List of Symbols

a	Fiber Dimension of Simplified One-Dimensional Models
α	Thermal Coefficient of Expansion
α_F	Thermal Coefficient of Expansion for Fiber
α_I	Thermal Coefficient of Expansion for Interphase
α_M	Thermal Coefficient of Expansion for Matrix
b	Interphase Dimension of Simplified One-Dimensional Models
β	Symmetric Angle Defining the Weak Bond Portion of the Interface for the Finite Element Combined Interphase Zone / Weak Bond Model
$2\beta/90$	Weak Bone Ratio(β in degrees) for Finite Element Combined Interphase Zone / Weak Bond Model
c	Matrix Dimension of Simplified One-Dimensional Models
d	Weak Bond Dimension in Combined Interphase Zone / Weak Bond Simplified One-Dimesional Model
d/a	Weak Bond Ratio for One-Dimensional Combined Interphase Zone / Weak Bond Model
E	Young's Modulus
E_F	Young's Modulus of Fiber
E_I	Young's Modulus of Interphase
E_M	Young's Modulus of Matrix
ε	Total Strain
ε_F, ε_{I_1}, ε_{I_2}	Total Strain in Regions F, I_1, and I_2 in Simplified One-Dimensional Models
ε_{M_1}, ε_{M_2}, ε_{M_3}	Total Strain in Regions M_1, M_2, and M_3 in Simplified One-Dimensional Models

ε_{EI_1}, ε_{EI_2}	Elastic Strain in Regions I_1 and I_2 in Simplified One-Dimensional Models
ε_{PI_1}, ε_{PI_2}	Plastic Strain in Regions I_1 and I_2 in Simplified One-Dimensional Models
e_p	Load Error Fraction
e_w	Energy Error Fraction
f	Coefficient of Friction
H'	Strain Hardening Parameter
ν	Poisson's Ratio
RVE	Representative Volume Element
RVE#1	Representative Volume Element for 35% Fiber Volume Fraction and Square Fiber Array(Aspect Ratio=1.0)
RVE#2	Representative Volume Element for 32% Fiber Volume Fraction and Rectangular Fiber Array(Aspect Ratio=1.2)
σ	Stress
σ_F, σ_{I_1}, σ_{I_2}	Stress in Regions F, I_1, and I_2 in Simplified One-Dimensional Models
σ_{M_1}, σ_{M_2}, σ_{M_3}	Stress in Regions M_1, M_2, and M_3 in Simplified One-Dimensional Models
σ_a	Applied Transverse Load
σ_{ys}	Yield Stress
σ_{ysI}	Initial Interphase Yield Stress
σ_{ysI_1}	Present Yield Stress in Region I_1 Accounting for Strain Hardening in Simplified One-Dimensional Models
σ_{ysI_2}	Present Yield Stress in Region I_2 Accounting for Strain Hardening in Simplified One-Dimensional Models
σ_x, σ_y, σ_z	Normal Stresses Along Axes

$\sigma_{\text{VON MISES}}$	Von Mises Stress
T	Temperature After Cooldown
T_P	Processing Temperature
τ_{xy}, τ_{yz}, τ_{zx}	Shear Stresses Parrallel to Faces Defined by Axes x, y, and z
u	Displacement
u_F, u_{I_1}, u_{I_2}	Displacement of Right Hand Faces of Regions F, I_1, and I_2 in Simplified One-Dimensional Models
u_{M_1}, u_{M_2}, u_{M_3}	Displacement of Right Hand Faces of Regions M_1, M_2, and M_3 in Simplified One-Dimensional Models
u_G	Displacement of Left Hand Face of Region M_1 in Simplified One-Dimensional Model with Combined Interphase / Weak Bond
V_F	Fiber Volume Fraction

AFIT/GAE/ENY/90D-22

Abstract

In order to develop reasonable analytical models and to better understand how the integrity of the fiber/matrix interface in high temperature titanium based metal matrix composites effects the overall transverse normal characteristics, a parametric study of various fiber/matrix interface conditions was performed. Analysis methods included both a simplified one-dimensional mathematical model and a finite element analysis using MSC/NASTRAN. First, both strong and weak interfacial bonds were examined. Subsequently, to provide for partial bonding, a model that used an elastic-plastic interphase zone between the fiber and matrix was examined. Finally, a combined model was investigated which assumed that a portion of the interface behaved as a weak bond and the remainder as if an elastic-plastic interphase zone existed between the constituents.

Results from a weak fiber/matrix bond indicate that interfacial separation and slip have a major impact on the response, resulting in substantial matrix plastic flow. At the point of separation a significant nonlinearity in the transverse response curve appears, so that the modulus after separation is considerably weakened. Slip along the interface was also found to significantly effect the transverse response, and increasing the interfacial friction arrested the slip only before separation had occurred. Therefore, after separation, no capability existed for varying the transverse response. An additional weak bond model was created that allowed only fiber/matrix separation(no slip was allowed). The additional constraint of no slip was found to greatly stiffen the response.

xiii

Since a weak bond model offered no capability for varying the level of bonding, the elastic-plastic interphase zone model was incorporated to determine if partial bonding could be obtained. It was found that by varying the plastic properties(i.e. yield stress and strain hardening) any level of interfacial bonding was possible, from perfectly strong to perfectly weak. The elastic-plastic interphase zone model also allows for energy dissipation. However, for low interphase yield stresses, a relaxation of the thermal residual stresses occurs. The combined interphase zone / weak bond model arrested this relaxation of thermal stresses, but did not offer as much flexibility for varying the level of bonding.

MICROMECHANICAL MODELING OF THE FIBER/MATRIX INTERFACE REGION IN A METAL MATRIX COMPOSITE

I - Overview

1.1   Introduction

For over two decades micromechanical analysis of unidirectional composites has proven to be a useful tool in predicting the overall properties of composite lamina and in understanding how the fiber/matrix interaction effects these overall properties. Correct modeling of the fiber/matrix interface is a crucial factor in a micromechanical analysis. Traditionally, for polymer or epoxy based composites a perfectly strong bond is assumed at the interface. A vast amount of research has been performed on these types of composites, and as a result a large body of knowledge exists to confirm the strong bond assumption. Unfortunately, such materials are only useful for low temperature applications. Therefore, all-metallic structures have remained the obvious choice for structures subjected to high temperatures.

It has long been a desire to incorporate the benefits of composite materials in high temperature applications. This desire has intensified as a result of programs such as the National Aerospace Plane (NASP) and the Integrated High Performance Turbine Engine Technology (IHPTET) Initiative. A key element in the success of these programs is the effective implementation of high temperature materials with vastly improved capa-

1

bilities. This technology thrust for advanced high temperature materials has fueled an interest in other classes of composites than the traditional polymer based composites. Among these are fiber reinforced metal matrix composites which are considerably attractive from the manufacturing technology and material performance aspects. In particular, systems using titanium or titanium aluminides as the matrix and silicon carbide for the fiber are appealing due to their ability to maintain high strength and stiffness at temperatures in excess of 800°C without the severe weight penalties associated with most existent high temperature metals.

High temperature metal matrix composites present a new challenge in micromechanical analysis. The metal matrix typically possesses a much higher thermal coefficient of expansion than the fiber, and in addition, processing temperatures are necessarily much greater than those used for conventional thermosetting composites. Such a combination results in relatively large thermal residual stresses in the composite after cooldown to room temperature. Also, at the fiber/matrix interface a reaction zone is present where the fiber has penetrated into and reacted with the matrix resulting in a third phase material which is likely to possess distinct properties from either the fiber or matrix. Further, it has become apparent from experiment that the fiber/matrix contact cannot be modeled as a strong bond[1]. Such conditions necessarily make transverse micromechanical modeling of high temperature metal matrix composites a complex task.

The extent to which these unique conditions may effect the overall material properties are not clear at present. Moreover, in order to develop reliable micromechanical models for titanium based metal matrix composites thorough investigations must be performed that will ascertain which

2

characteristics need to b.. included and how they should be modeled.

1.2   Background

Performing a micromechanical analysis of transverse normal loading in a unidirectional composite while incorporating both a weak fiber/matrix bond and thermal residual stresses requires a nonlinear material analysis. Residual compressive stresses exist at the interface after cooldown, and must be overcome before the matrix will separate from the fiber. Thus, before separation the composite behaves as if a strong bond exists at the interface while afterward it demonstrates weak bond characteristics. This was experimentally observed by Johnson et. al.[1]. Also, Nimmer[2; 3] analytically examined this effect using both a one-dimensional square fiber model and a nonlinear finite element analysis.

Substantial energy dissipation occurs during a loading and unloading sequence. This energy loss is most likely due to mechanisms at the fiber/matrix interface. The only means of energy dissipation in Nimmer's model were transverse friction along the fiber/matrix contact and plastic flow of the matrix. Since much of the energy loss in Nimmer's model occurred in the form of matrix plastic flow, it exhibited significant permanent strain after unloading which has not been observed experimentally. In addition, the model demonstrated a weaker secondary stiffness that occurs after fiber/matrix separation than demonstrated in experiment.

Thus, the problem suggests that there are additional constraints at the interface that cannot be modeled using a perfectly weak bond assumption alone. If accurate load histories of the composite are to be reproduced, these additional mechanisms must be incorporated.

1.3   Proposal

To develop accurate models, parametric studies must first be per-
formed to see how various interface conditions effect the overall compos-
ite characteristics. The present study will examine transverse normal
loading using a variety of interface conditions and seek to model the ener-
gy dissipation mechanisms using a third zone. First, an examination simi-
lar to Nimmer's [2; 3] will be undertaken analyzing the effect of a strong(no
separation or slip) versus weak(both separation and slip allowed) interface
on the matrix stress and overall characteristics. Comparisons will be
made with Nimmer's results for validation. Second, the drawbacks of a
completely weak interface model will be examined through adding an ad-
ditional constraint that prevents slip at the fiber/matrix interface. Third-
ly, a reaction zone at the interface will be added to model the three phase
system. The zone will possess different material properties than the fiber
or matrix in an attempt to model the energy dissipation mechanisms
present near the fiber/matrix interface. Finally, a portion of the reaction
zone will be removed to model a partially bonded interface.

The problem at hand is a highly nonlinear one. Therefore, even
though a simplified one dimensional model will also be used, the mode of
analysis will mainly be the finite element method. The finite element pro-
gram, MSC/NASTRAN, is a highly versatile code that possesses nonlinear
capability and a gap element essential for modeling contact type problems
such as a weak fiber/matrix bond.

This investigation will demonstrate possible models and discuss their
credibility. Such studies will advance the knowledge base of high temper-
ature metal matrix composites, and lead to their ultimate application.

II - Perspective

2.1 Motivation

Before a new material may be incorporated into structural designs it is essential to be able to reliably predict its useful life under a given loading. The mechanisms involved in fatigue failure operate on the microscopic level. Therefore, before such predictions are possible a thorough understanding of the micromechanics involved is necessary.

As mentioned in the introduction the recent technological push for improved high temperature materials has resulted in new classes of composites being brought to the forefront of composite research. Titanium based metal matrix composites have the potential to meet this new challenge, but they possess unique characteristics which must first be understood. Among these : e the imperfect fiber/matrix bond and the significant thermal residual stresses after processing.

Many questions arise when studying such phenomena. For instance, what level of debonding occurs at the interface and in what directions, or how much relaxation of the thermal stresses occurs during both cooldown and afterward? Most importantly, how can these effects be modeled and which ones are significant? Before such questions may be answered, more research must be performed, both analytically and experimentally. The goal being to develop proper micromechanical models which will lead to a clearer understanding of the behavior of high temperature metal matrix composites.

2.2   Micromechanical Methods

The work presented in this paper will analyze transverse normal load-
ing using a simplified one-dimensional model and a numerical finite ele-
ment approach. However, many micromechanical theories have been pro-
posed over the years, and it is helpful to present a brief history for the
reader. Also, before attempting a micromechanical analysis it is benefi-
cial to possess an overall view on both closed form and numerical meth-
ods that have been used in the past.

Chamis and Sendeckyj[4] render a comprehensive critique on various
techniques in micromechanics. They divide the approaches into many
classes: netting analyses[+], mechanics of materials approaches, self-con-
sistent models, variational techniques using energy bounding principles,
exact solutions, statistical approaches, discrete element methods, semiem-
pirical approaches, and microstructure theories. Many of these approach-
es are summarized by Jones[5:85-146]. Except for the first two, all ap-
proaches use at least some of the elements of the theory of elasticity.
Only a few will be briefly mentioned here.

The self-consistent model[6] is constructed of a fiber and matrix mod-
eled as concentric cylinders embedded in the composite. In this method
the isotropic plane strain elasticity solution in cylindrical coordinates is
solved for a transverse applied stress in the surrounding material. Such
an approximation is advantageous because it results in a closed form elas-
ticity theory solution allowing stresses at the fiber/matrix contact to be
analyzed. Therefore, it has been widely used. However, it completely ig-

---

+ Netting analysis assumes the fibers provide all the longitudinal stiffness and the ma-
  trix provides all the transverse, shear, and Poisson's effect.

6

nores the effects of adjacent fibers(assumes no packing array).

Other elasticity solutions in micromechanics include closed form series solutions such as developed by Sendeckyj[7] for longitudinal shear loading. Nevertheless, the application of such solutions can be tedious since it involves the truncation of an infinite series.

Also, a very useful set of equations for overall stiffness were developed by Halpin and Tsai[8]. Their result represents a good approximation to the self-consistent model in the transverse direction without the complexity. Overall stiffness properties may be obtained quickly and easily from relatively simple equations. In the Halpin-Tsai equations a single parameter is used to incorporate fiber geometry, packing geometry, and loading conditions. The value of this parameter must be assessed by relating the equations to exact solutions. Also, no fiber or matrix stresses are determined, only overall stiffness properties.

Except for the self-consistent model, micromechanical analysis generally requires assuming a regular array of fibers. After assuming a fiber array, symmetry is used to produce a representative volume element consisting of a single fiber and its surrounding matrix. In doing this the analyst has taken a completely random distribution of fibers and assumed it to be ordered. The influence of random filament packing on transverse stiffness was examined by Adams and Tsai[9]. They studied two types of random arrays: square and hexagonal. The arrays were not entirely random since they still contained repeating units of several fibers. Regardless, results indicated that a random hexagonal array analysis agrees more closely with experiment than a square random array analysis. This confirms the notion that a hexagonal array seems more physically realistic.

On the other hand, if an analysis that is not random is used, the square fiber array tends to agree more closely with experiment. In addition, a square array possesses greater flexibility by allowing for two independent dimensions in defining a unit cell while the hexagonal array contains only one dimension. Therefore, since most analysis assumes a repeating regular array of fibers, a square array is more widely used.

Much work has been done using numerical approaches to obtain discrete approximations to the elasticity equations, and since the study presented in this paper will use a numerical finite element technique, a strong review of these methods is in order. Early on in 1966 Foye[10] used a finite element approach with a regular square array of fibers to analyze the transverse properties of a unidirectional composite. Subsequently, Adams and Doner[11; 12] analyzed longitudinal shear as well as transverse normal loading of a unidirectional composite using a finite difference technique. Stress concentration and stiffness were analyzed as functions of fiber volume fraction, constituent stiffness ratio, and fiber shape. However, the method allowed for only linear elastic analysis.

Later Adams[13] used a nonlinear material analysis to analyze transverse normal loading. A plane strain finite element scheme was incorporated to obtain the stress field throughout the matrix, but the greatly increased computational requirements resulted in only a limited amount of data being produced. However, substantial matrix yield was shown to induce only a mild nonlinearity in the composite.

Others sought to incorporate inelastic micromechanics through numerical techniques. Foye[14] examined longitudinal shear as well as transverse normal loading for carbon/epoxy, boron/epoxy, and boron/aluminum

8

using a nonlinear finite element program. Again, the computational requirements limited the analysis to an extremely coarse grid and sparse data. Nevertheless, it demonstrated the capability of inelastic micromechanics using the finite element technique. Later, Crane and Adams[15] performed a more extensive inelastic analysis of longitudinal shear loading of a unidirectional composite

Seeking to advance the capability of computational micromechanics, in 1973, Adams[16] presented a rudimentary crack propagation scheme to model failure in the matrix around the fiber duri .g transverse loading. Once an element reached its critical octahedral shear strain for failure, its stiffness was reduced to zero. Of course, such a scheme is not entirely accurate since it produces relatively large gaps in the material after failure of a matrix element. Also, modeling crack propagation in such a discrete fashion resulted in a highly irregular transverse stress-strain response. In spite of such approximations, the two points on the stress-strain curve associated with directly before an element failure and directly after tended to bound the experimental data, but not in a way that could be easily predicted. In addition, these earlier nonlinear analysis studies were only capable of monotonically increasing loads.

Continued work in the micromechanics field has resulted in many varied prediction techniques available for today's engineer. The underlying assumption in most of these is a strong fiber/matrix bond. Also, only a few methods are able to account for the thermal residual stresses due to processing. Such limitations produce no difficulty for epoxy based composites that possess apparent strong bonds and are processed at relatively low temperatures. However, as previously mentioned, such assumptions

are grossly in error for high temperature titanium-based metal matrix composites. Therefore, if reliable micromechanical models are to be developed for such composites, an imperfect bond must be incorporated.

2.3   Imperfect Bonding

An interphase zone between the constituents is known to exist in all composites. This zone comprises imperfections due to absorption and reaction of the two constituents, voids, imperfect adhesion, and microcracks. Since the load transfer between fiber and matrix depends on the strength of this interphase zone, the thermomechanical properties of the composite are strongly affected by its integrity. However, due to high temperature processing and the constituents involved, the effect of the interphase zone in high temperature metal matrix composites is amplified. Therefore, even though an accurate representation of the zone is very complex, incorporating its effect into a micromechanics model is necessary for such composites.

Various attempts have been made to model an imperfect fiber/matrix bond. Several researchers have used linear elastic methods while more recently some inelastic models have been proposed. In the elastic realm, three studies[17-19] employed the finite element analysis with an interfacial layer between the constituents. The elastic properties of the layer were varied to model various levels of debonding. Later, Lene and Leguillon[20] allowed tangential slip at the interface using a finite element approach. Only linear elastic properties were examined.

Aboudi[21] developed a theoretical model for an imperfect bond based on the simplifying assumptions of Jones and Whittier[22], who expressed an imperfect bond as a thin elastic film containing two parameters. Each parameter represents the stiffness in the tangential and normal directions, respectively. Aboudi's results agreed favorably with those of Benveniste [23; 24] who used a concentric cylinder three phase model. Other theoretical models of debonding have appeared for determining a weak bond's affect on longitudinal shear[25], for analyzing wave propagation in unidirectional composites[26], and for particulate composites possessing imperfectly bonded spheres[27] have also appeared.

In addition, Pagano and Tandon[28-31] used a circular concentric cylinder elastic model they had previously developed similar to the self consistent model to analyze interfacial debonding. Complete separation was modeled by replacing the fibers with cylindrical voids, and a slipping condition was simulated by forcing the shear traction at the interface to vanish.

All of these linear elastic methods meet with the same difficulty. When attempting to model an imperfect bond using linear elastic methods alone, a weak interfacial bond condition necessarily exists in compression as well as in tension since the stiffness must remain constant. In other words, such an analysis will result in the interface being incapable of sustaining a compressive load, and consequently, the fiber and matrix will be allowed to pass through one another. Therefore, no constraints will exist during the application of thermal strains, and hence, no thermal stresses will result. This is a major drawback to the models discussed so far when analyzing high temperature metal matrix composites.

11

In an effort to model thermal residual stresses Hopkins and Chamis[32] developed a set of micromechanics equations for high temperature metal matrix composites based on a concentric cylinder mechanics of materials approach. However, in order to include thermal effects, it was necessary to assume a strong bond between the constituents.

Including both a weak fiber/matrix bond and thermal residual stresses in a micromechanical analysis is necessarily a nonlinear problem. Residual compressive stresses at the interface must be overcome before the matrix will separate from the fiber. As mentioned in the first chapter, this was experimentally observed by Johnson et. al.[1]. A distinct "knee" in the transverse load-displacement curve occurred. It was postulated that a weaker modulus existed after fiber/matrix separation resulting in the approximate bilinear behavior.

Residual thermal stresses are not the only mechanism controlling fiber/matrix separation. The fiber/matrix bond seems to possess a finite ultimate strength. Naik et. al.[33] found that during initial loading of an actual specimen the characteristic "knee" occurred at a slightly higher load than in subsequent cycles. The additional loading before nonlinearity occurred during the first cycle was assumed to be the load required to fail the fiber/matrix bond. Since bond failure had already occurred, subsequent loadings demonstrated bilinear behavior earlier. Other than for purposes of discussion, a finite ultimate strength of the fiber/matrix bond will not be considered in the present study. Since it is present during initial loading only, it will not be of concern in most structural applications.

Highsmith and Naik[34] attempted to determine the onset of separation analytically using both a concentric cylinder self consistent model and a linear elastic finite element analysis. Again, due to the linear elastic nature of the analysis it was necessary to assume a strong bond for the calculations, and as a result the analysis could not determine the characteristics beyond the point of separation. If one desires to determine the composite characteristics after this point, as a minimum, a bilinear capability must be present at the interface. Therefore, using the types of linear analyses discussed so far is not practical.

However, even a bilinear elastic analysis will not allow for energy dissipation, and it is apparent that there is a significant amount of energy dissipation during transverse loading and unloading of a titanium-based composite. If only a small portion of the matrix yields during loading, the unloading phenomena will be dominated by the elastic stresses in the matrix which contains significant thermal residual strain. Therefore, upon unloading, the elastic stresses in the matrix will tend to close the separated fiber/matrix interface before complete unloading occurs. However, a significant amount of energy will be lost at the interface due to frictional effects, crack propagation, and plastic flow[1].

Nimmer[2] performed a nonlinear analysis of a weak interfacial bond coupled with thermal residual stresses using both a simplified square fiber model and a finite element analysis. He examined a monotonically increasing transverse normal load and compared the characteristics of a strong and weak interfacial bond. A uniform square array of fibers was assumed and then symmetry used to isolate one quarter of a unit fiber/matrix cell. The fiber was assumed to be a circular cylinder with no voids

13

between it and the surrounding matrix. His work agreed at least qualitatively with the experimental results of Johnson et. al.[1]. A key part of the analysis was the incorporation of a contact element at the fiber/matrix interface. This type of two noded element allows for high stiffness in compression and extremely low stiffness in tension. Also, a friction coefficient may be included for transverse slippage along the interface.

Figure 1 presents Nimmer's results on the effect of thermal residual stresses in the presence of a weak fiber/matrix bond. A 35% fiber volume fraction was used, and the zero stress state was taken to be 1000°C. The model was subsequently cooled to 23°C followed by a monotonically increasing load. For the weak interface solution the Coulomb friction coefficient(friction coefficient between two dry surfaces) was taken to be 1.0, and the material properties are given in Table 1. The strong interface model does not experience yielding until approximately 950 MPa while the weak interface solution shows an apparent yielding at less than 200 MPa. Nimmer demonstrated that this point of apparent yield was actually fiber/matrix separation. True yielding of the matrix in the weak interface model did not occur until well above 200 MPa. Thus, the weak model was still elastic well after it experienced the nonlinearity.

Subsequently, Nimmer[3] attempted a more in-depth investigation of his finite element model and compared it to experimental data(Figure 2). A composite of silicon carbide fiber and titanium aluminide matrix was used for the experiment, and its associated constituent properties were input into the analysis. An attempt was made in the computations to match the experimental specimen's fiber distribution aspect ratio and volume fraction. Finally, analysis and experiment were brought through a

14
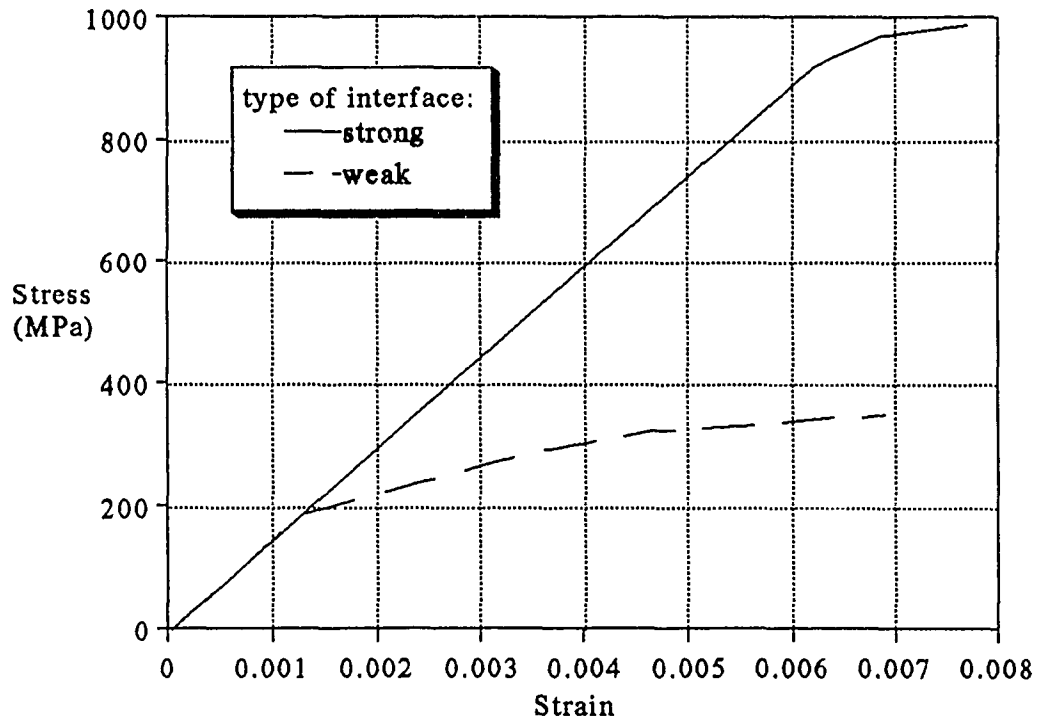
Figure 1. Nimmer's Results for Strong vs. Weak Interface, Plane Stress Finite Element Solution[2]

Table 1. Material Properties Used in the Finite Element Solutions of Figure 1.

	E (GPa)	ν	α (°C)$^{-1}$	σ$_{ys}$ (MPa)
Fiber	400.	0.3	5.0x10^{-6}	-
Matrix	100.	0.3	10.0x10^{-6}	1000.

15
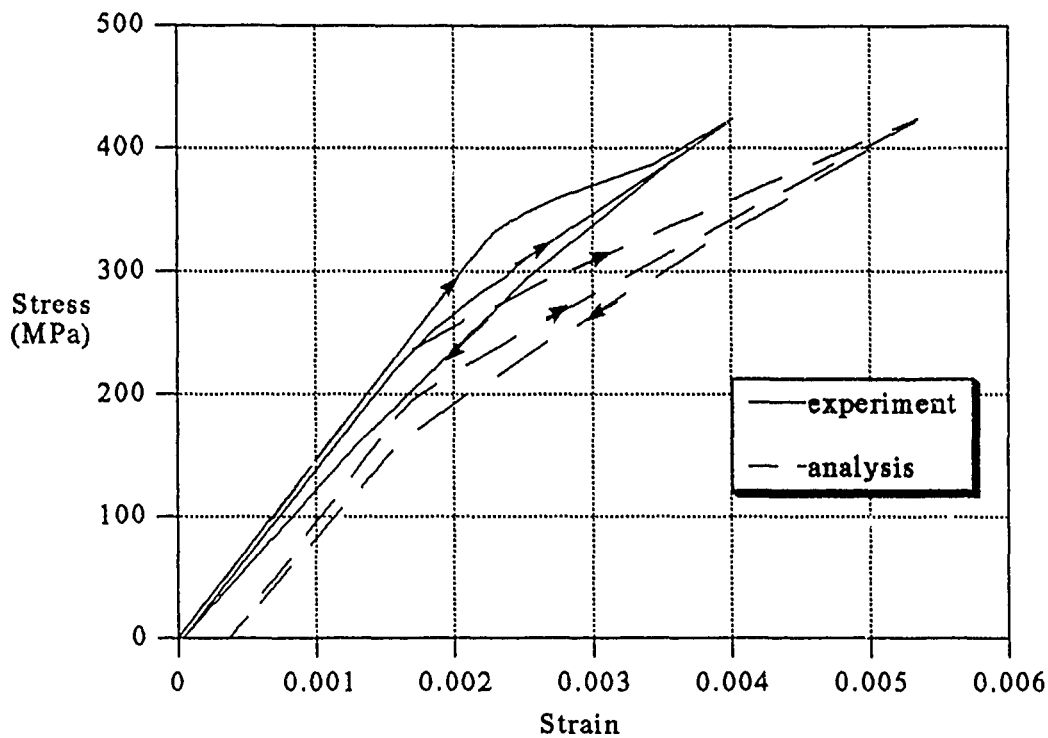
Figure 2. Nimmer's Results of Analysis vs. Experiment, 3-D General-
ized Plane Strain Finite Element Solution[3]

similar thermomechanical loading sequence consisting of cooldown fol-
lowed by loading, unloading, and then reloading. The experimental re-
sults exhibited almost no permanent strain upon unloading confirming that
little matrix plasticity occurs. In addition, the small finite strength of the
fiber/matrix bond is demonstrated in the difference between the initial
loading curve and reload.

Nimmer's generalized plane strain model does an excellent job of
predicting the initial modulus as well as the point of fiber/matrix separa-
tion. Since the experimental specimen demonstrates interfacial bond fail-
ure upon initial loading and the analysis models the interface as weak, the

16

initial loading in the analysis should compare most favorably with the reloading of experiment. Nevertheless, the secondary stiffness after separation is considerably weaker than the empirical data, and in addition, upon unloading the model fails to return to its approximate original strain state as observed experimentally. This indicates that modeling the fiber/matrix contact as perfectly weak is not an adequate representation of the actual mechanism. Hence, there must be additional constraints existing at the interface after separation. Also, since the model exhibits significant plastic strain after unloading, it does not correctly model a matrix dominated by elastic forces.

The only means of energy dissipation in Nimmer's model were transverse friction along the fiber/matrix contact and plastic flow of the matrix. However, the experimental data indicates that a significant amount of energy dissipation occurs even when the matrix is dominated by elastic forces. Since very little of the matrix yields, the bulk of the energy loss must occur at the fiber/matrix interface. It is essential to model this energy loss if correct load histories of the composite are to be reproduced in a micromechanical analysis.

Energy absorption is a prime factor in determining the life cycle of a material. In many cases, fatigue failure criteria is based on the energy dissipated during loading and unloading [35]. Therefore, before reliable life prediction techniques for high temperature metal matrix composites may be obtained, a strong understanding of the energy dissipation process is needed. To develop accurate models, parametric studies must first be performed using various interface conditions to determine what mechanisms must be included.

The results of such studies will demonstrate the effect of various interface conditions on the composite characteristics. In the study presented here an attempt will be made to determine if the energy dissipation mechanisms existent at the interface may be adequately modeled by representing the reaction zone as a material with different material properties as compared to the matrix.

Much work remains to be done in understanding high temperature metal matrix composites. In this effort, micromechanical analysis can provide both the ability to predict macroscopic characteristics of the composite and furnish a clearer understanding into the mechanisms surrounding interfacial debonding. Once equipped with a stronger understanding of these microscopic mechanisms, micromechanical analysis can bridge the gap between experimental data and developing reliable life cycle prediction capabilities. Therefore, it is imperative that a reasonable model of the interface zone be developed.

III - Methods of Analysis

3.1   Hardware and Software

Two types of analysis will be used in this study: the finite element method and a simplified one dimensional model. A nonlinear material finite element method will receive the most attention. However, the simplified one dimensional model will also be employed for rapid calculation of trends in the data. Since this will be a parametric study where many conditions will be examined, using a finite element method alone would be quite tedious. Each nonlinear solution may take anywhere from 2 to over 24 hours of CPU time. When one also considers the time required for grid generation and application of constraints, it becomes a task far from attractive. Additionally, unless another means of verification is available, using a simplified analysis alone makes one to question the results. Therefore, a mixture of finite element and one dimensional solutions will be used.

Computer system hardware included the aeronautical engineering department's SUN 4/330 workstation for the finite element calculations and pre/post processing of results. When the workstation was unavailable, the computer directorate's VAX 11/785 (Hercules) was employed. Finally, an Apple Macintosh IIx was used for the one dimensional model calculations.

Important software consisted of the Macneal-Schwendler Corporation's MSC/NASTRAN finite element analysis program and the Structural Dynamics Research Corporation's SDRC-IDEAS computer aided de-

sign/engineering package. The SDRC-IDEAS package was used only as a pre/post processor for MSC/NASTRAN. Additionally, the one dimensional calculations were performed using Mathematica™, a versatile mathematics program capable of symbolic operations.

The remainder of this section will present a brief discussion of the capabilities of MSC/NASTRAN for nonlinear material analysis, software utilization, and some of the difficulties encountered. MSC/NASTRAN's nonlinear material static analysis solver(solution sequence 66) uses a modified Newton-Raphson approach for convergence. The tangent method is employed, and the user maintains the option of when to update the stiffness matrices. Other convergence parameters available to the user include the number of load increments per subcase, the type of convergence test(displacement, load, or energy error fractions), and the error tolerance limits. Both load error fraction, e_p, and energy error fraction, e_w, were incorporated to control convergence. These quantities are defined in the MSC/NASTRAN Application Manual[36: 2.14-52]. The solution was assumed to have converged when $e_p \leq 1.0 \times 10^{-3}$ and $e_w \leq 1.0 \times 10^{-7}$.

In linear elastic analysis the loading sequence is immaterial, but for nonlinear elastic-plastic problems the solution is dependent on the load history. NASTRAN incorporates a load history by applying the load through user specified subcases. Each subcase may further be incremented for more stable convergence. Once a solution for the subcase is achieved the next subcase's calculations are begun starting from the previous solution.

Several types of yield criteria are available in MSC/NASTRAN. The Von Mises criterion gives good results for most metals, and since a metal

20

matrix material was to be analyzed, this criterion was chosen for the
present study. The Von Mises stress is defined as follows:

$$\sigma_{VON\ MISES} = \sqrt{\frac{1}{2}\left[(\sigma_x - \sigma_y)^2 + (\sigma_y - \sigma_z)^2 + (\sigma_z - \sigma_x)^2 + 6\left(\tau_{xy}^2 + \tau_{yz}^2 + \tau_{zx}^2\right)\right]}$$

(1)

where σ_x, σ_y, and σ_z are the normal stresses along any orthogonal set of
axes, and τ_{xy}, τ_{yz}, and τ_{zx} are the respective shear stresses for the axes.
The Von Mises criterion states that yielding occurs when the Von Mises
stress exceeds the yield stress.

MSC/NASTRAN incorporates the Prandtl-Reuss flow relations, and
possesses the capability for either isotropic, kinematic, or a combined
hardening. Since a loading and unloading sequence is planned, kinematic
hardening was chosen in order to account for the Bauschinger effect in the
simplest manner.

The types of elements used in this study included a three noded con-
stant strain, constant curvature triangular shell element, a four noded iso-
parametric shell element, a six noded three dimensional isoparametric
wedge element, an eight noded three dimensional isoparametric brick ele-
ment, and a two noded gap element. The user input for the shell and solid
element's material properties is the one-dimensional stress-strain curve
for tension. The gap element provides a unique capability necessary for
the present study. It is an element intended to model surfaces which may
come into contact. It connects two grid points(nodes) which may be ini-
tially coincident, and the local element coordinate system defines a con-
tact plane which does not change with deflection. When compressive
normal stress exists, the gap element may possess a longitudinal stiffness

21

comparable to the surrounding material and carry a transverse shear load of a magnitude less than the normal load times the coefficient of friction. When the element is in tension, its longitudinal stiffness may be dramatically reduced to approximately zero and it is no longer capable of resisting a transverse shear load.

A good portion of the grid generation and data reduction was performed using the SDRC-IDEAS software. Using this program it was possible to minimize the number of manual inputs to a NASTRAN data deck. A few minor difficulties arose. It was found that IDEAS was unable to write out temperature loads, and incorrect Direct Matrix Abstraction Programming (DMAP) statements for creating the necessary post processing files from NASTRAN were listed in the IDEAS manual [38]. For the correct DMAP statements see appendix-A which lists a sample MSC/NASTRAN input deck used in this study.

A couple of significant software problems in using MSC/NASTRAN are worth mentioning for future reference. Rigid body elements are ignored when thermal loads are present. Therefore, rather than using rigid body elements to ensure constant displacement, multipoint constraints (MPCs) must be written. Also, in the nonlinear material solution sequence there was a major discrepancy in the solutions between MSC/NASTRAN version 65C and the recently released version 66A. Since the 65C results demonstrated excellent agreement with Nimmer's solutions calculated using the finite element program ADINA, all results presented in this study are from the 65C version. Due to this discovery the MacNeal-Schwendler Corporation is presently looking into this discrepancy, and until the problem is overcome the author recommends using version 65C

22

for any nonlinear material solutions.

3.2   General Information on Models Used in this Study

In order to perform the investigation several assumptions were necessary. First, a regular rectangular array of fibers was assumed for all models. A unit fiber/matrix cell or representative volume element (RVE) consists of a single fiber and the surrounding matrix material. Symmetry was used in the analysis to isolate one quarter of a unit fiber/matrix cell for the calculations(Figure 3). The fiber diameter was taken to be 0.14 mm, and the remaining dimensions of the analysis cell were determined from the fiber volume fraction and aspect ratio. The material properties of the fiber, matrix, and interphase zone were assumed to be isotropic.

Boundary conditions along the external faces of the analysis cell were chosen as the simplest to satisfy compatibility. Thus, the lower face is fixed in the vertical direction only, and the left face in the horizontal direction only. The other two in-plane faces are free to move parallel to their faces, but perpendicularly they are constrained to move uniformly. The loading for all models consisted of a cooldown from a specified processing temperature to room temperature followed by a transverse normal load applied to the right-hand face.

Two representative volume elements will be used throughout this study: a 35% fiber volume fraction with an assumed square fiber array(aspect ratio=1.0), and a 32% fiber volume fraction of a rectangular array with an aspect ratio of 1.2. The 35% fiber volume fraction square array representative volume element which at times will be referred to as RVE#1 was used as a generic model for determining how the composite

23
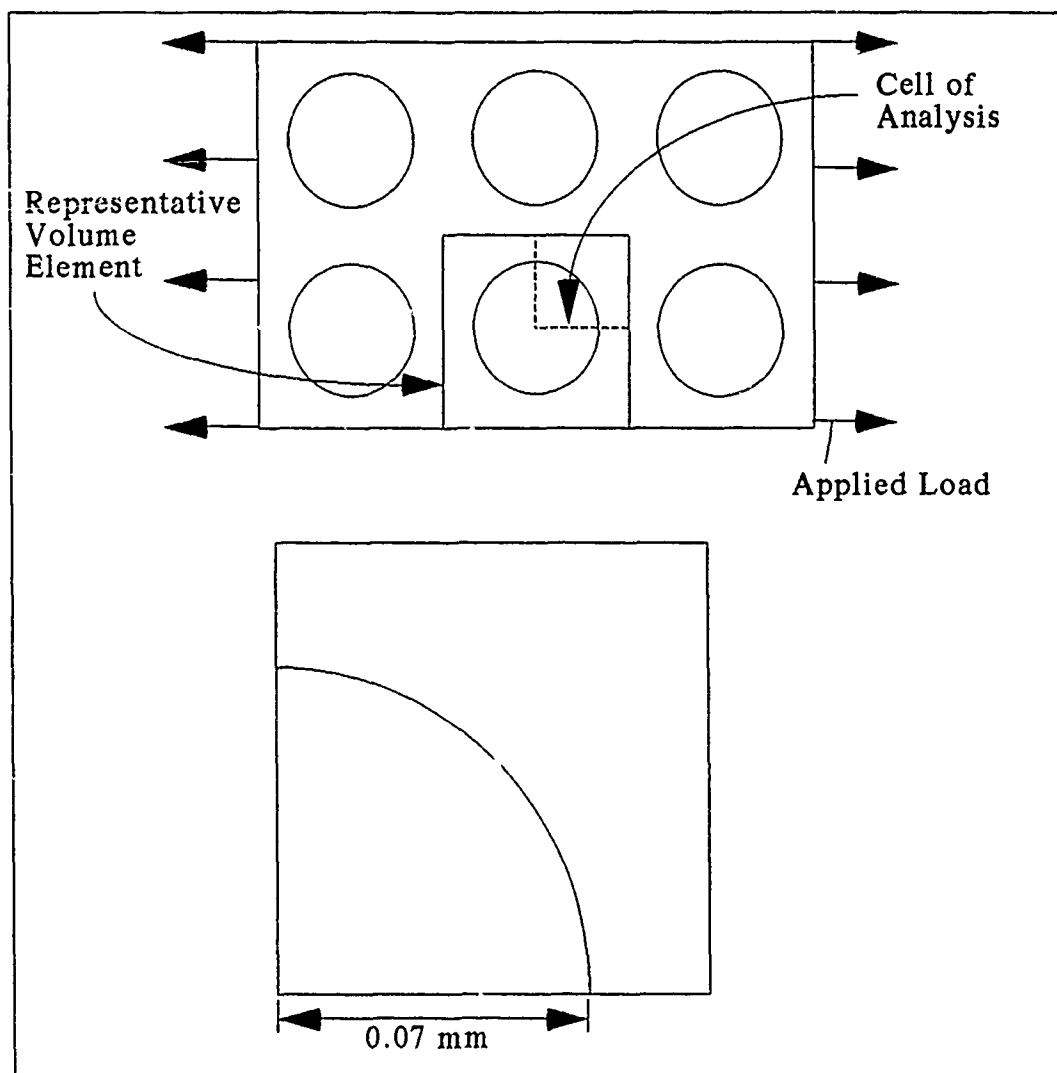
Figure 3. Basic Cell Used in Analysis

behaved under various interface conditions. The properties used were similar to those used previously by Nimmer[2]. Since this is a parametric study, RVE#1 will be employed most often. The 32% fiber volume fraction rectangular array representative volume element with the 1.2 aspect ratio(RVE#2) is for specific comparison with an actual specimen from previously published experimental data where micrographs were used to

obtain the correct fiber volume fraction and aspect ratio[3].

3.3   Finite Element Models for Strong and Weak Interfaces

The strong and weak interface models were created mainly for comparison with Nimmer's previous work as a check for the calculations and to provide a baseline. However, in a few of the cases there was some extrapolation on his work, and in one instance an additional constraint applied. The strong and weak interface finite element models consisted of both two dimensional and three dimensional grids. Both plane stress and plane strain solutions were performed on the two dimensional models.

For the strong bond calculations only RVE#1 was used. The two dimensional strong interface model consisted of quadrilateral isoparametric four noded shell elements and triangular constant strain constant curvature three noded shell elements. Since only membrane effects were needed, all rotations and out of plane displacements were removed through single point constraints. Also, since the strong interface model experiences little or no nonlinearities at the load levels considered(no fiber/matrix separation occurs and the transverse load is less than half of the matrix yield stress), then only a linear analysis was necessary. The finite element grid is shown in Figure 4 and was biased towards regions of expected maximum stress. This biasing ratio is approximately 3 to 1.

The boundary conditions along the four faces were applied through single point and multipoint constraints as well as nodal applied loads. Single point constraints are simply specified displacements at particular nodes, while a multipoint constraint is a linear equation that relates a set of degrees of freedom to each other. Thus, a multipoint constraint for the

Fiber/Matrix
Interface

2-D Model

3-D Model
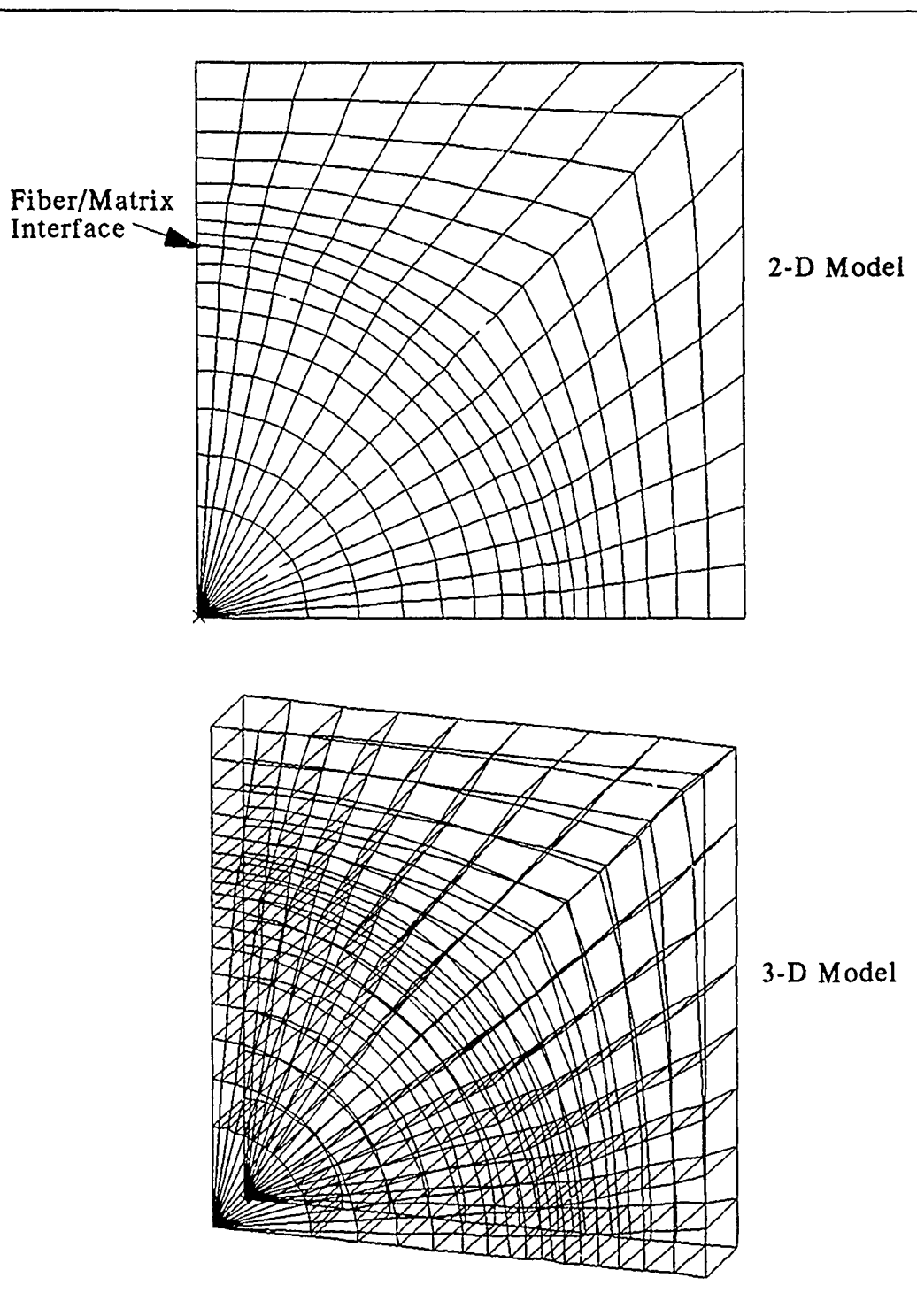
Figure 4. 35% Fiber Volume Fraction Square Array Finite Element
Grids for Both Strong and Weak Interfacial Bonds

26

set of degrees of freedom, $\{u_1, u_2, ..., u_n\}$, will take the form

$$\sum_{i=1}^{n} a_i u_i = 0 \qquad (2)$$

where a_i are constant coefficients.

The nodes on the lower face were restrained in the vertical direction only, and the nodes on the left face were restrained in the horizontal direction only. Multipoint constraints were applied on the right and upper faces to provide for equal displacement. All nodes on the right face are tied through a multipoint constraint to the node on the lower right corner in such a way that they will displace equally in the horizontal direction. The same is true for the upper face in the vertical direction where the node on the upper left corner is used. Transverse loading was applied at the lower right-hand node. Determining equivalent nodal loads for an evenly applied face pressure was not necessary since all the nodes along the face will displace equally.

To create the finite element grid for the three-dimensional strong bond model the two dimensional grid was simply extruded into three dimensional space by a thickness of .01 mm. Therefore, it was made up of eight noded brick elements and six noded wedge elements. The purpose of the three dimensional model was to analyze behavior under a generalized plane strain condition. Since the composite longitudinal direction is the out-of-plane direction in the analytical models, it is assumed that this direction is very thick, and hence, a generalized plane strain solution is the most physically realistic. No change of the in-plane boundary conditions

27

were necessary for the three-dimensional model, but an additional degree of freedom in the out-of-plane, z-direction, must be dealt with. These additional boundary conditions consist of the back face being fixed in the z-direction and the nodes on the front face being constrained to displace uniformly in the z-direction through the use of multipoint constraints. All the strong bond calculations provided a good reference for the weak interface solutions.

The weak interface models contained finite element grids of both RVE#1 and RVE#2. The finite element grid for the weak bond RVE#1 model was identical to the strong bond model except for the incorporation of gap elements to allow for the weak fiber/matrix interface condition. The weak model possessed coincident nodes at the interface where one set is attached to the matrix and the other to the fiber. These coincident interface nodes are then connected to one another through gap elements that prevent the fiber and matrix from passing through one another but on the other hand offer no resistance under separation. In addition, a weak r face model of RVE#2 was also developed. Its finite element grid played in Figure 5, and except for the dimensions all other characteristics of it are similar to the RVE#1 model. Finally, as would be expected, the boundary conditions for the weak bond models were identical to those discussed in the previous paragraphs for the strong interface models.

In order to distinguish the effect of interfacial slippage between the fiber and matrix, an additional constraint which prevents any transverse slippage along the interface but still allows for separation was developed for the RVE#2 model. Again multipoint constraints were utilized to only allow the coincident nodes to displace perpendicularly from the interface.

28

Fiber/Matrix
Interface

2-D Model

3-D Model
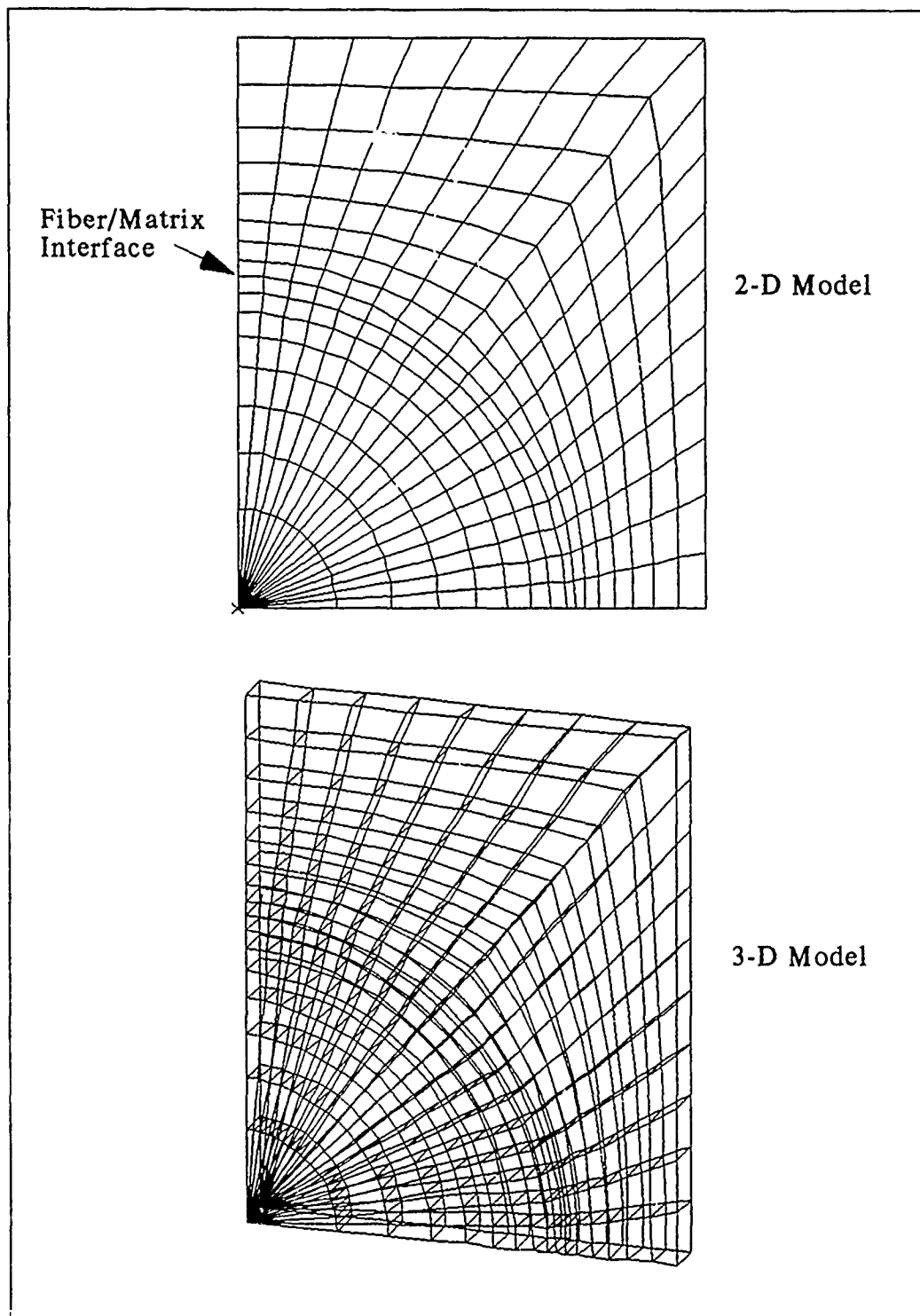
Figure 5. 32% Fiber Volume Fraction Rectangular Array(Aspect
Ratio=1.2) Finite Element Grids for Weak Interfacial Bond

29

This constraint could be optionally applied, so it was possible to make direct comparisons between the free slip and no slip conditions.

3.4 Models for Incorporating an Interphase Zone

A considerable portion of this study was an attempt to model the imperfections that exist in the reaction zone by incorporating a third zone at the fiber/matrix interface possessing isotropic material properties. This zone will be modeled with various material properties in order to simulate the imperfect bond characteristics and to allow for energy dissipation in a loading and unloading cycle. Both a simplified one dimensional model and finite element analysis will be used for analyzing the effect of an interphase zone.

The one dimensional model is patterned after a bilinear elastic analysis proposed by Nimmer for a weak bond[2]. However, a higher level of sophistication is needed to model an interphase zone and its elastic-plastic characteristics. A visualization of the model is depicted in Figure 6 where a square fiber is assumed and the entire model is divided into five regions consisting of two matrix regions, two interphase zone regions, and a single fiber region. The stress and strain is assumed constant throughout each region, and to reduce the equations into one dimension both the shear and Poisson's effect are neglected. Hence, only the stress and strain in the direction of applied load is necessary which in this case is the x-direction. Since the left face is fixed, the strains in each region may be related to the displacements shown in Figure 6 as follows:

$$\varepsilon_F = \frac{u_F}{a} \qquad (3)$$

30
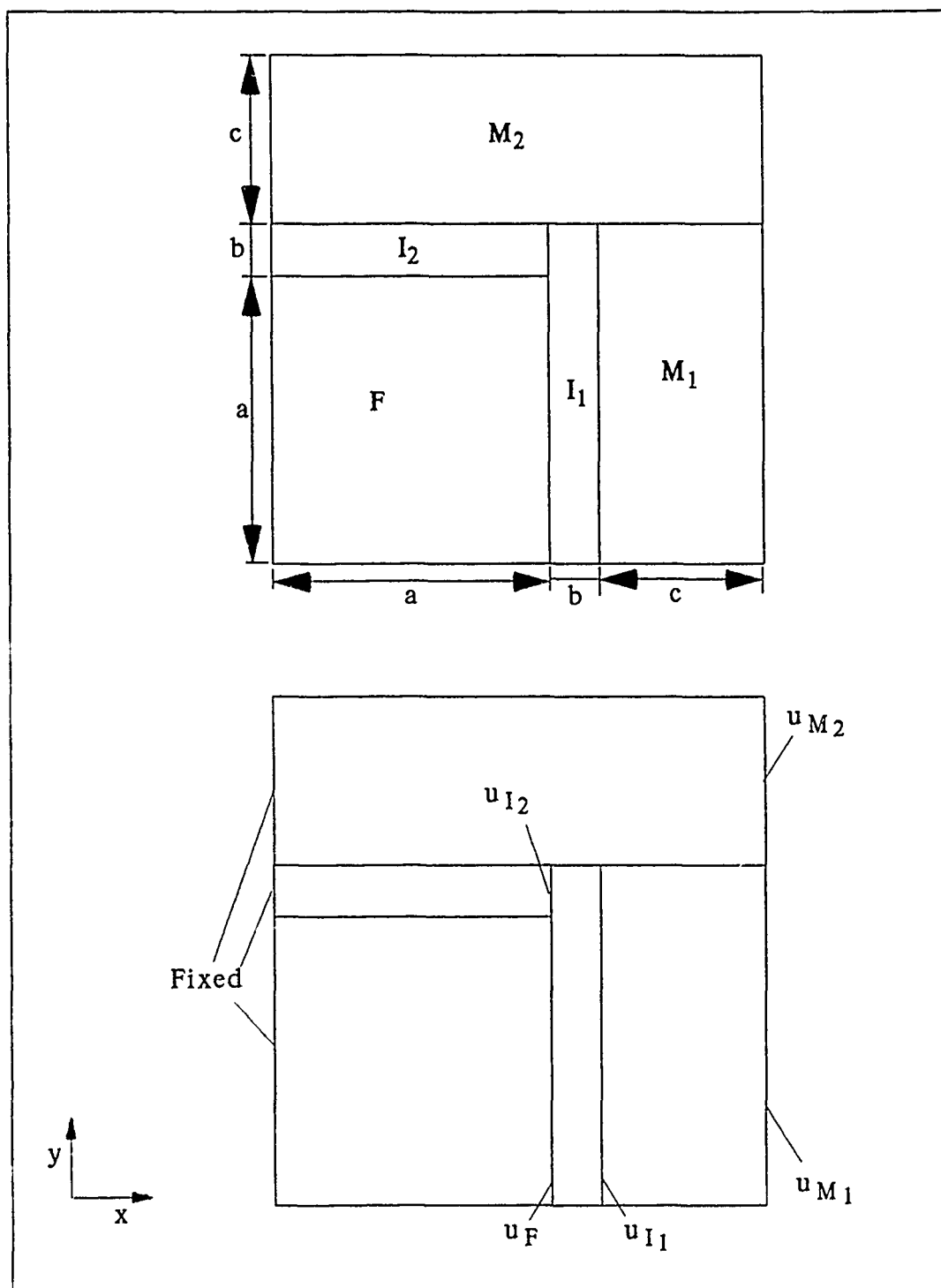
Figure 6. Simplified One Dimensional Model Incorporating an Interphase Zone

$$\varepsilon_{I_1} = \frac{u_{I_1} - u_F}{b} \tag{4}$$

$$\varepsilon_{M_1} = \frac{u_{M_1} - u_{I_1}}{c} \tag{5}$$

$$\varepsilon_{I_2} = \frac{u_{I_2}}{a} \tag{6}$$

$$\varepsilon_{M_2} = \frac{u_{M_2}}{(a + b + c)} \tag{7}$$

where u is displacement, ε is strain, and subscripts are the specified regions shown in Figure 6.

Both the fiber and matrix regions are assumed to be linearly elastic, and therefore the only material properties needed for these regions are Young's modulus and thermal coefficient of expansion. The interphase zone is assumed to be elastic-plastic with isotropic hardening during plastic deformation. Therefore, the material properties required for the interphase zone are Young's modulus, thermal coefficient of expansion, initial yield stress, and a strain hardening parameter. Incorporating the plastic strains in both interphase zone regions and denoting the cooldown temperature by T and the processing temperature by T_P the one dimensional stress-strain relations for the model become:

$$\varepsilon_F = \frac{\sigma_F}{E_F} + \alpha_F (T - T_P) \tag{8}$$

$$\varepsilon_{I_1} = \varepsilon_{E_{I_1}} + \varepsilon_{P_{I_1}} \tag{9}$$

32

$$\varepsilon_{E_{I_1}} = \frac{\sigma_{I_1}}{E_I} + \alpha_I (T - T_P) \tag{10}$$

$$\varepsilon_{M_1} = \frac{\sigma_{M_1}}{E_M} + \alpha_M (T - T_P) \tag{11}$$

$$\varepsilon_{I_2} = \varepsilon_{E_{I_2}} + \varepsilon_{P_{I_2}} \tag{12}$$

$$\varepsilon_{E_{I_2}} = \frac{\sigma_{I_2}}{E_I} + \alpha_I (T - T_P) \tag{13}$$

$$\varepsilon_{M_2} = \frac{\sigma_{M_2}}{E_M} + \alpha_M (T - T_P) \tag{14}$$

where σ is stress, α is the thermal coefficient of expansion, E is Young's modulus, the subscripts E and P denote elastic and plastic strains, and the other symbols and subscripts are the same as in Eqs (3-7).

Designating the applied stress on the right-hand face by σ_a, the equilibrium equations for this simplified model are:

$$\sigma_F a + \sigma_{I_2} b = \sigma_{I_1} (a + b) \tag{15}$$

$$\sigma_{I_1} (a + b) = \sigma_{M_1} (a + b) \tag{16}$$

$$\sigma_{M_1} (a + b) + \sigma_{M_2} c = \sigma_a (a + b + c) \tag{17}$$

There are nineteen unknowns in this set of fifteen equations, so additional information is required. Two more equations may be obtained by applying certain constraints on displacements. These constraints come

33

from the boundary condition on the right-hand face and compatibility of the interior. They are:

$$u_{I_2} = u_F \qquad (18)$$

$$u_{M_2} = u_{M_1} \qquad (19)$$

The problem is still in need of more information. This comes in the form of the one dimensional yield criteria and the strain hardening relation. The yield criteria states that if the interface stress exceeds the yield stress, then plastic deformation occurs, otherwise the material behaves elastically. Since plastic solutions are dependent on the load history, the load must be applied in incremental steps so that the plastic strains from the previous load step may be used in the present calculation. The one dimensional model presented here employs the following solution sequence. If yielding does not occur during an applied load, then the previous load step's plastic strains are used in the above 17 equations to solve for the 17 unknowns. If yielding does occur, then the yielded region's stress is set equal to the yield stress of the region which could be either in compression or tension, and its associated plastic strain becomes the unknown to be solved for. The yield stress for each interphase region is given by the following strain hardening relations.

$$\sigma_{ysI_1} = \sigma_{ysI} + H' \, \varepsilon_{P_{I_1}} \qquad (20)$$

$$\sigma_{ysI_2} = \sigma_{ysI} + H' \, \varepsilon_{P_{I_2}} \qquad (21)$$

where σ_{ysI} is the initial yield stress for the interphase material, and H' is

34

the strain hardening parameter.

A Mathematica™ program was written to solve Eqs (3-21) for all possible interphase zone yielding combinations of the two regions both in compression and tension. Any transverse rmal loading sequence may be applied to the mathematical model, but in this study only a single loading and unloading sequence will be used. The program is listed in Appendix-B. During an applied load step the stresses are initially assumed to be elastic, and upon evaluation of the stresses in the interphase regions a judgment is made through the use of a logic sequence as to what set of equations apply. This procedure is continued until two successive solutions are identical.

The one dimensional model provided a good supplement to the finite element solutions by providing rapid calculations of how varying a specific property or parameter generally affected the overall structure. As a result, more effective use of the finite element solutions were possible. In addition, it provided a good check for the finite element calculations by preventing gross errors from being overlooked as might occur if no other analysis tool was available.

Similar to the perfectly weak bond calculations, the finite element solutions that incorporated an interphase zone contained both two and three dimensional models. The same boundary conditions were employed, and the three dimensional models were again obtained by extruding the two dimensional ones into three dimensional space. Since the effect of the interphase zone size was to be examined, separate grids had to be created for each size investigated. Three sizes were examined. Their thicknesses were 5%, 7.5%, and 10% of the fiber radius. Such thicknesses were cho-

Interphase Zone

Coarse Grid
337 Nodes

Interphase Zone

Fine Grid
1313 Nodes
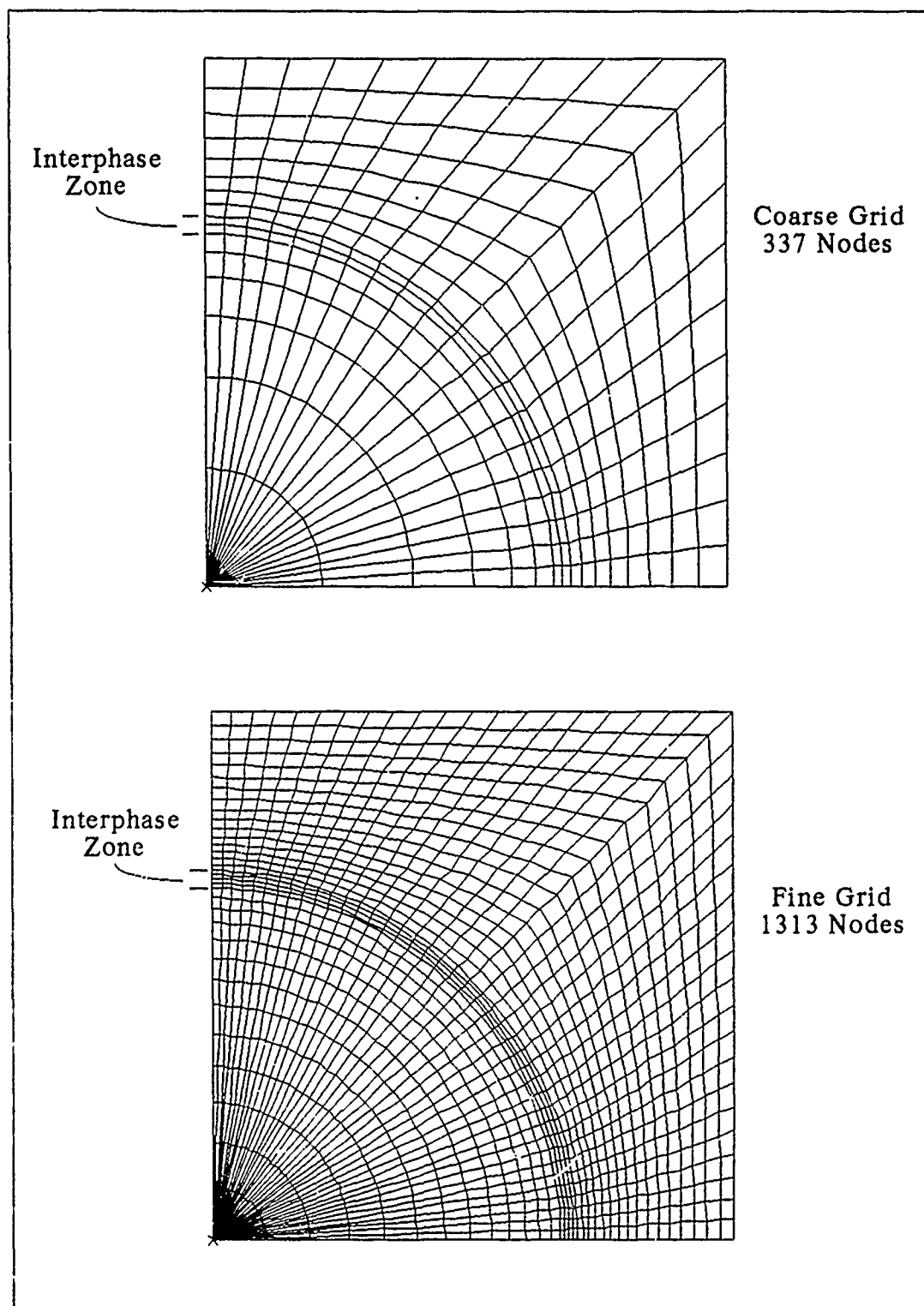
Figure 7. Coarse and Fine Grids for Interphase Zone Size 5% of Fiber Radius
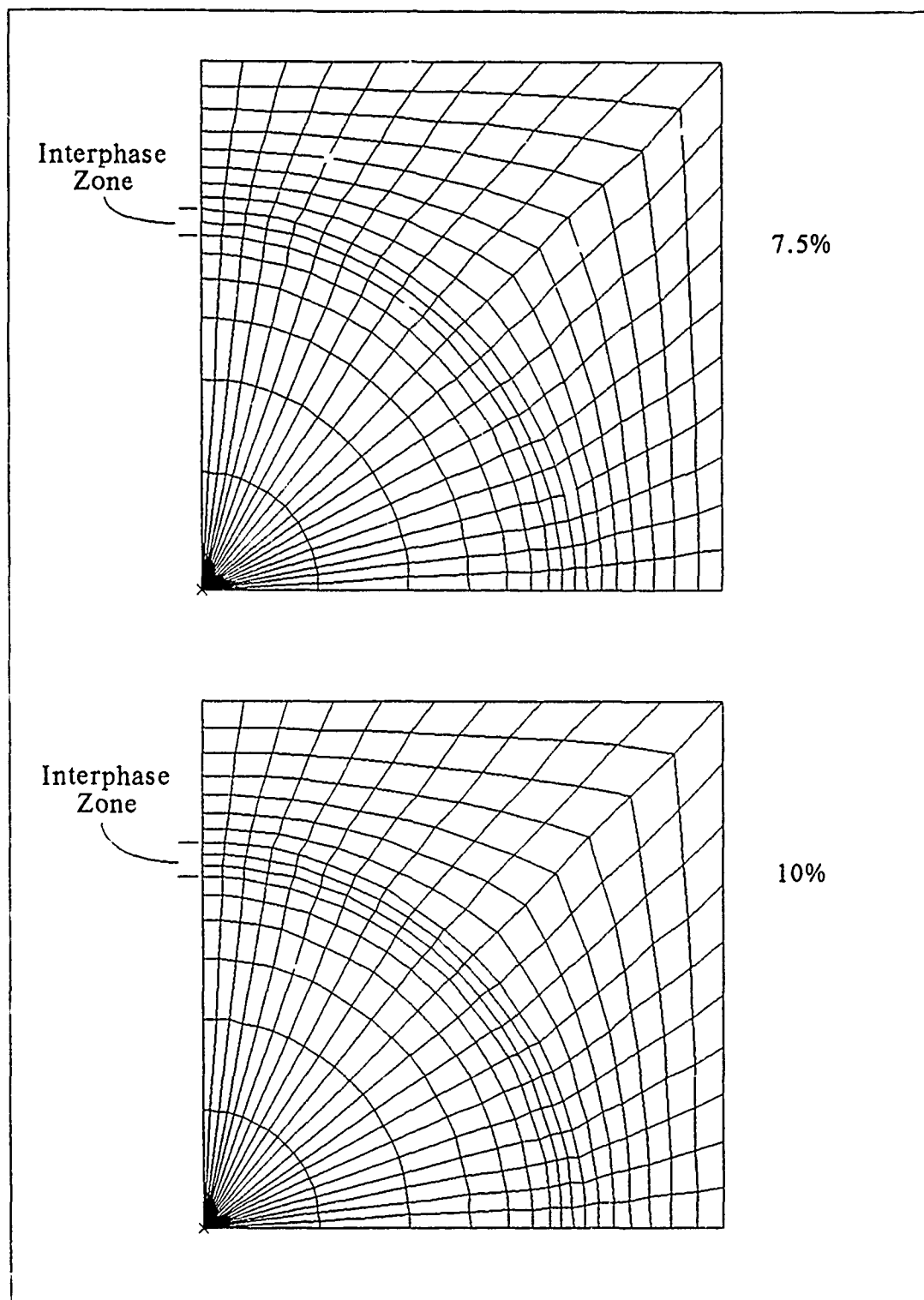
Figure 8. Finite Element Grids for Interphase Zone Sizes of 7.5% and 10% of Fiber Radius

3.5   Combined Interphase Zone and Weak Bond Models

All the models to this point have assumed that the fiber/matrix inter-facial region possesses identical properties at all points around the fiber. Most likely this is not the case in an actual specimen. Portions of the interface may represent a perfectly weak bond while other portions may still offer resistance either in separation or an irregular fracture surface may arrest transverse slippage at the interface. Therefore, additional models were developed to analyze a combination of fiber/matrix interface conditions. These models consist of a section of the interface taken to be perfectly weak while the remainder is assumed to behave as a third phase material possessing unique properties. A parametric study was then performed by varying the percentage of the interface modeled as perfectly weak.

Again, a simplified one dimensional mathematical solution and both two and three dimensional finite element solutions were used in this analysis. The one dimensional model is a modification of the previous model mentioned in the last section. However, an additional matrix region has been added, and the contact between it and the fiber is assumed to be perfectly weak(Figure 9). Neglecting shear and the Poisson's effect the one dimensional stress-strain and strain-displacement equations are obtained as before.

$$\varepsilon_F = \frac{u_F}{a} = \frac{\sigma_F}{E_F} + \alpha_F(T - T_P) \tag{22}$$

$$\varepsilon_{I_1} = \frac{u_{I_1} - u_F}{b} = \frac{\sigma_{I_1}}{E_I} + \alpha_I(T - T_P) + \varepsilon_{P_{I_1}} \tag{23}$$
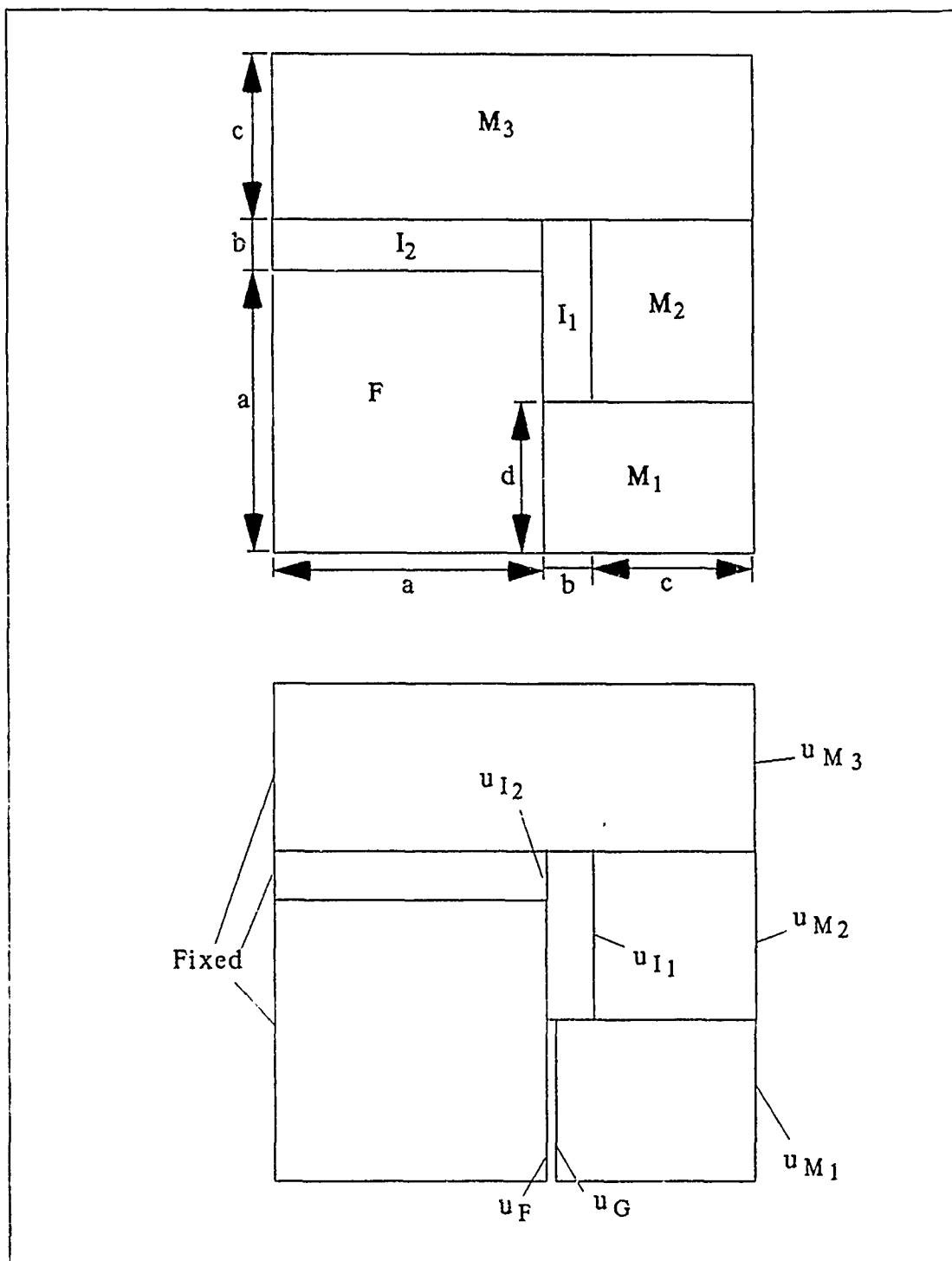
Figure 9. Simplified One Dimensional Model With Combined Interphase
Zone / Weak Bond

$$\varepsilon_{M1} = \frac{u_{M1} - u_G}{c} = \frac{\sigma_{M1}}{E_M} + \alpha_M(T - T_P) \qquad (24)$$

$$\varepsilon_{I2} = \frac{u_{I2}}{a} = \frac{\sigma_{I2}}{E_I} + \alpha_I(T - T_P) + \varepsilon_{PI2} \qquad (25)$$

$$\varepsilon_{M2} = \frac{u_{M2} - u_{I1}}{c} = \frac{\sigma_{M2}}{E_M} + \alpha_M(T - T_P) \qquad (26)$$

$$\varepsilon_{M3} = \frac{u_{M3}}{(a + b + c)} = \frac{\sigma_{M3}}{E_M} + \alpha_M(T - T_P) \qquad (27)$$

The three equilibrium equations become

$$\sigma_F a + \sigma_{I2} b = \sigma_{M1} d + \sigma_{I1}(a + b - d) \qquad (28)$$

$$\sigma_{I1}(a + b - d) = \sigma_{M2}(a + b - d) \qquad (29)$$

$$\sigma_{M1} d + \sigma_{M2}(a + b - d) + \sigma_{M3} c = \sigma_a(a + b + c) \qquad (30)$$

and the constraints on displacements

$$u_{I2} = u_F \qquad (31)$$

$$u_{M1} = u_{M2} = u_{M3} \qquad (32)$$

The same procedure is followed for plastic deformation of the inter-phase regions as in the previous section. However, the weak bond be-tween region F and M_1 must be taken into account. This is done by exam-ining the stress in region M_1 after each load step. If the stress is com-

41

pressive, then u_G is set equal to u_F. If the stress in region M_1 is tensile, then this stress is set equal to zero and u_G becomes the unknown. As before, a set of logic sequences are followed in solving the equation sets until two successive solutions are identical. The Mathematica™ program incorporated for solving this combined interphase zone / weak bond simplified one dimensional model is listed in appendix-C.

Unlike the one dimensional model where only the percentage of interface modeled as perfectly weak enters into the calculations, the finite element solutions also are affected by the location. A choice must therefore be made as to where to place the perfectly weak bond interface in the model. For both the two and three dimensional models a symmetric scheme was incorporated. The portion of the interface that was assumed to behave as if an isotropic interphase zone existed between the fiber and matrix was centered about a 45° line intersecting the center and upper right corner of the representative volume element as depicted in Figure 10.

The grid used was the same as of the 5% of fiber radius interphase zone size coarse grid model shown in Figure 7. Gap elements were added symmetrically as the size of the interface modeled as a weak bond increased. The elements outside the fiber attached to the gap elements were then given properties identical to the matrix.

The combined interphase zone / weak bond models provide a good extension on the effects of the interface conditions on the overall characteristics. The results from it and the other models already mentioned are presented in the following chapters. As a final note, no mention of specific material properties given to a particular model have been made in

42
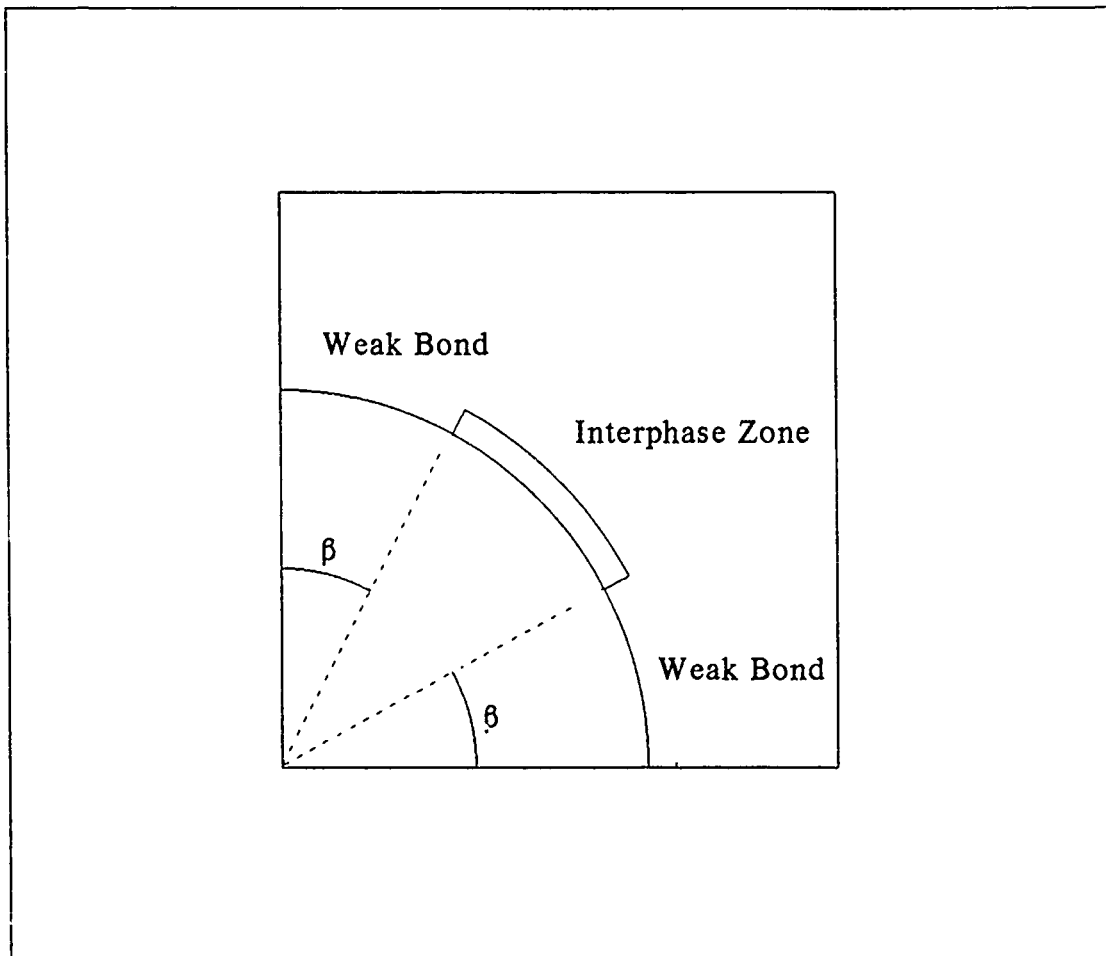
Figure 10. Interphase Zone Location Scheme for Combined Finite Element Model

the previous model descriptions. This was intentional. The following parametric study will require many material property variations to be made. Therefore, it was thought to be less confusing to call out the specific material properties used in a particular model in the results section.

IV. Results and Discussion

The main thrust of this thesis is to investigate how various properties and conditions at the fiber/matrix interface in a high temperature metal matrix composite effect its overall transverse normal properties. The following discussion presents the results of such a parametric study completed by using the techniques revealed in the previous chapter. All thermomechanical loading sequences consisted of cooldown to room temperature from a specified processing temperature followed by a transverse normal loading at constant temperature and in most cases, unloading. The transverse stress-strain response during the mechanical loading and unloading will be analyzed in detail. First, the results from perfectly strong and perfectly weak interfaces will be presented and compared with previous calculations obtained by an independent researcher[2; 3]. Subsequently, the results from models containing an interphase zone between fiber and matrix will be presented, and finally, an investigation where part of the interface is modeled as perfectly weak and part as if an interphase zone exists will be put forth.

4.1   Strong and Weak Interfacial Bond Results

The initial portion of this study will examine the behavior of a finite element micromechanics model where the interface is modeled both as perfectly strong and perfectly weak. Since previous work on this subject has been performed, it provides an excellent means for validation of the calculations. If the results presented in this section show good agreement with previous work, then further calculations may be attempted with a

44

high degree of confidence. Therefore, much of the material properties and other parameters will be matched with those used by Nimmer[2; 3].

4.1.1   Results from Perfectly Strong Interface

As described in section 3.3, both two and three dimensional finite element models possessing a strong interface were created. A 35% fiber volume fraction with a square fiber array was assumed, and the calculations were performed using the material properties listed in Table 2. One of the goals during the strong bond calculations was to determine what type of two-dimensional representation, either plane stress or plane strain, more accurately portrayed a generalized plane strain analysis. Therefore, all three methods were used and comparisons made between the plane stress and plane strain analyses against the three-dimensional generalized plane strain analysis. The loading sequence consisted of cooldown from a 1000°C zero stress state to room temperature at 23°C followed by a monotonically increasing transverse normal load. The Von Mises stresses after cooldown for plane stress and plane strain are shown in Figure 11, and the generalized plane strain model contours are shown in Figure 12.

Table 2. Material Properties Used for Strong Bond Models and Weak Bond RVE#1 Models

	E(GPa)	ν	$\alpha \ x10^{-6}(°C)^{-1}$
Matrix	100.0	0.3	10.0
Fiber	400.0	0.3	5.0
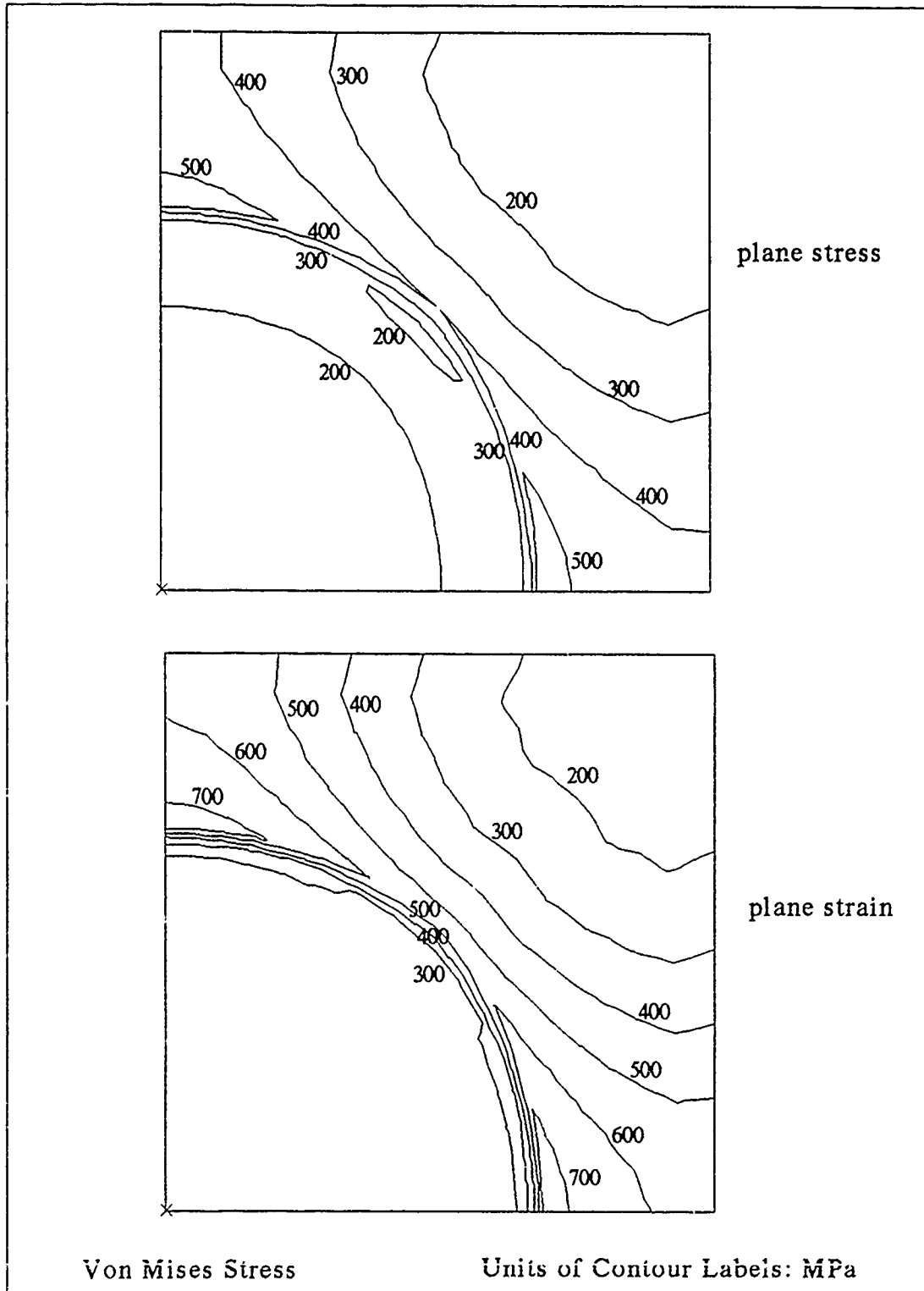
Figure 11. Strong Interface Plane Stress and Plane Strain Finite Element Model Residual Stress After Cooldown

46
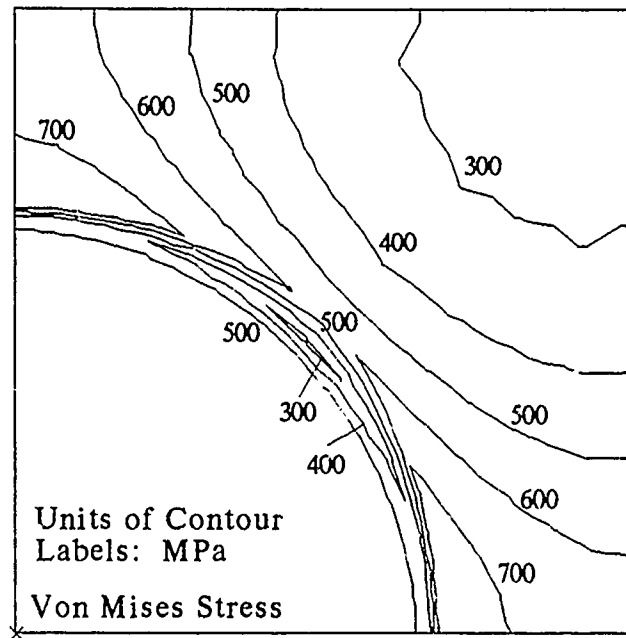
Figure 12. Strong Interface Generalized Plane Strain Finite Element
Model(3-D Model) Residual Stress After Cooldown

The maximum Von Mises stress is 543 MPa from the plane stress anal-
ysis and 745 MPa from the plane strain analysis while the generalized
plane strain model gives 794 MPa. Also, it is apparent after examination
of the stress contours in the above figures that from a stress field stand-
point the plane strain analysis more accurately approximates the three-di-
mensional generalized plane strain model. However, since the goal of mi-
cromechanics is to approximate the overall behavior, the load-deflection
curve of the entire structure is of primary importance.

The overall composite horizontal strain is the displacement of the
right-hand face referenced to the after cooldown state divided by the hori-
zontal width, and the overall composite stress is the applied load on the
right-hand face divided by its respective area. Thus, the overall compos-

47

ite transverse normal stress-strain behavior may be plotted from the finite element solutions. This is done in Figure 13 for plane stress, plane strain, and the generalized plane strain model, and the same procedure will be used throughout this paper for plotting all transverse response curves.

Surprisingly, the plane stress rather than the plane strain solution agrees more closely with generalized plane strain. As expected, plane stress and plane strain bounds the generalized plane strain solution, but the plane strain solution is too stiff. Therefore, when considering transverse response of a high temperature metal matrix composite, a plane stress analysis seems to be the best two-dimensional substitute for a three-dimensional generalized plane strain solution.
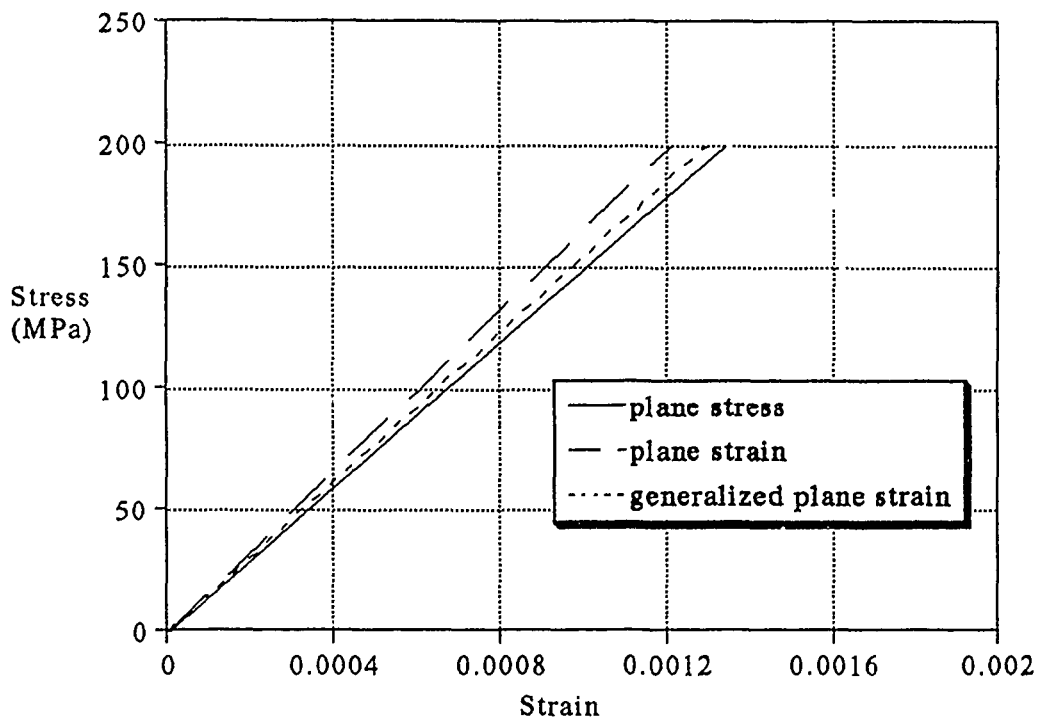
Figure 13. Strong Interface Transverse Response for Plane Stress, Plane Strain, and Generalized Plane Strain Finite Element Solutions

48

A possible explanation for this apparent anomaly lies with the thermal strains. The thermal strains, which are not shown in the figure since the zero strain state is taken to be the position of the right-hand face after cooldown, are on the order of 10^{-3} while the mechanical strains are on the order of 10^{-4}. Thus, the thermal strains are an order of magnitude greater than the mechanical strains, and since thermal strains are triaxial in nature, a significant amount of contraction will occur in the out-of-plane direction. Hence, the type of out-of-plane constraint will have a pronounced effect on the behavior. A pictorial explanation is given in Figure 14. A generalized plane strain analysis allows uniform out-of-
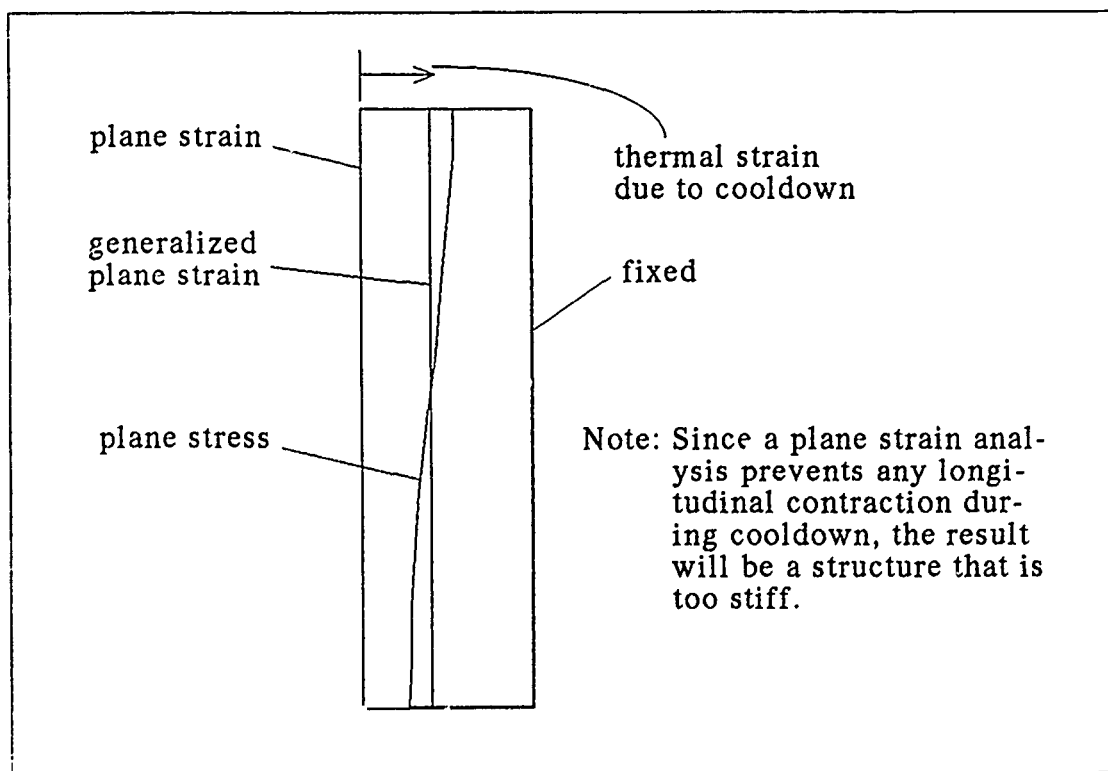
Figure 14. Schematic of Out-of-Plane Constraints Showing Difficulty of a Plane Strain Solution in the Presence of Large Thermal Strains

plane longitudinal contraction during cooldown while the plane stress analysis allows free longitudinal contraction. On the other hand, if a plane strain solution is used, no thermal contraction is allowed in the longitudinal direction, but this contraction is large when compared to the mechanical displacements. Therefore, the plane strain constraint will result in unduly large stresses in the longitudinal direction. The Poisson's effect of these longitudinal stresses will produce a stiffer structure in the lateral or transverse direction.

This last observation is important from the computational aspect since three-dimensional nonlinear finite element solutions are costly in CPU time. For the strong interface models where very little nonlinearity occurs it was possible to use a linear analysis, but for all other models a nonlinear analysis was necessary. Therefore, appropriate two-dimensional solutions must be sought. Nimmer used a plane stress type solution while performing his two-dimensional finite element analysis, and therefore, if appropriate comparisons are to be made with his results, then plane stress solutions must be used. In addition, a programming error presently exists in MSC/NASTRAN for solutions involving a plane strain nonlinear material analysis in the presence of thermal loads. Hence, for these reasons, in subsequent sections all two-dimensional models will use a plane stress type solution.

4.1.2   Results from Perfectly Weak Interface

The finite element solutions of a strong interface provided a good comparison to the weak interface models since before fiber/matrix separation occurs under transverse loading the weak and strong bond models

should behave in the same manner. Since nonlinear solutions must be used, the weak interface greatly increases the complexity of the problem. Therefore, to be assured that the results were reasonable several calculations were performed using a weak bond.

Initially, a 35% fiber volume fraction representative volume element (RVE#1) similar to that used for a strong bond was incorporated. The loading sequence for the RVE#1 weak bond models was the same as for the strong bond models. The overall composite transverse stress-strain response after cooldown for a monotonically increasing load using a plane stress analysis is given in Figure 15 and compared with a strong bond. The material properties were the same as listed in Table 2 on page 45, and
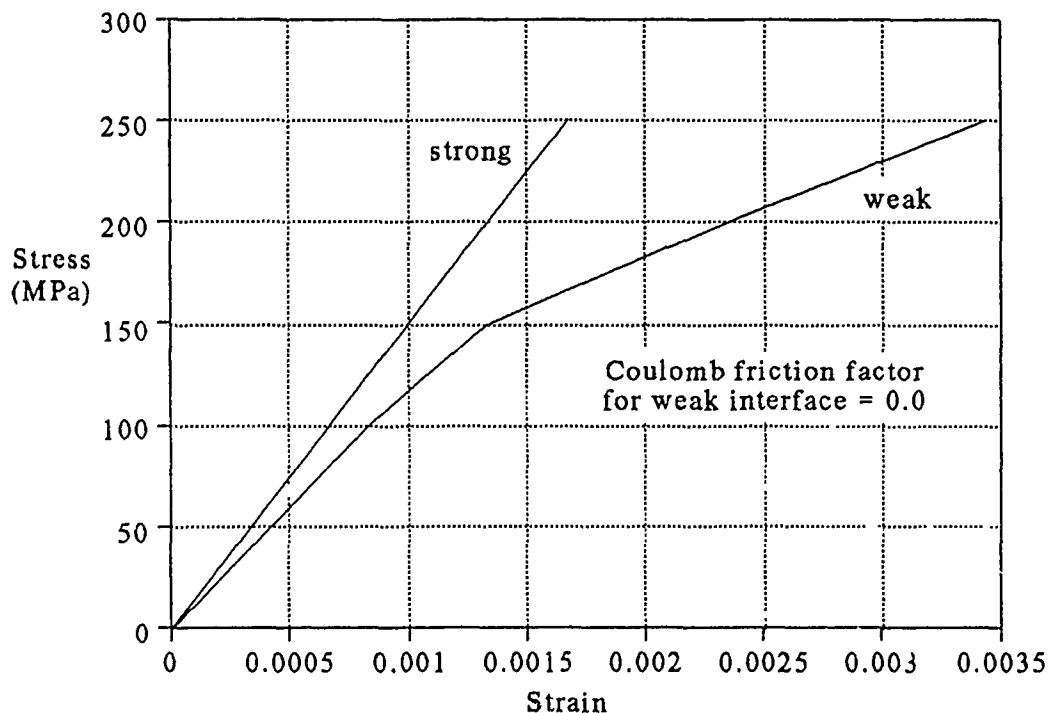
Figure 15. Weak Interface Transverse Response of RVE#1 Assuming Linear Elastic Matrix and Using a Plane Stress Finite Element Solution

51

the matrix was assumed to be linearly elastic. Also, a Coulomb friction coefficient of 0.0 was input for the gap elements along the interface. The classical bilinear shape of the weak interface curve is demonstrated, and fiber/matrix sep. ration occurs at approximately 150 MPa.

Notwithstanding, the initial slope of the weak bond curve does not match that of the strong bond as expected. An investigation into this difference requires an examination of the displaced geometry (Figure 16). The deformed structure is given for a transverse load of 140 MPa and 210 MPa. The 140 MPa load point occurs before separation, but upon further examination of the displaced geometry it is apparent that there is another mechanism acting besides just fiber/matrix separation. A weak interface with no friction will also experience slip along the interface. Therefore, even though the fiber and matrix are still in contact at 140 MPa, the structure has been considerably weakened as opposed to the strong interface due to the fiber/matrix slip. Interfacial slip was found to occur at all load levels, and hence, the decreased initial slope in the stress-strain curve resulted.

As a side note, the plots in this paper that show deformed geometry are presented with deformations grossly exaggerated, usually by multiplication factors above 100. Many of the stress contour plots are shown with their deformed geometry.

The addition of Coulomb friction at the interface has a pronounced effect on the results since it tends to arrest the fiber/matrix slip (Figure 17). As the friction coefficient is increased, the initial modulus before fiber/matrix separation also increases until it becomes equal to that of a strong bond. However, the addition of friction has no effect on the sec-

52
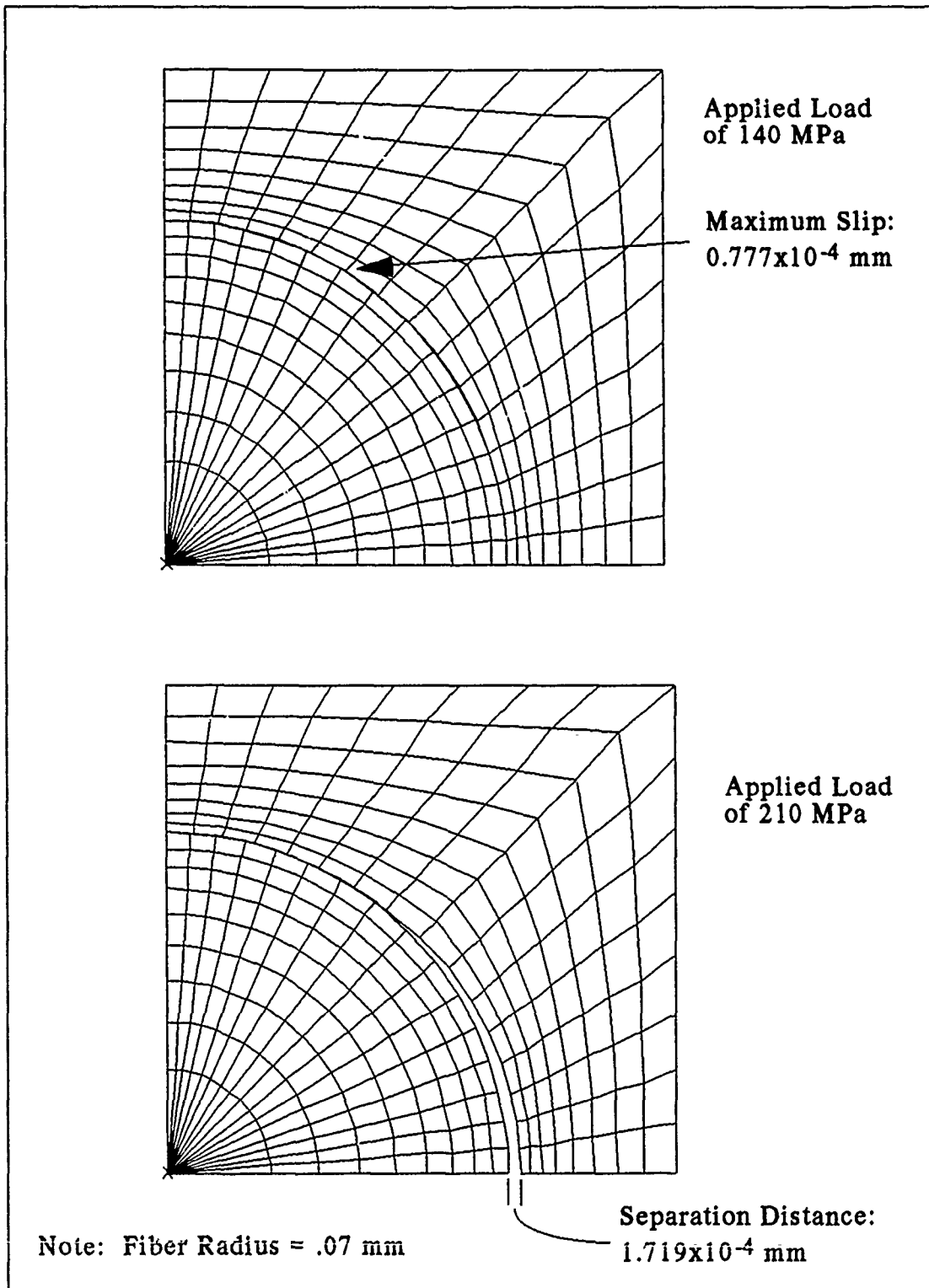
Figure 16. Weak Interface Deformed Geometry of RVE#1 at 140 MPa and 210 MPa.
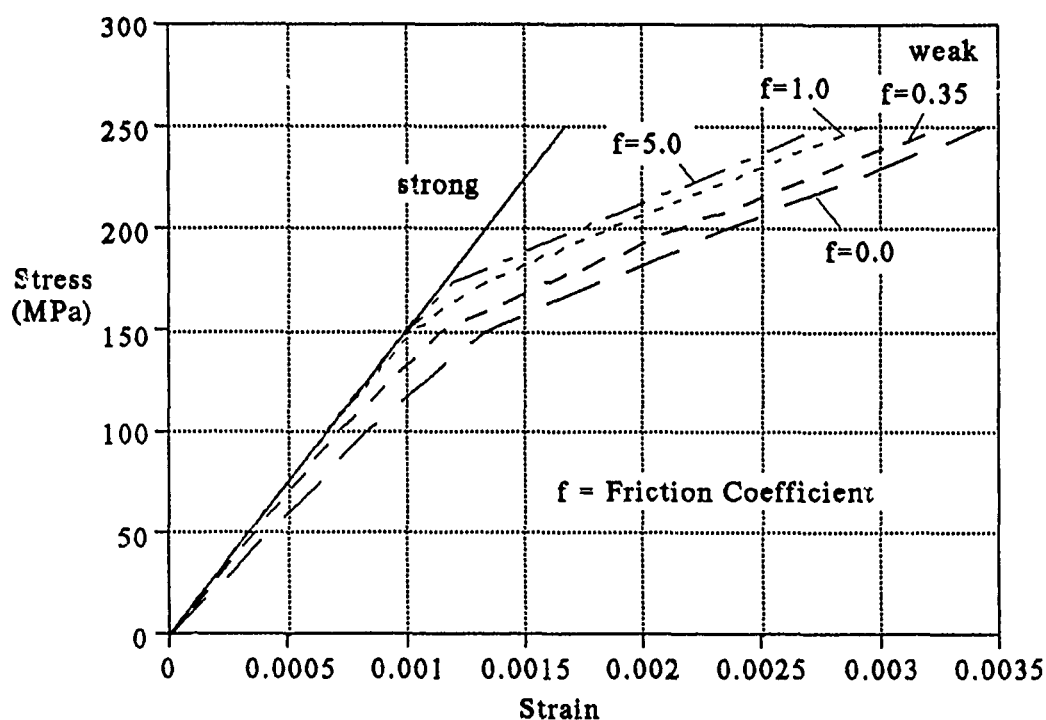
Figure 17. Weak Interface Transverse Response of RVE#1 With and Without Friction at the Interface and Assuming a Linear Elastic Matrix

ondary slope that occurs after separation. Since a large portion of the fiber and matrix surfaces are no longer in contact, the frictional constraint vanishes.

The final calculation using a monotonically increasing load incorporated an elastic-perfectly plastic matrix with a yield stress of 800 MPa and a friction coefficient of 0.0 at the interface(Figure 18). All other material properties remained the same as in Table 2. The results are plotted alongside that obtained by Nimmer using the finite element program ADINA for comparison[2]. As shown, the agreement between the calculations is excellent. Especially when one considers that the grids were cre-
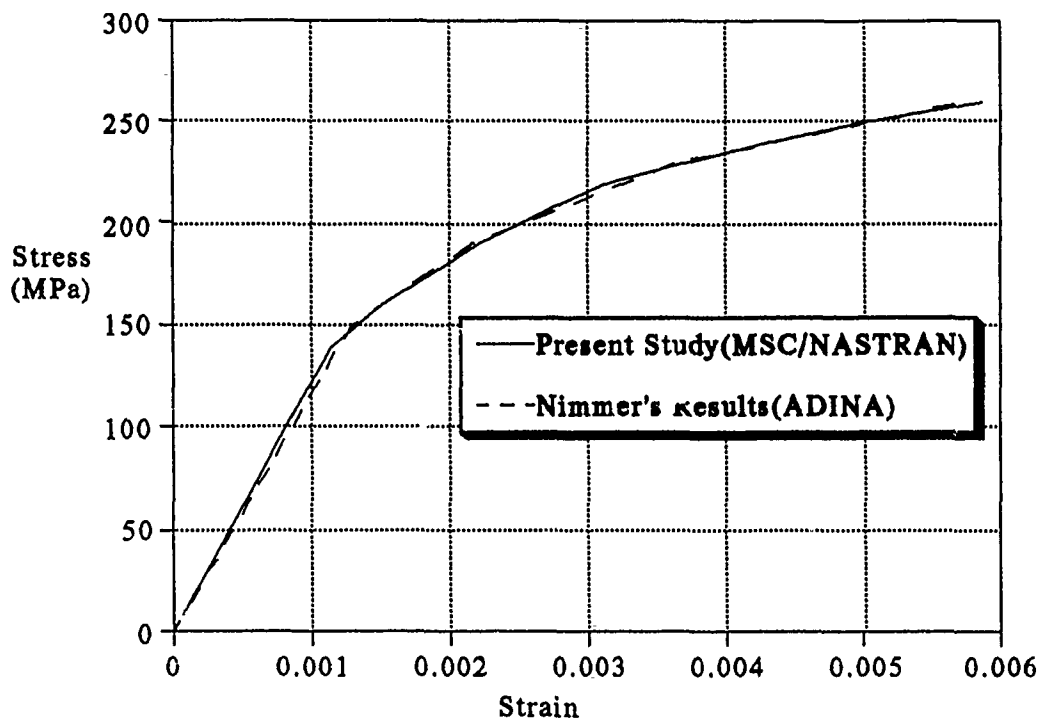
Figure 18. Weak Interface Transverse Response of RVE#1 Assuming Elastic-Plastic Matrix With a Yield Stress of 800 MPa and No Interfacial Friction as Compared to Nimmer's Results[2]

ated independently. Fiber/matrix separation again occurs at approximately 150 MPa, but the transverse response after separation is not linear since the matrix exhibits yielding.

A more clear understanding of the effects of the monotonically increasing load may be obtained by examining the history of the stress field during loading. The Von Mises stress contours after cooldown and at the onset of fiber/matrix separation are presented in Figure 19. The stress for transverse loads of 210 MPa and 260 MPa are then shown in Figure 20. The maximum Von Mises stress after cooldown is 621 MPa. Therefore, for a matrix yield stress of 800 MPa the residual stresses during cooldown

After Cooldown

Points of Maximum
Compressive Stress Normal
to the Interface: 258 MPa

150 MPa Applied
Transverse Load
(Onset of Separa-
tion)

Units of Contour
Labels: MPa
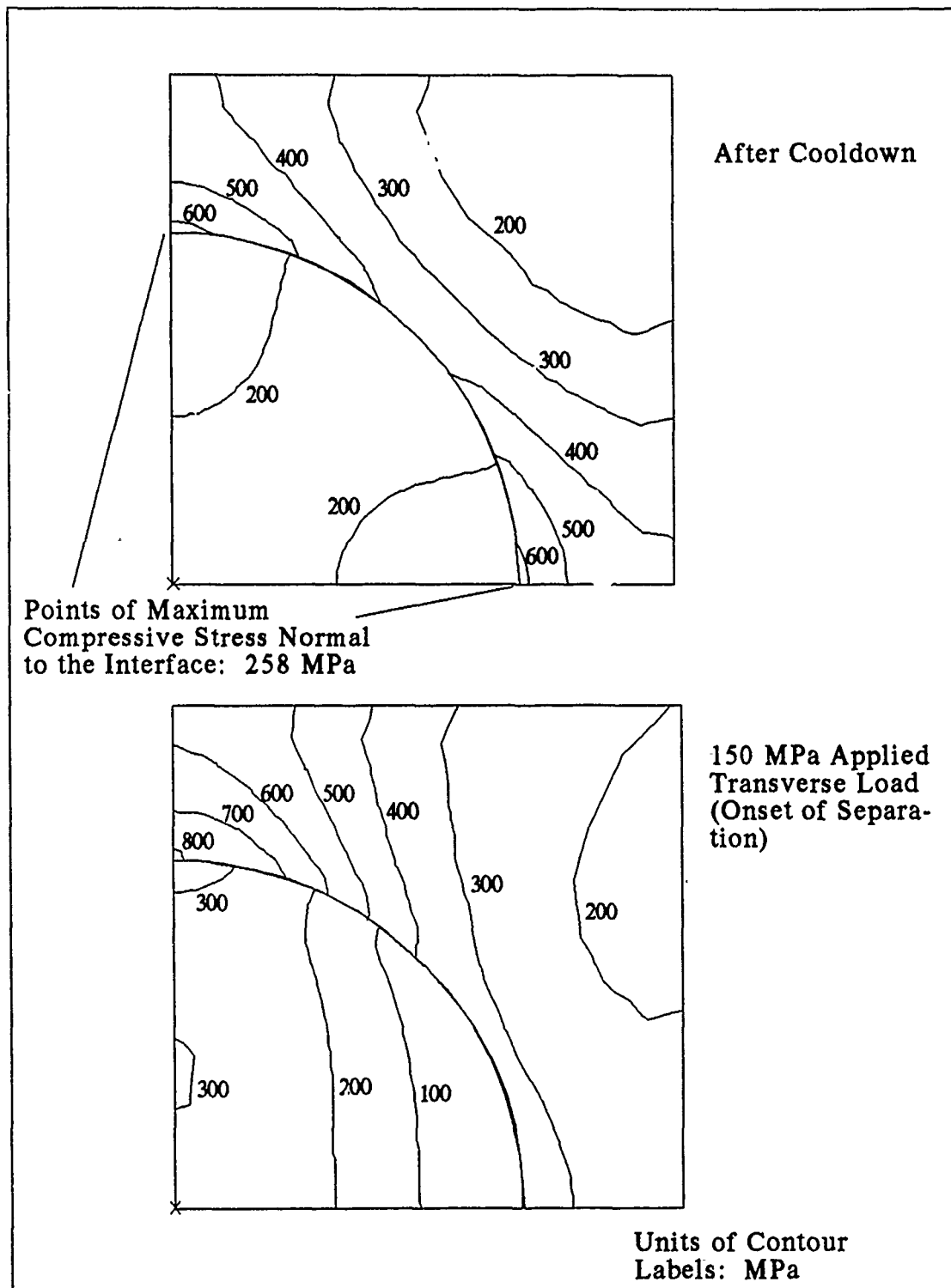
Figure 19. Weak Interface Von Mises Stress Contours for RVE#1 With
Elastic-Plastic Matrix and Frictionless Interface at Cooldown
and Onset of Fiber/Matrix Separation
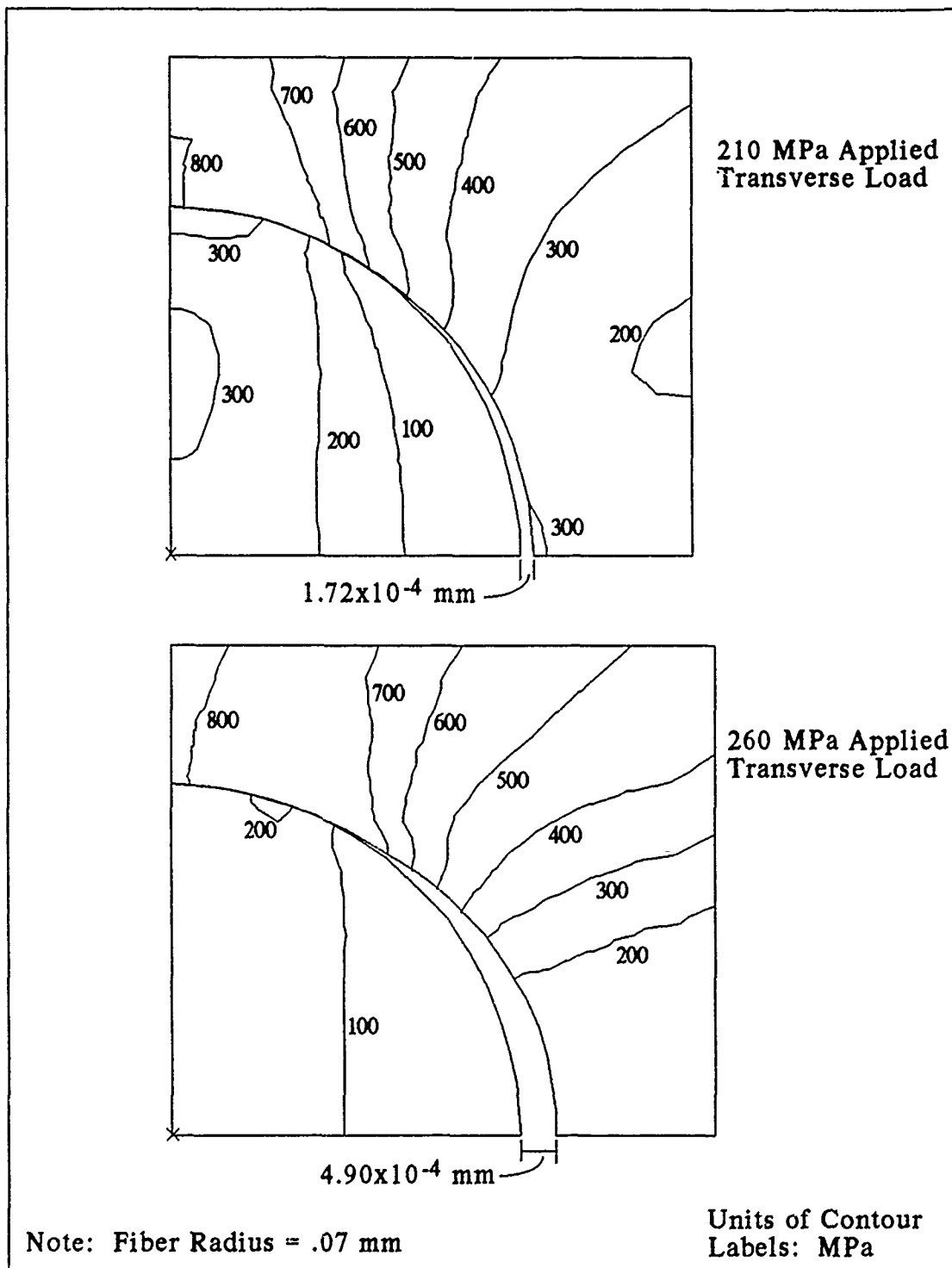
Figure 20. Weak Interface Von Mises Stress Contours for RVE#1 With Elastic-Plastic Matrix and Frictionless Interface at 210 MPa and 260 MPa Transverse Load

57

are not sufficient to cause matrix plastic flow. Also, when compared to Figure 11 on page 46 the stress field after cooldown for a weak and strong bond are not identical as one might at first imagine. The weak interface with no friction is unable to transmit shear across its face since friction is absent, so slip occurs and causes what seems to be an apparent discontinuity at the interface in the stress contours. Large compressive stresses normal to the interface exist after cooldown. These compressive stresses are maximum along the fixed edges as shown in Figure 19.

Interfacial compressive stresses must be overcome before the fiber and matrix will separate. This separation occurs at 150 MPa, and as shown in the figure a very small portion of the matrix has exceeded the yield stress at this point, indicating that for the model considered, matrix yield occurs simultaneously with fiber/matrix separation. This was merely a coincident. In general, fiber/matrix separation and matrix yield are not required to occur at the same load level.

As the model is further loaded past the separation point, plasticity in the matrix grows. Also, as more of the matrix separates from the fiber the overall stress in the fiber begins to decrease(Figure 20).

Weak interface calculations involving a loading and unloading sequence used the 32% fiber volume fraction, RVE#2, finite element grid. Both plane stress and three-dimensional generalized plane strain solutions were performed. As mentioned in chapter 3, this finite element model was created to match published experimental data[3]. Therefore, specific material properties associated with the published material were used and are given in Table 3. A coefficient of friction at the interface of 0.30 was chosen to match Nimmer's results, and the loading sequence consisted of

Table 3. Material Properties Used for Weak Bond RVE#2 Models

	E(GPa)	ν	$\alpha \times 10^{-6} (°C)^{-1}$	σ_{ys} (MPa)	H' (MPa)
Matrix	113.7	0.3	9.44	900.0	4600
Fiber	414.0	0.3	4.86	-	-

cooldown from a 900°C zero stress state to 21°C followed by a transverse applied load at constant temperature to 425 MPa and unload[3].

The transverse response after cooldown for both plane stress and generalized plane strain is presented in Figure 21. Results from Nimmer's generalized plane strain analysis are plotted alongside for comparison. The difference between the plane stress and generalized plane strain results are significant. The point of fiber/matrix separation is slightly increased and the overall response is considerably stiffer for the generalized plane strain model. However, the initial moduli are approximately the same, so the deviation occurs after the separation point. This deviation between the generalized plane strain solution and plane stress is linked to the high triaxial state of stress that exists for generalized plane strain due to the extra constraint in the out-of-plane direction. High triaxial stress fields may still possess low octahedral shear stress which may not be sufficient to cause yielding. Hence, if a triaxial stress field is the cause of the large difference between the generalized plane strain and plane stress solutions, then a significant reduction in matrix yield should be visible in the stress contours(Figure 22). Such is found to be the case as the
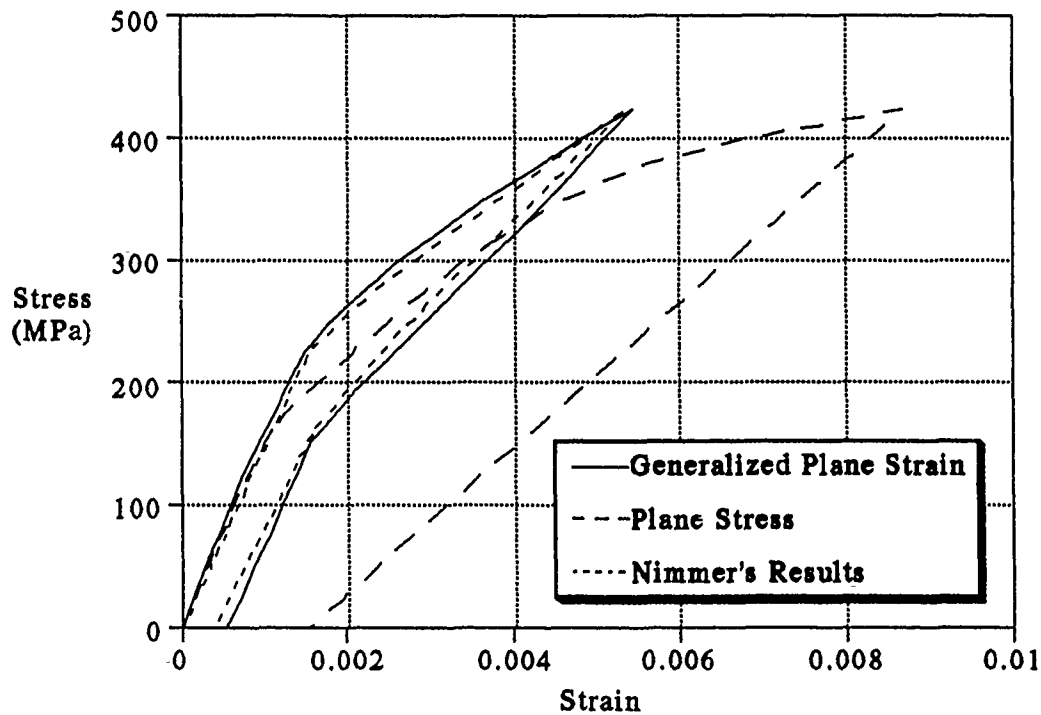
Figure 21. Weak Interface Transverse Response for RVE#2 Using Plane Stress and Generalized Plane Strain Solutions With Comparison to Nimmer's Results [3]

900 MPa contour line which represents the extent of matrix yield is greatly reduced in area for the generalized plane strain solution.

Nevertheless, as pointed out early on in Figure 2 on page 16 the weak bond generalized plane strain solutions do not always match experiments. Hence, it is possible that additional constraints exist in the actual specimen that are not modeled with a completely weak interfacial bond. A partially weak bond is more physically realistic, but the finite element weak bond model presented in the literature [2; 3] and also up to this point in the present study offers little flexibility for incorporating additional constraints; interfacial friction is the only variable. An increase in the in-
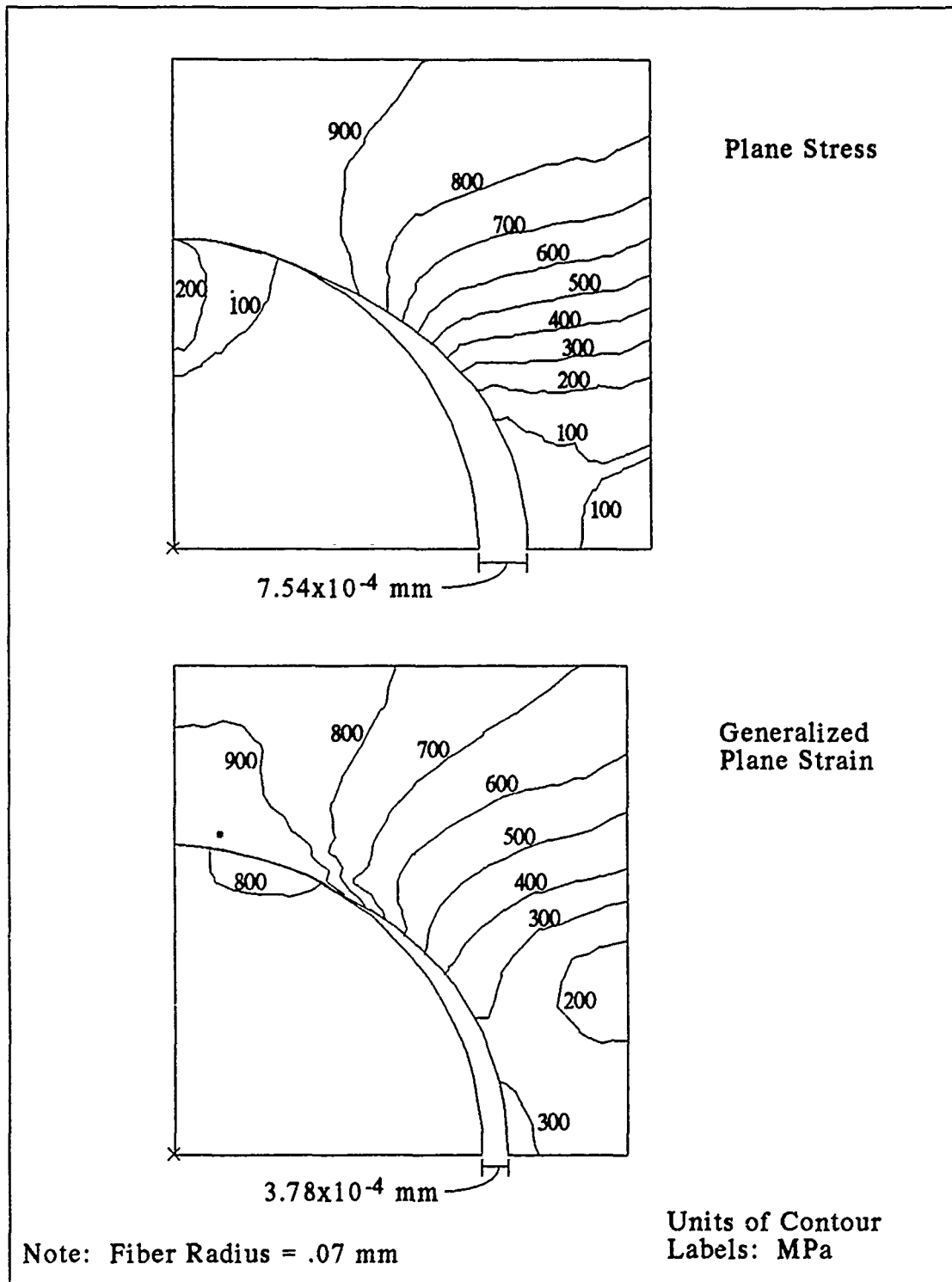
Figure 22. Weak Interface Von Mises Stress Contours for RVE#2 at Maximum Load for Both Plane Stress and Generalized Plane Strain

61

terfacial coefficient of friction was previously found to increase the modulus before separation but had little or no effect after separation. However, the problem at hand requires a constraint that exists both before and after separation.

The zone between fiber and matrix is very complex. During high temperature processing a reaction zone is formed where the fiber material has penetrated into and reacted with the matrix. Many flaws exist in this zone and its failure occurs early during initial loading[1]. After failure of the fiber/matrix bond a fracture surface exists. Most fracture surfaces are not smooth but rather jagged in nature, especially at the microscopic level. Therefore, the surface will possess a high resistance to slip between the two faces, and as long as the separation between the two fracture surfaces is small, this resistance to slip will persist.

Hence, a reasonable constraint to add to the perfectly weak bond model is one that prevents slip between fiber and matrix both before and after separation. Such a constraint was added to the plane stress and generalized plane strain models to determine its effect. Figure 23 presents the plane stress solution. The added constraint of preventing slip at the interface has a pronounced effect on the result, greatly stiffening the structure. In fact, it increases the overall stiffness to the point that no plastic deformation occurs in the matrix making the loading and unloading elastic. The initial modulus remains the same, and fiber/matrix separation occurs at approximately the same point, but the slope after separation is greatly increased.

The generalized plane strain solution is shown in Figure 24 with the experimental results from Figure 2 on page 16 plotted alongside for com-
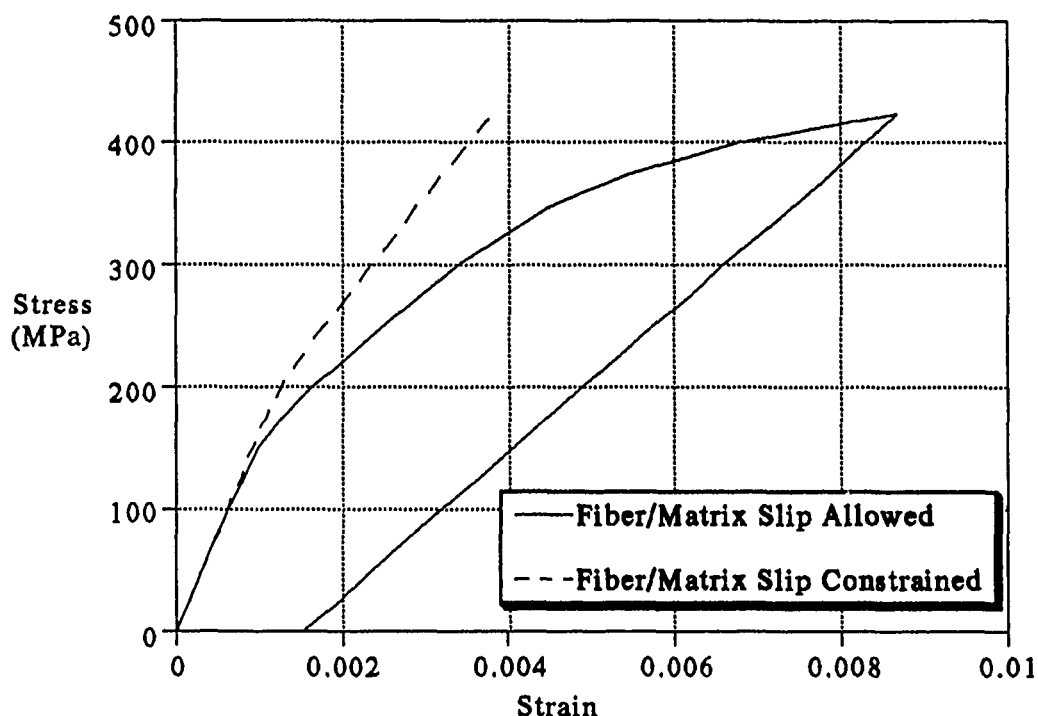
Figure 23. Weak Interface Transverse Response for RVE#2 Plane Stress
Solution With and Without Fiber/Matrix Slip at the Interface

parison. In addition, the stress contours at maximum load are given in
Figure 25. The results again indicate a substantial effect from the addi-
tional constraint. In the same way as in the plane stress solution the
structure has been greatly stiffened. In fact, the Von Mises stress of the
matrix never exceeds its yield stress of 900 MPa. Instead, the overall
transverse stress-strain response becomes a nonlinear elastic curve.
Fiber/matrix separation still occurs, but due to the extra constraint that
prevents slip, the overall transverse response is dramatically changed, and
ne separation distance at maximum load is greatly reduced. Also, a very
encouraging development is that the with and without slip constraint cal-
culations form a bound for the experimental data.

63
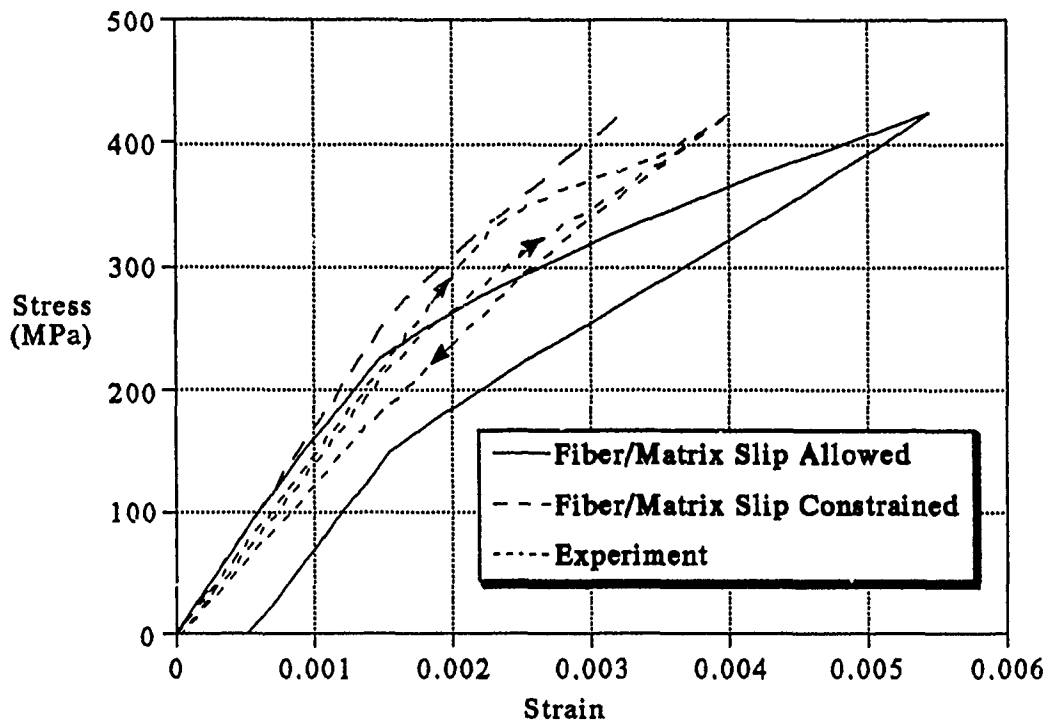
Figure 24. Weak Interface Transverse Response for RVE#2 General-
ized Plane Strain Solution With and Without Fiber/Matrix
Slip and Comparison to Nimmer's Experiment[3]

As a reminder, the experimental data is from a load, unload, and re-
load sequence. The difference between the initial load and reload curves
in the experimental data are from the finite fiber/matrix bond strength
which fails during initial loading. The experiment exhibits energy dissi-
pation during the cycle, but very little permanent strain. Therefore, it is
reasonable to assume that much of the energy dissipation is caused by
something other than plastic deformation. During the opening and closing
of jagged fracture surfaces frictional losses will occur that otherwise
would not if the two surfaces were smooth. Hence, the motivation for the
additional constraint also serves as an explanation for the energy dissipa-
tion observed in experiment. It was not possible to account for this fric-
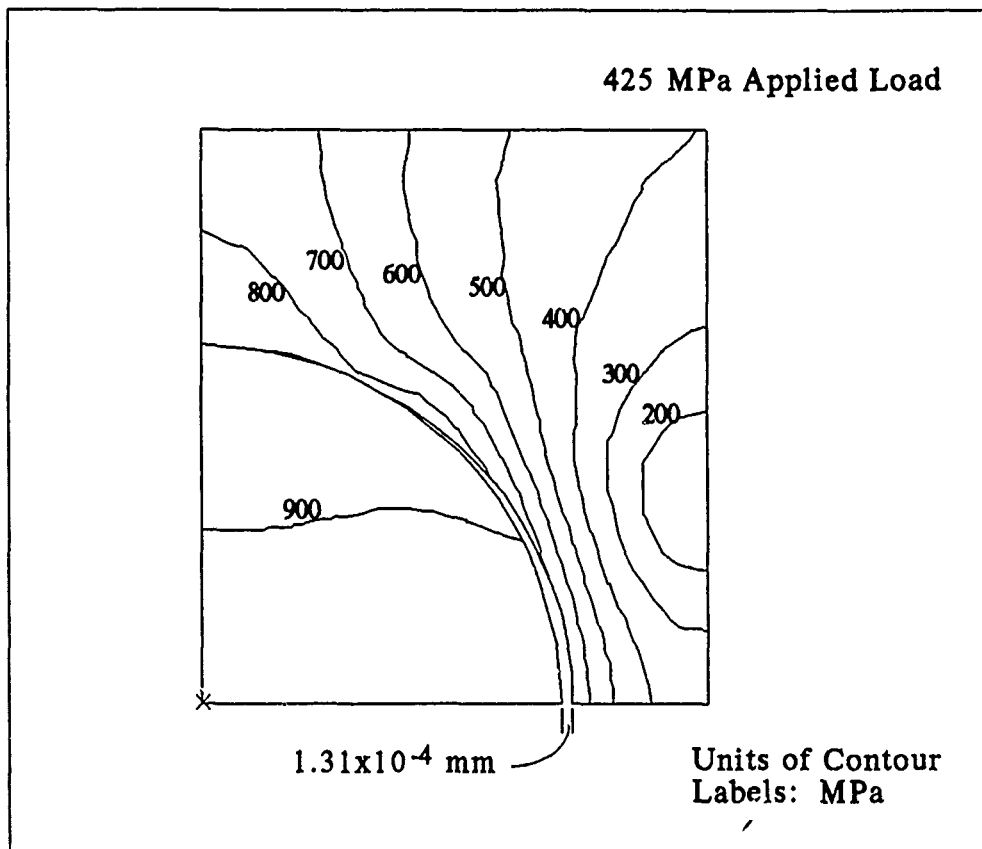
Figure 25. Weak Interface Von Mises Stress Contours for RVE#2 at
Maximum Load Using Generalized Plane Strain Solution and
Preventing Fiber/Matrix Slip

tional energy loss in the calculations as that would almost certainly in-
volve the development of a new type of element in MSC/NASTRAN.

The assumption of a jagged fiber/matrix fracture surface provides a
possible explanation for the phenomena observed. However, as demon-
strated, incorporating its effects in an analysis is difficult. In spite of the
jagged surface a certain amount of fiber/matrix slip will still be allowed,
and frictional losses during opening and closing make the problem even
more formidable. At present, it is impossible to include such effects with
the finite element tools available. Therefore, an attempt is made to model

65

the problem in a simplified manner by including a third zone between fiber and matrix possessing its own unique properties. This interphase zone should provide for energy dissipation and for additional constraints at the interface not modeled by a perfectly weak bond.

4.2   Results from Models Possessing an Interphase Zone

Many mechanisms are acting at the fiber/matrix interface. Imperfections exist that have a pronounced effect on the composite's overall characteristics. The challenge is to model these mechanisms in the simplest way. As demonstrated in the previous section assuming the interface behaves as if it is perfectly weak exhibits modest success, but due to inadequate constraints at the interface and because there is no means of modeling energy dissipation such an assumption meets with difficulty. In this section the attempt is made to model the interface as a third zone possessing unique properties. Previous studies have used such an approach, but they only examined the elastic realm[17-19]. This study will emphasize the plastic properties. The assumption being that all the nonlinearities existent at the interface may be adequately modeled by an isotropic elastic-plastic interphase zone between the fiber and matrix.

4.2.1   One-Dimensional Results With Interphase Zone

The simplified one-dimensional model discussed in section 3.4 was incorporated for analyzing parameter variations associated with an inter- phase zone. The advantage of the one-dimensional solutions over the finite element calculations rests with the speed at which answers could be

obtained. Solutions that took on the average ninety seconds with the one-dimensional model would require several hours for a finite element solution. In addition, the finite element solutions would generally require the creation of a new grid which in itself might take several hours. Therefore, the mode of analysis presented here proved to be very helpful in this study.

Due to the fact that several parameter variations were to be examined a suitable baseline was chosen from which a single parameter could be varied while holding the others fixed. This baseline set is listed in Table 4 and was chosen to match the material properties from some of the weak bond calculations of the previous section. All parameters associated with the interphase zone were varied to determine their overall effect. These include interphase zone yield stress, strain hardening, Young's

Table 4. Baseline Parameters for One-Dimensional Model With Interphase

σ_{ys_I} = 125 MPa		V_F	= 0.35
H' = 0 MPa	(see Figure 6)	a	= 0.07 mm
T_P = 1000°C		b	= 5% of fiber
T = 25°C		E_F	= 400 GPa
α_F = 5 x 10^{-6} (°C)$^{-1}$		E_I	= 100 GPa
α_I = 10 x 10^{-6} (°C)$^{-1}$		E_M	= 100 GPa
α_M = 10 x 10^{-6} (°C)$^{-1}$			

modulus, thermal coefficient of expansion, and thickness. Each solution consisted of transverse normal loading to 27.5 MPa followed by a complete unloading.

Some of the results are compared to a one-dimensional model with a strong and weak bond[2]. This is the case in Figure 26 where interphase zone yield stress is varied from 200 MPa to 75 MPa. As shown, the initial slopes of all curves match the strong interfacial bond slope exactly. This is as expected since the initial compressive thermal stresses at the interface must be overcome before nonlinearities may occur. The weak bond presents a bilinear behavior where the "kink" in the curve results from fiber/matrix separation. The model containing an elastic-plastic inter-
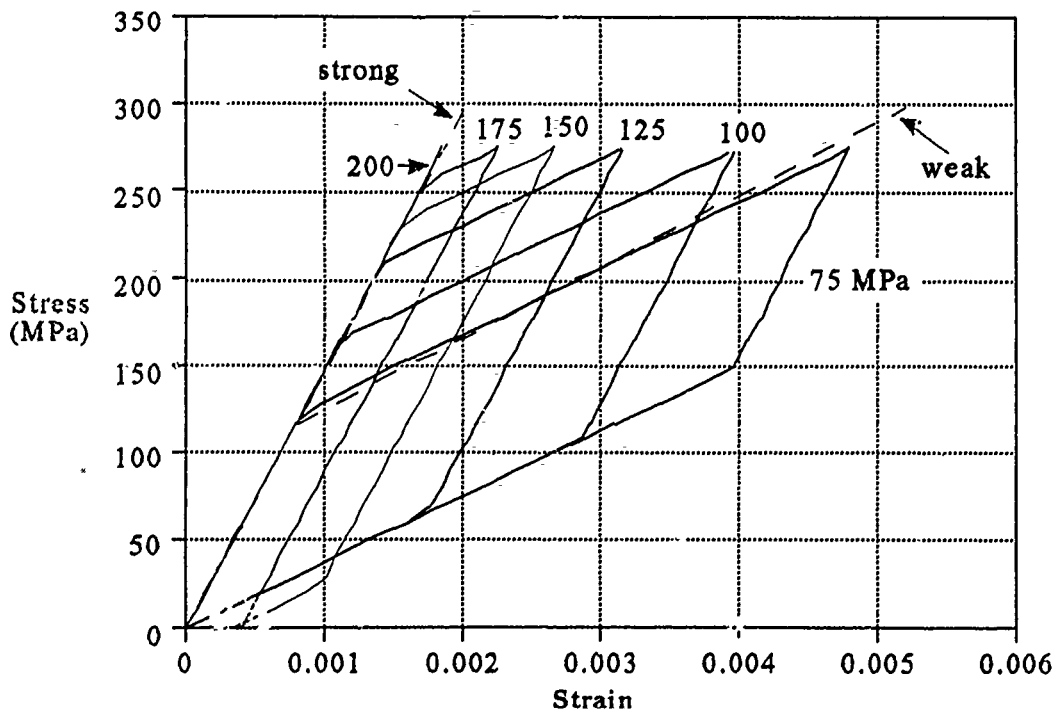
Figure 26. One-Dimensional Solutions With Interphase Zone for Interphase Yield Stresses from 75 MPa to 200 MPa as Compared to Nimmer's Strong and Weak Bond Model[2]

phase zone must further be loaded before nonlinearity develops because the interphase yield stress must also be overcome. Similarly, unloading is characterized by elastic followed by plastic deformation which involved compressive yielding of the interphase. The plastic deformation during unloading is a result of the thermal residual stresses and elastic energy in the matrix overcoming the interphase zone yield stress. As shown, for the given loading condition a yield stress of 200 MPa does not experience yielding, and hence a linear elastic curve that matches the strong bond results.

At first one might reason that a yield stress of zero should match the weak bond model, but in actuality a zero yield stress results in a complete relaxation of all thermal residual stresses as the interphase zone deforms during cooldown. The compressive stress at the interphase after cooldown is 130 MPa. Therefore, any yield stress below this will result in some relaxation of the thermal stresses. This was observed in the solutions and c_n be visualized in Figure 26. For yield stresses above 130 MPa the point where nonlinearity first occurs is controlled by the applied load overcoming an initial compressive stress of 130 MPa at the interphase and then exceeding the tensile yield stress. For yield stresses below 130 MPa the initial compressive stress that the applied load must overcome is equal to the yield stress. Hence, the point of nonlinearity will occur sooner. This can be seen by observing that all curves ith yield stresses below 130 MPa demonstrate a greater difference between points of nonlinearity for two successive yield stresses than can be seen in the curves with yield stresses above 130 MPa. Therefore, rather than zero yield stress matching the weak bond, a yield stress of 75 MPa closely approximates the behavior

of a weak bond during loading. Thus, an incorrect stress field calculation will result due to the relaxation of the thermal residual stresses.

In addition, the simplified one-dimensional solutions demonstrate that a significant amount of energy dissipation occurs when modeling the fiber/matrix interface as a third zone possessing relatively low yield stress. The area traced out by each loading and unloading sequence depicts this energy dissipation. Also, for yield stresses of 125 MPa and below the model returns close to its approximate initial strain state after unloading. This results from the residual thermal compressive stresses being equal to the yield stress, and hence they are capable of plastically deforming the interphase zone back to its original state. Therefore, this approach's ability to model energy dissipation and allow for additional interface constraints that may be varied to approximate any level of bonding from strong to weak holds some promise over the weak bond model.

Varying the plastic parameters(i.e. yield stress and strain hardening) was found to effect the overall transverse behavior the most. The effect of strain hardening on the solution is shown in Figure 27, and it indicates that the main effect is on the secondary slope during loading. As a result, when the interphase strain hardening parameter is increased the energy dissipated during loading and unloading is decreased. Also, a mirror image of these slopes about the $H' = 0$ MPa secondary slope line occurs when plastic deformation becomes present upon unloading. This is a result of the isotropic strain hardening assumption. In fact, for the $H' = 2000$ MPa curve the interphase has been sufficiently hardened during loading that the residual thermal stresses are unable to induce plastic deformation when the structure is unloaded.

70
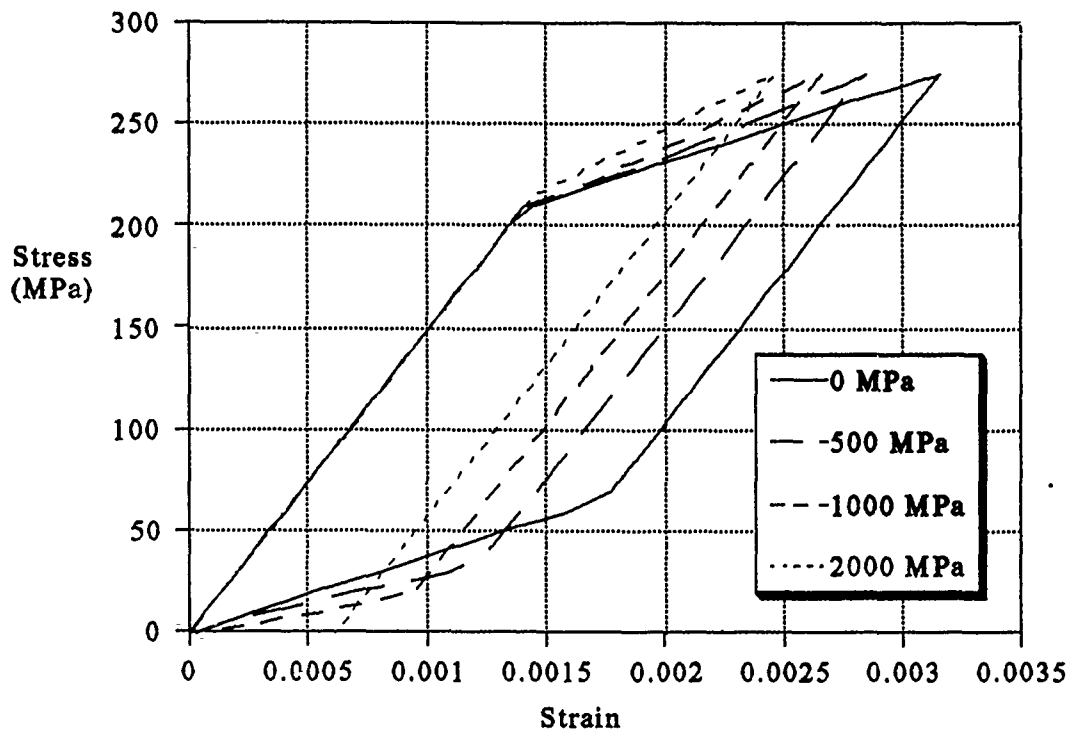
Figure 27. One-Dimensional Solutions of Interphase Zone Strain Hardening Parameter Variation

The three other parameters varied were the interphase zone size, Young's modulus, and thermal coefficient of expansion. The effect of zone size is depicted in Figure 28. As shown, it has only modest impact on the results. A slight change in the secondary slope occurs reducing the amount of energy dissipated as the zone size is decreased. This is as expected since the matrix is stronger than the interphase zone. Therefore, as the interphase zone size is decreased and replaced by matrix material the overall structure will become stronger.

Young's modulus was also found to have only a slight effect on the overall stress-strain response during loading and unloading(Figure 29).
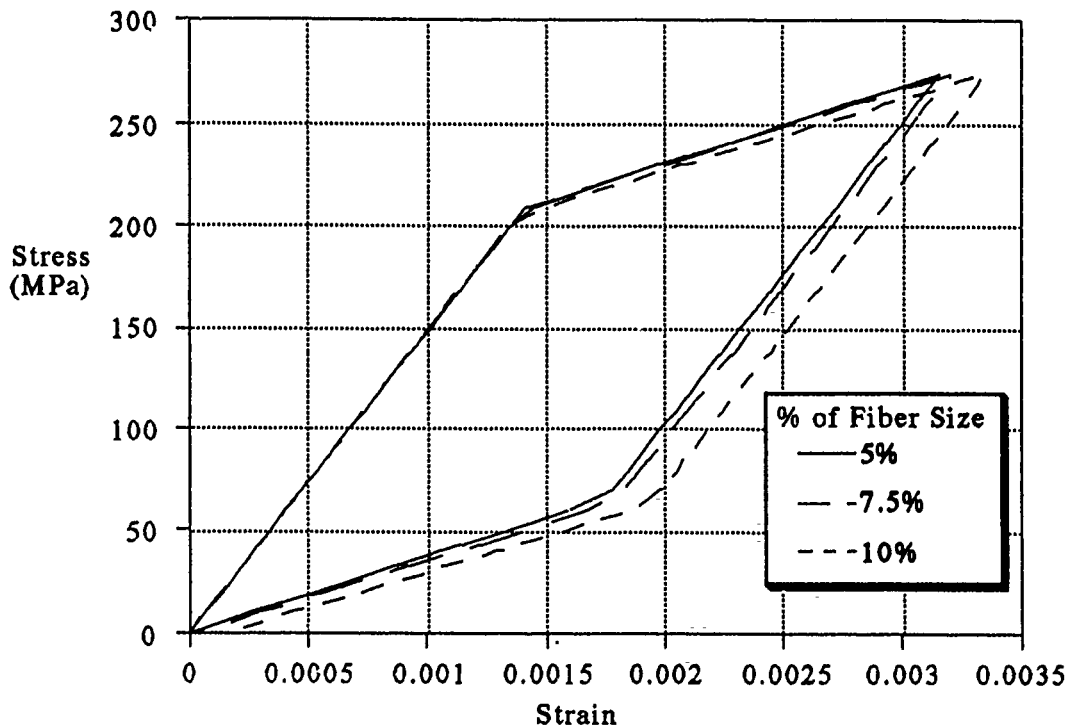
Figure 28. One-Dimensional Solutions of Interphase Zone Size Variation

Since the interphase zone is small in comparison to the fiber and matrix, its elastic characteristics exert little influence on the entire structure. In the figure below the interphase modulus is first set equal to that of the matrix(100 GPa) and then the fiber(400 GPa). Only a slight change in the elastic slope of the structure results.

Finally, the thermal coefficient of expansion of the interphase is varied and shown in Figure 30. As with the modulus, the expansion coefficient is varied from the the matrix's value to the fiber's. The plot shown deviates from the baseline parameter set by taking the interphase yield stress to be 150 MPa. This was necessary since the effect of changing the
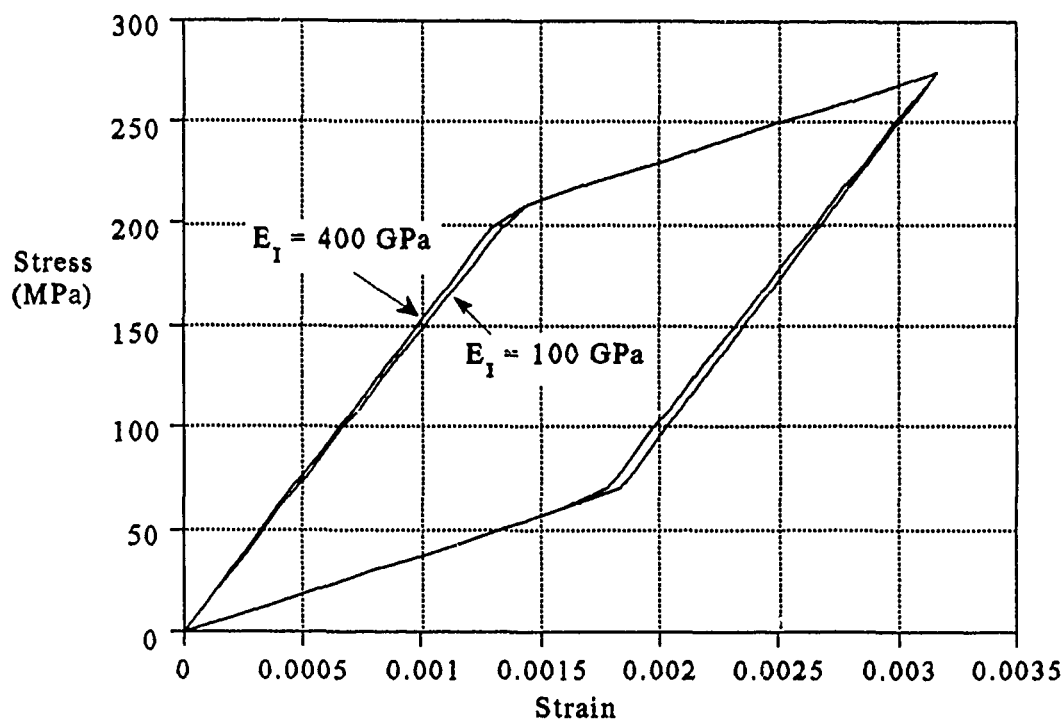
Figure 29. One-Dimensional Solutions of Interphase Young's Modulus Variation

expansion coefficient is reflected in the compressive residual stresses, and in order to prevent a relaxation of these stresses a yield stress was chosen so that yielding would not occur during cooldown. With transverse loading as the expansion coefficient is increased the stress at which nonlinearity begins decreases. This results from the interphase zone with a higher expansion coefficient contracting more during cooldown and hence the matrix experiences less resistance when it contracts thereby lowering the compressive residual stresses. However, this effect is small.

In summary, the one-dimensional solutions have provided a good introduction into how the properties of the interphase zone effect the over-

73
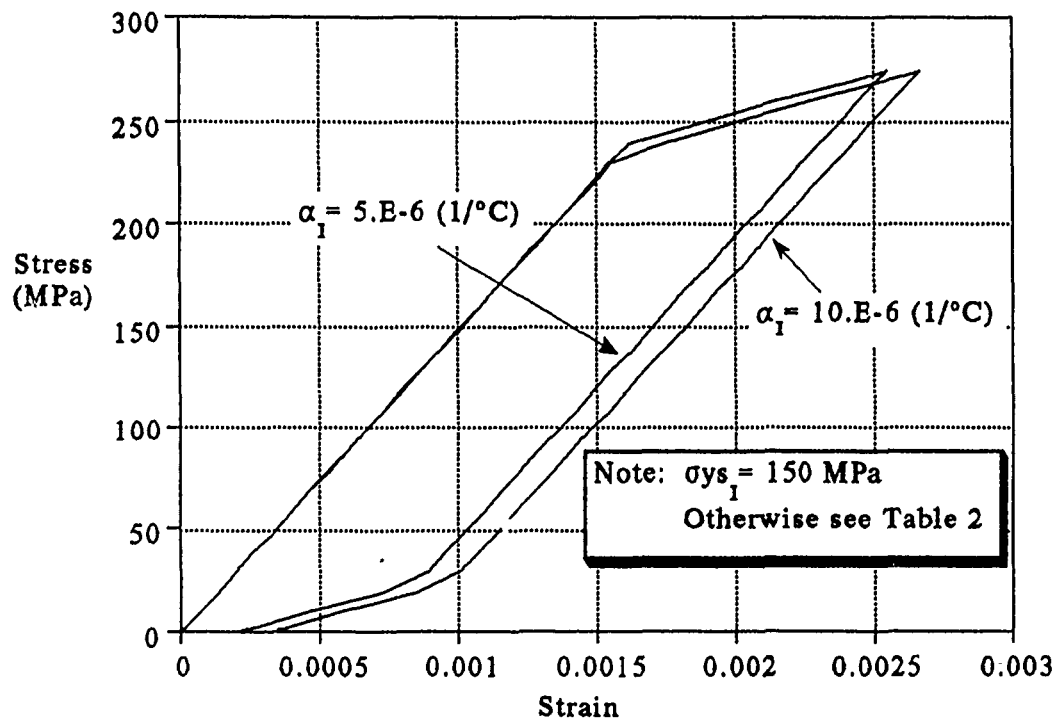
Figure 30. One-Dimensional Solutions of Interphase Zone Thermal Expansion Coefficient Variation

all characteristics of the composite. Yield stress and strain hardening were found to have the most profound effect. Increasing the yield stress was found to increase the point of nonlinearity(Figure 26), and increasing the strain hardening parameter was found to increase the secondary slope (Figure 27). Significant energy dissipation occurs during a loading and unloading sequence, and for sufficiently low interphase zone yield stress the overall structure returns to its approximate original strain state after unloading. A more thorough investigation using finite element analysis is presented in the following section, and some comparisons will be made between it and the one-dimensional solutions.

4.2.2 Finite Element Solutions With Interphase Zone

An examination into the effects of an interphase zone between fiber and matrix using finite element analysis utilized the finite element grids presented in section 3.4 for a 35% fiber volume fraction and a fiber radius of 0.07 mm. The bulk of the calculations consisted of plane stress type solutions, but a few three-dimensional generalized plane strain solutions were also performed.

Just as for the one-dimensional solutions, a baseline parameter set was chosen from which a single parameter could be varied while holding the others fixed. This baseline set is given in Table 5, and except for the added matrix plastic properties, it is the same as was used in the one-dimensional solutions. The loading sequence is also the same, cooldown from a 1000°C processing temperature to room temperature at 25°C followed by transverse loading at constant temperature to 275 MPa and then unload.

Table 5. Baseline Parameters for Finite Element Models With Interphase Zone

	E(GPa)	ν	$\alpha \times 10^{-6}(°C)^{-1}$	σ_{ys} (MPa)	H′ (MPa)
Matrix	100.0	0.3	10.0	800.0	0.
Interphase	100.0	0.3	10.0	125.0	0.
Fiber	400.0	0.3	5.0	-	-

Interphase Zone Size(thickness) = 5% of Fiber Radius

75

The plane stress solutions will be presented first. The effect of vary-
ing the yield stress is shown in Figure 31 along with the solutions for a
perfectly strong bond and a perfectly weak bond. The behavior is very
similar to that seen in the one-dimensional solutions. The initial modulus
for all curves matches that of a strong bond, and the main effect of in-
creasing the interphase zone yield stress is increasing the stress at which
nonlinearity first occurs. An interphase yield stress of 200 MPa experi-
ences very little yielding, and hence this curve does not deviate much
from the strong bond solution.

Relaxation of the thermal residual stresses during cooldown occurred
in the one-dimensional solutions for interphase yield stresses below
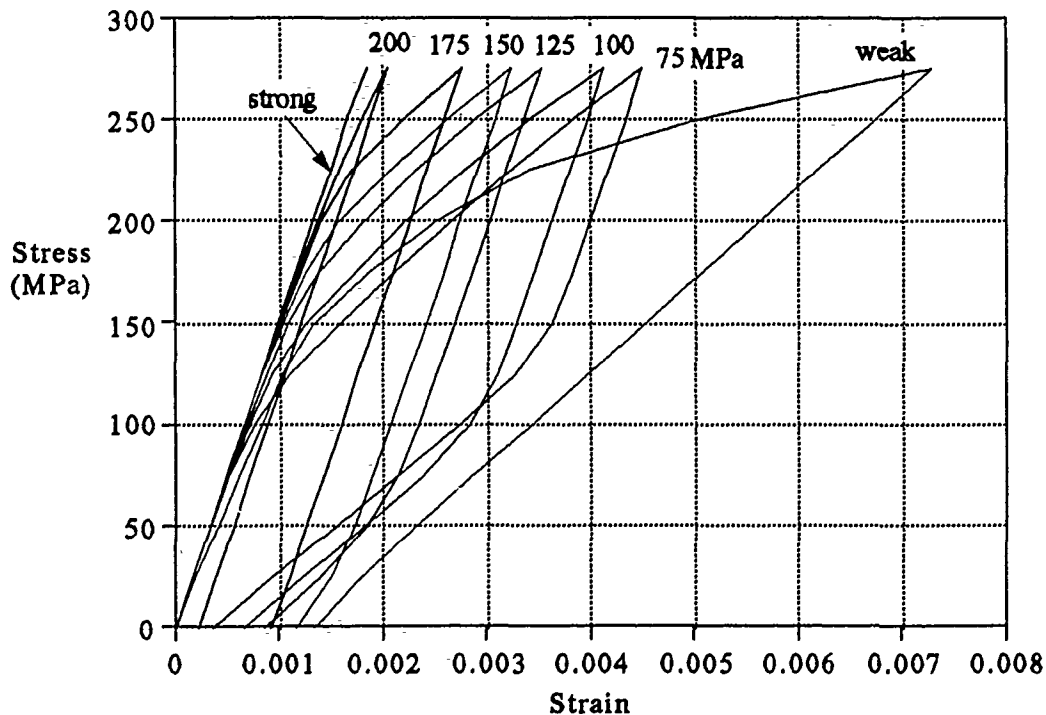
Figure 31. Finite Element Plane Stress Solutions of Interphase Zone
Yield Stress Variation as Compared to Perfectly Strong and
Perfectly Weak Bonds

76

130 MPa. A more thorough examination into this problem by using the stress fields from the finite element solutions may provide greater insight. The Von Mises stress contours after cooldown for a strong bond and an interphase yield stress of 175 MPa are given in Figure 32. The stress contours for interphase yield stresses of 125 MPa and 75 MPa are given in Figure 33. One can see that a relaxation of the stresses from a perfectly strong bond stress field occurs to a certain extent in all three solutions shown containing an interphase zone. Of course, the most dramatic effect occurs with the 75 MPa interphase yield stress solution. The maximum Von Mises stress after cooldown for the strong interface is 545 MPa. If an interphase zone with a yield stress of 75 MPa is used, this maximum stress is reduced to 345 MPa. Therefore, just as in the one-dimensional solutions a relaxation of the thermal stresses also occurs in the finite element solutions, but in a more gradual fashion. Portions of the interphase zone in the finite element solutions are at a relatively high state of stress after cooldown. All yield stresses examined were below this maximum stress, and therefore yielding would occur in these regions. On the other hand, the one-dimensional solutions required the stress throughout the interphase to be constant, and hence the entire interphase zone was either above or below the yield stress.

A major difference between the one-dimensional and finite element solutions was that for all interphase zone yield stresses using the finite element analysis the composite experienced permanent strain after unloading. However, the one-dimensional solutions returned to their approximate original strain state after unloading for interphase yield stresses below 130 MPa. This is most likely attributed to the added matrix plastic-

77
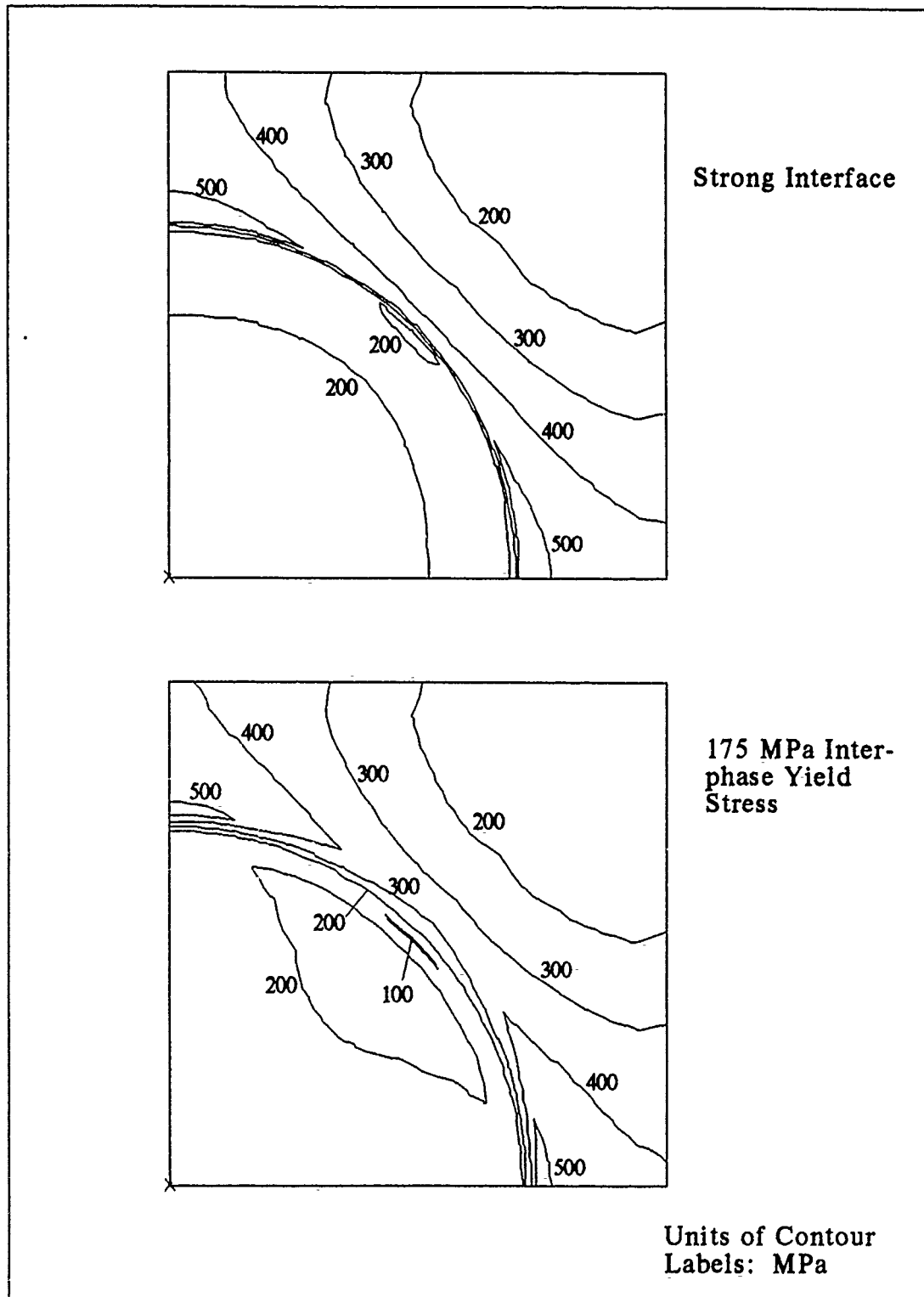
Figure 32. Von Mises Stress Contours After Cooldown Using Plane Stress Solution for Strong Interface and for an Interphase Zone Yield Stress of 175 MPa
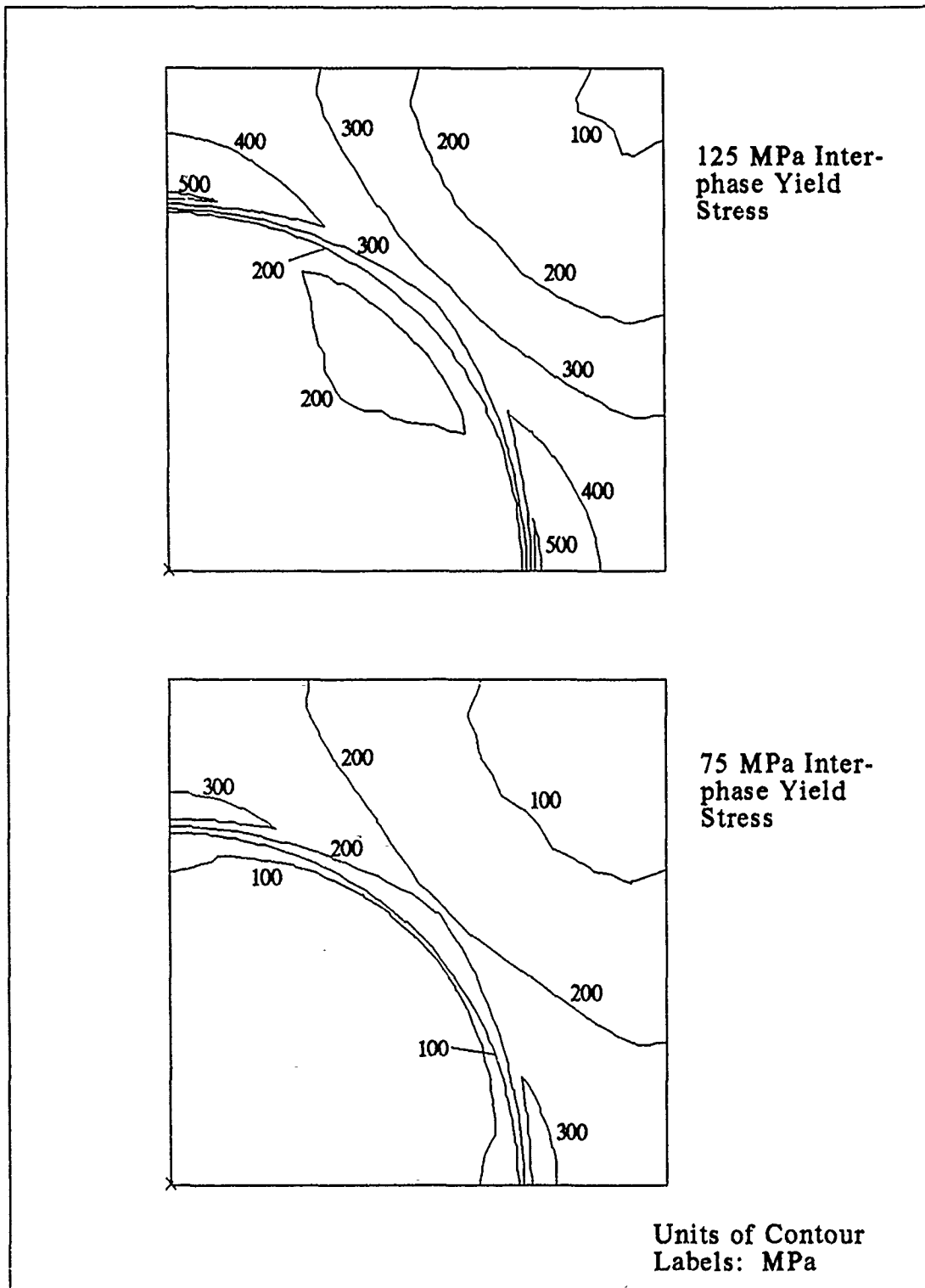
Figure 33. Von Mises Stress Contours After Cooldown Using Plane Stress Solution for Interphase Yield Stresses of 125 MPa and 75 MPa

79

ity.

The effect of varying the interphase zone strain hardening parameter on the transverse response is depicted in Figure 34. The one-dimensional solutions again provided a good introduction into the behavior found using the finite element analysis. Varying the interphase zone strain hardening parameter changes the secondary slope of the stress-strain curve and this effect can be easily seen in the figure.

Unloading is characterized by elastic followed by plastic deformation, and varying the strain hardening parameter was found to change the slope of the stress-strain curve during the plastic part of unloading. This effect was earlier observed in the one-dimensional solutions, but the change in slope was of opposite sign(see Figure 27, page 71). This difference be-
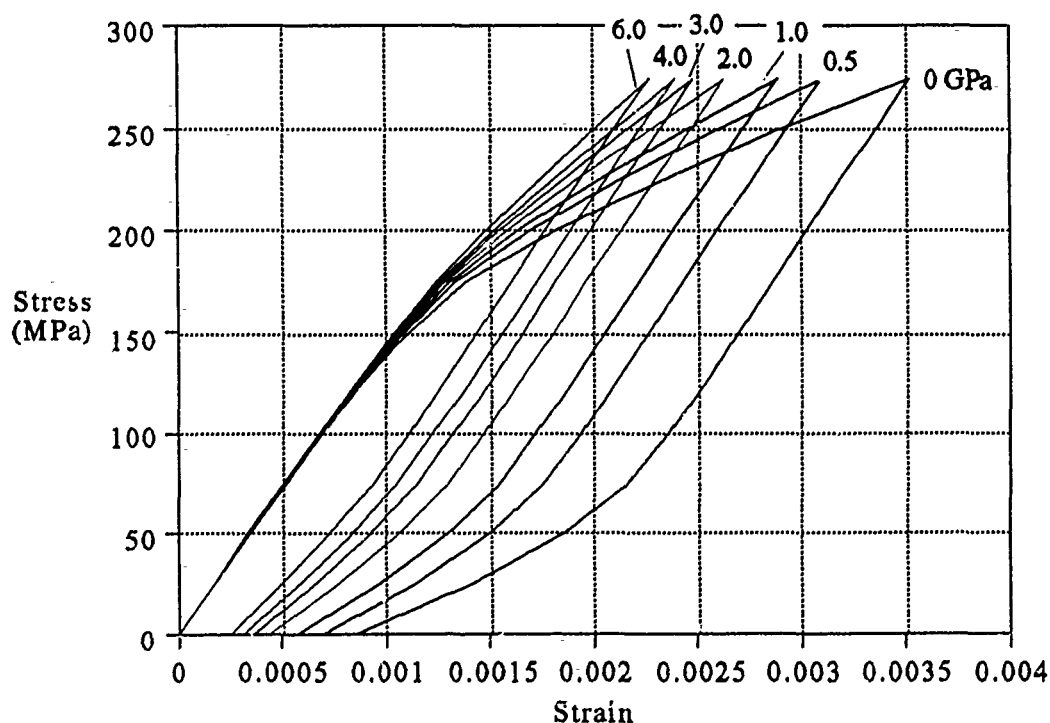
Figure 34. Finite Element Plane Stress Solutions of Interphase Zone Strain Hardening Parameter Variation

tween the one-dimensional solutions and the finite element results from the fact that the one-dimensional models used isotropic hardening while the finite element models used kinematic hardening. Therefore, plastic deformation during loading would increase the compressive yield stress in the one-dimensional models but decrease it in the finite element models.

Plane stress solutions were also performed on various interphase zone sizes. These results are presented in Figure 35. The same general trends observed in the one-dimensional results were also observed here, but the effect was more pronounced. Enlarging the interphase zone lowers the point at which nonlinearity first occurs, and therefore increases the energy dissipated during a loading and unloading cycle.
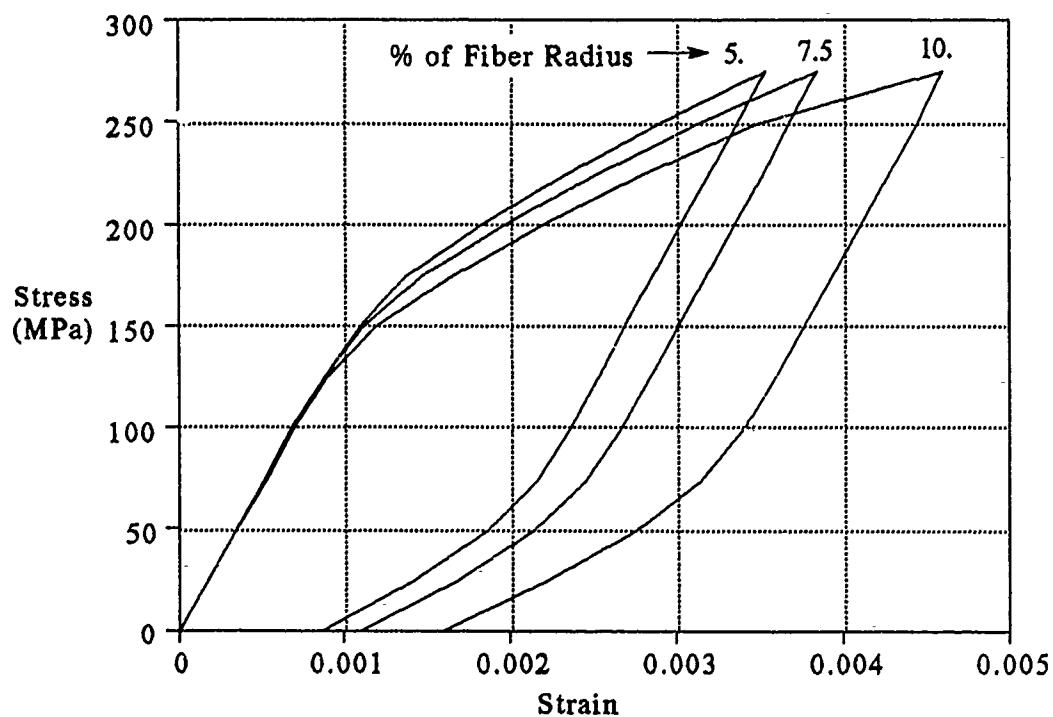
Figure 35. Finite Element Plane Stress Solutions of Interphase Zone Size Variation

Calculations involving the three-dimensional generalized plane strain model were costly from the computer resources standpoint. A complete solution would usually take over 24 hours of processing time, and many trial runs were required before the necessary choice of convergence parameters to complete a solution were achieved. Therefore, only one set of solutions were obtained. This set consisted of various interphase zone yield stresses. These results are given in Figure 36. As previously, perfectly strong and perfectly weak bonded interface solutions are plotted alongside for comparison.

The generalized plane strain solutions demonstrated the same trend as the plane stress, but were considerably stiffer. For instance, with an interphase yield stress of 100 MPa the overall transverse strain at maximum
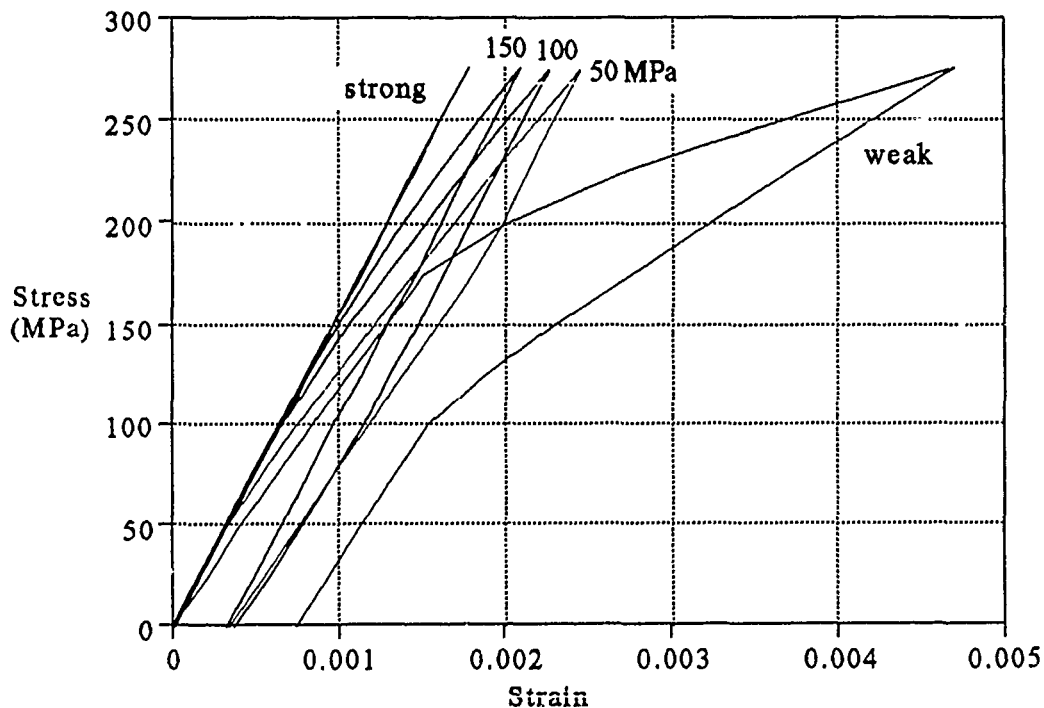
Figure 36. Finite Element Generalized Plane Strain Solutions of Interphase Zone Yield Stress Variation as Compared to Perfectly Strong and Perfectly Weak Bonds

load for the plane stress calculation was almost double that found using the generalized plane strain solution.

The additional constraint in the out-of plane direction will result in a triaxial stress state throughout the structure. Even though the yield stress of the interphase zone may be relatively low, the triaxial stress state will result in low Von Mises stresses, and therefore the extent of yielding will be greatly reduced.

In order to determine the approximate discretization error associated with the finite element grid chosen for this study, an additional grid containing approximately four times the number of nodes was developed (see Figure 7, page 37). A calculation using the baseline parameters of Table 5 was performed and a comparison made with the conventional grid. The transverse response, shown in Figure 37, demonstrates excellent agreement in the elastic realm, but when nonlinearity begins, the solutions drift apart. The greatest discrepancy occurs at maximum load where the difference in overall transverse strain is 0.00031, and remains at that level during the elastic portion of unloading. The maximum percent error occurs at the end of the elastic portion of unloading and is 12.5%. An error of this magnitude may seem excessive, but it is important to remember that the solutions represent the behavior after cooldown. Therefore, the error is an accumulation over an entire thermomechanical cycle consisting of cooldown, transverse loading, and then unloading. Also, it is encouraging that the basic characteristics of the transverse response are the same. Only a shift in the data has occurred.

In summary, the finite element solutions that incorporated an interphase zone between fiber and matrix in general demonstrated the same
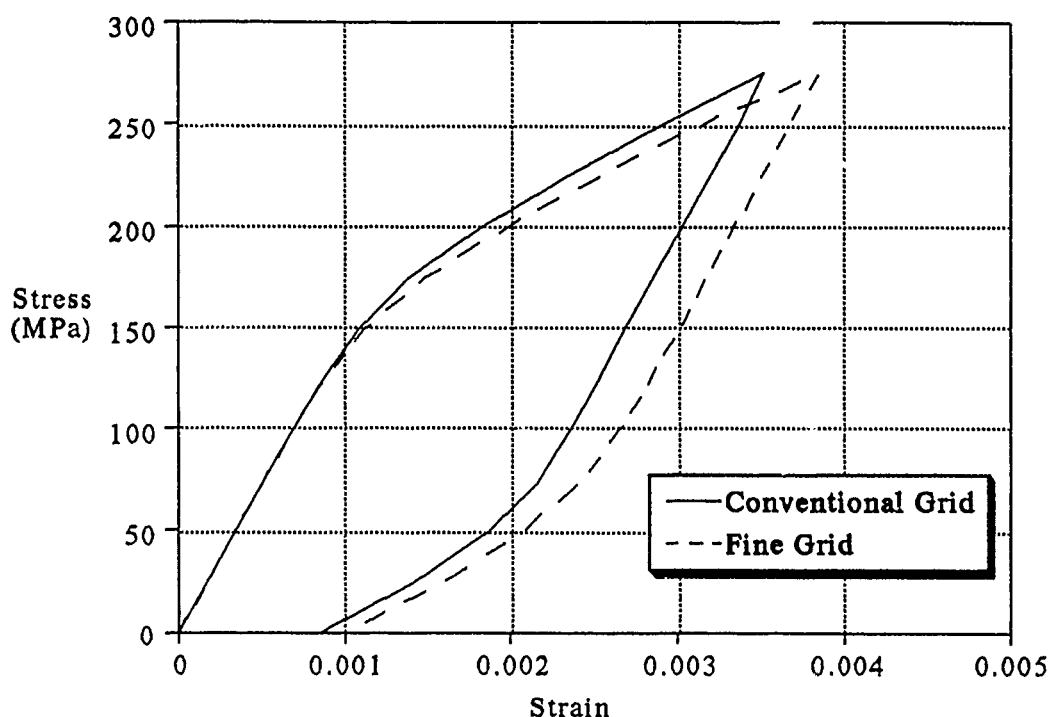
Figure 37. Finite Element Plane Stress Solutions of Conventional and Fine Grids Using Baseline Parameter Set of Table 5

trends as were observed with the one-dimensional solutions. The interphase plastic parameters(i.e. yield stress and strain hardening) were found to have the greatest effect on the overall behavior. Increasing the yield stress resulted in increasing the point of nonlinearity, and increasing the strain hardening resulted in increasing the secondary slope. Most importantly, modeling the interface as a third phase(interphase) elastic-plastic zone allowed for continuous variation in transverse behavior from strong to weak bonding(see Figure 31 on page 76). Thus, such a model allows for additional constraints at the interface region that may be tailored to match a particular composite's characteristics. Other attributes of the interphase zone model included significant energy dissi-

84

pation during a loading and unloading sequence, and a relaxation of the thermal residual stresses due to the interphase zone yielding during cooldown.

The main difference between the finite element and one-dimensional solutions was that the finite element solutions always experienced permanent strain after a loading and unloading cycle. This was most likely due to the added plasticity of the matrix in the finite element analysis.

Figure 38 gives a transverse response comparison between the one-dimensional and plane stress finite element analysis solutions of the baseline parameter set. The one-dimensional solution does an excellent job of predicting the general characteristics, producing only a 12% error in total strain at maximum load.
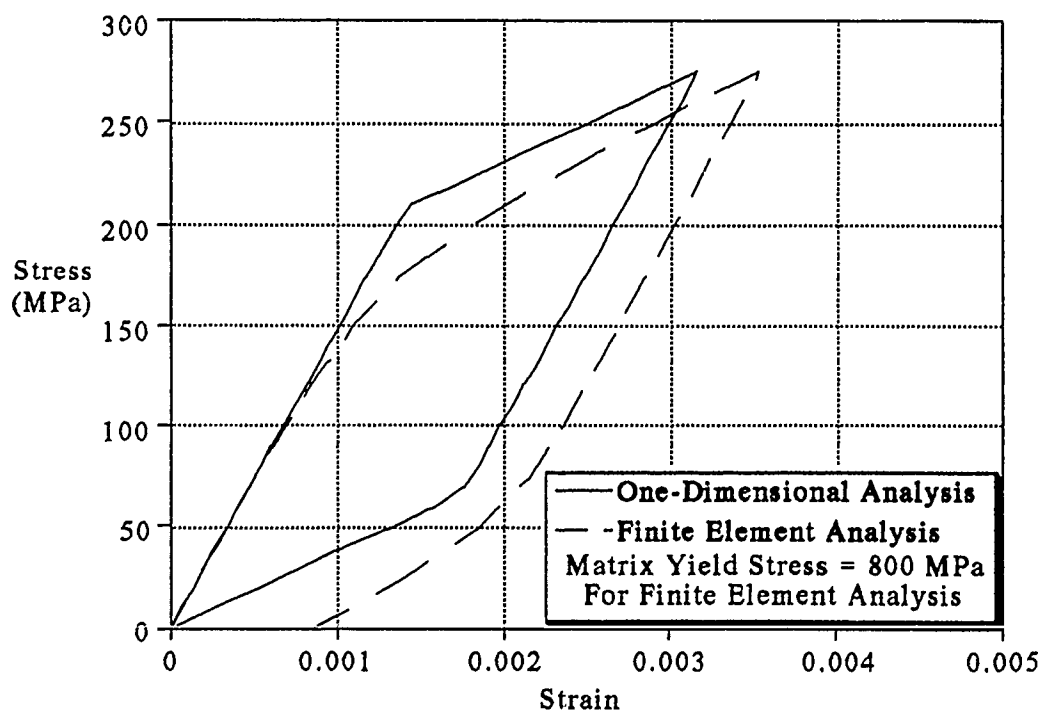
Figure 38. Comparison of One-Dimensional and Finite Element Transverse Response for Baseline Parameter Set of Table 4

A comparison of the nonlinear characteristics as calculated by the one-dimensional and finite element analyses is depicted in Figure 39. The one-dimensional analysis tended to overpredict the point of nonlinearity and underpredict the secondary slope. The point of nonlinearity varied with interphase yield stress in a bilinear nature. This behavior was more pronounced in the one-dimensional solutions, and it is interesting to note that the bilinearity begins at an interphase yield stress of approximately 125 MPa. This is the same yield stress at which a relaxation in the thermal residual stresses during cooldown began to occur in the one-dimensional solutions. However, as a final note, considering the simplifying assumptions made in the one-dimensional analysis, the overall agreement between it and the finite element calculations is excellent.

4.3   Results of Combined Interphase Zone / Weak Bond Models

The previous section points out that a major difficulty in modeling the fiber/matrix interface as a third zone possessing independent properties is the relaxation of the thermal residual stresses during cooldown as the interphase zone yields. Another drawback is that all models considered so far have assumed that the conditions are identical at all points along the interface (i.e. the interface behaves the same everywhere). Therefore, this section will examine models possessing an interface with combined effects. Part of the interface will be modeled as perfectly weak and part as possessing an interphase zone. The development of these models is discussed in section 3.5. The energy dissipation capability of an interphase zone coupled with a perfectly weak bond constraint to prevent the relaxation of thermal stresses could provide a superior micromechanics model.

86
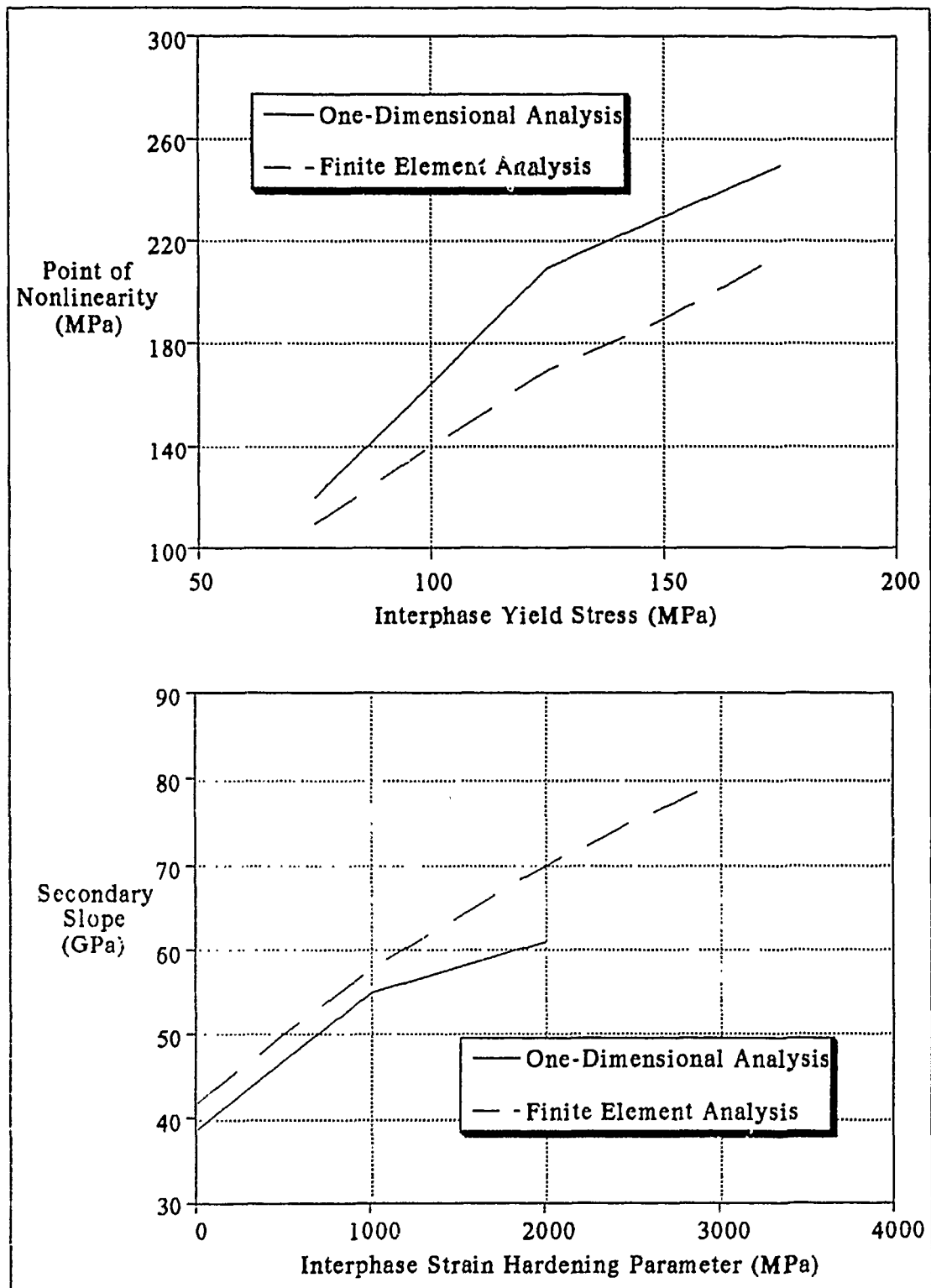
Figure 39. Comparison of Nonlinear Characteristics Between the One-Dimensional and Finite Element Solutions

4.3.1 One-Dimensional Results of a Combined Interphase Zone / Weak Bond Model

The loading sequence will be the same as in section 4.2, cooldown to room temperature followed by transverse normal loading and unloading. The baseline material properties and model dimensions will be the same as listed in Table 4. An additional dimension not listed in Table 4 is required. This dimension, d, shown in Figure 9 is a representation of the portion of the interface modeled as perfectly weak and will be given referenced to the fiber size, a. Therefore, since shear effects are neglected, the ratio d/a provides an approximate representation of the percentage of the interface modeled as perfectly weak and will be referred to as the weak bond ratio. Since it was found in section 4.2 that the plastic characteristics of the interphase zone effected composite behavior much more than the other interphase zone parameters, the parameters varied in this portion of the study were only interphase zone yield stress, strain hardening, and the weak bond ratio. For validation of the combined interphase zone / weak bond one-dimensional solutions the weak bond ratio was set to both 0% and 100% to see if the behavior would approach that of an all interphase zone model and a perfectly weak bond interface model.

Figure 40 depicts the transverse loading and unloading behavior for these two cases as well as a weak bond ratio of 50%. A weak bond ratio of zero matches exactly the results for the one-dimensional model possessing only an interphase zone. However, there is some energy dissipation that occurs for a weak bond ratio of 100% that is not seen in a perfectly weak bond model. This discrepancy results from the fact that in the one-dimensional solutions a portion of the interphase zone above the fiber remains intact in
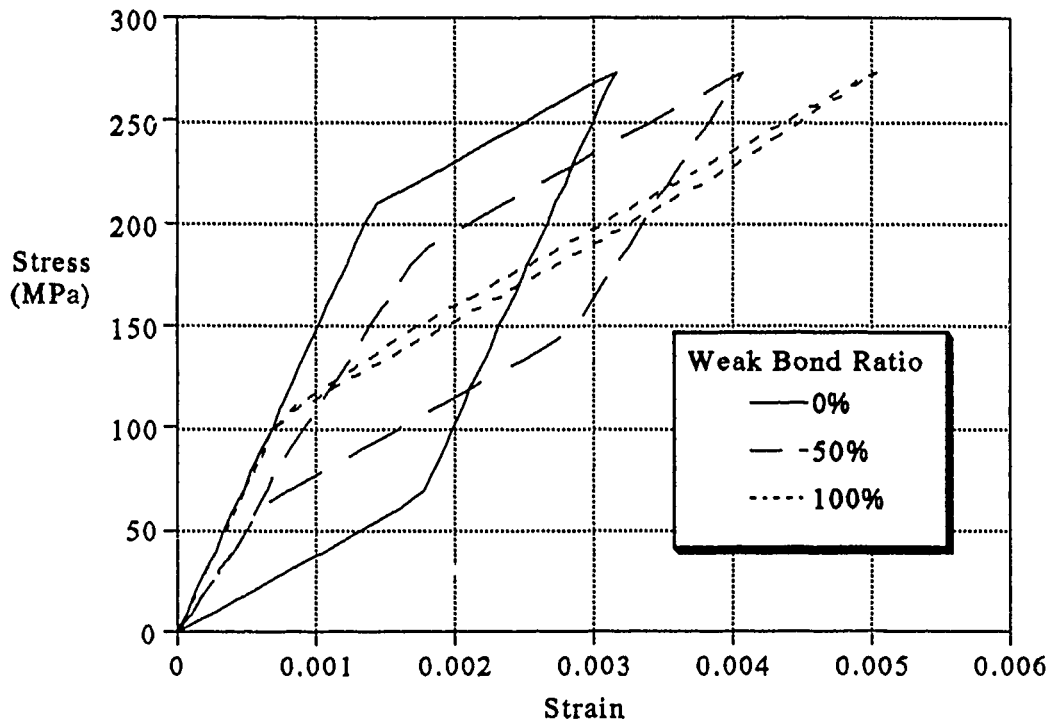
Figure 40. One-Dimensional Solutions of Combined Interphase Zone / Weak Bond for Weak Bond Ratios from 0.0 to 1.0

spite of a 100% weak bond ratio. The plastic deformation of this remaining third phase material causes the energy dissipation.

A rather surprising result from Figure 40 is the behavior of the 50% weak bond ratio. The behavior of this curve is difficult to interpret without examining the stresses and displacements in each region. A summary of what occurs during loading and unloading is given in Figure 41. The curve may be divided into several distinct linear fields. These characteristic linear fields existed for all the one-dimensional combined interphase zone / weak bond solutions. Only the slope and size of the fields changed.

89
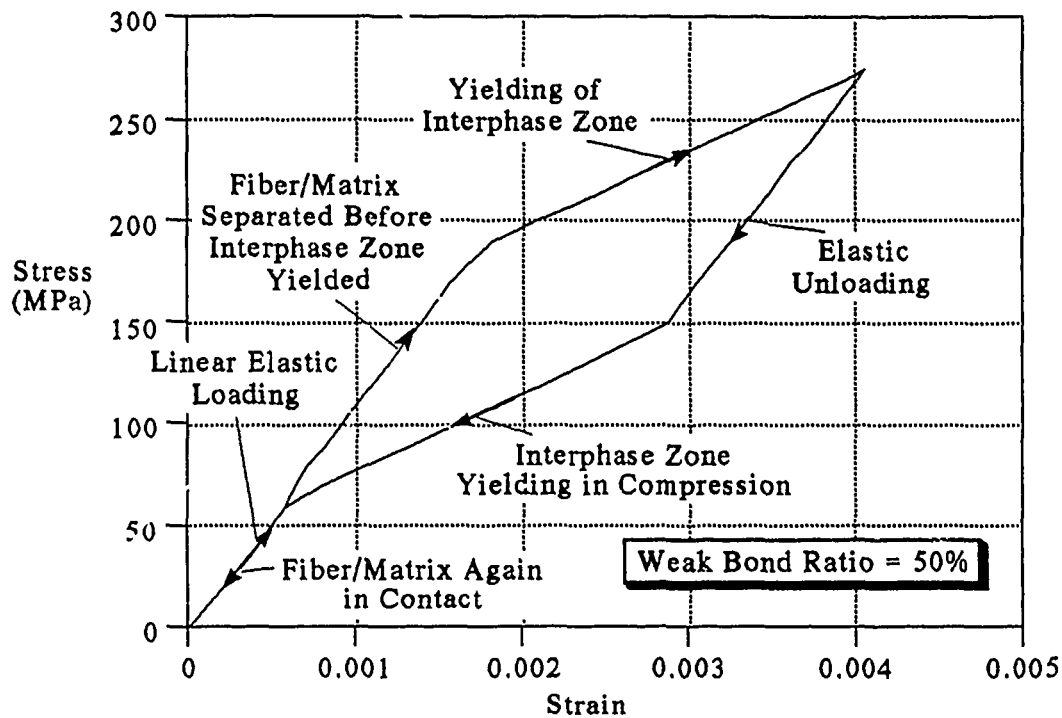
Figure 41. One-Dimensional Solution of Combined Interphase Zone / Weak Bond With Loading Sequence Explanations

An investigation into the effect of the weak bond ratio on the transverse behavior is depicted in Figure 42. A few characteristics of the one-dimensional model when increasing the weak bond ratio are worth mentioning. First, the stress at which fiber/matrix separation occurs increases. Also, the slope in the second linear field(after separation but before interphase zone yielding) decreases and approaches the slope that exists after interphase zone yield. The combined model was found to prevent relaxation of the thermal residual stresses by keeping the interphase zone from yielding during cooldown. Therefore, as the weak bond ratio was increased the solutions approached that of a completely weak bonded interface but still retained an energy dissipation mechanism in the form of a
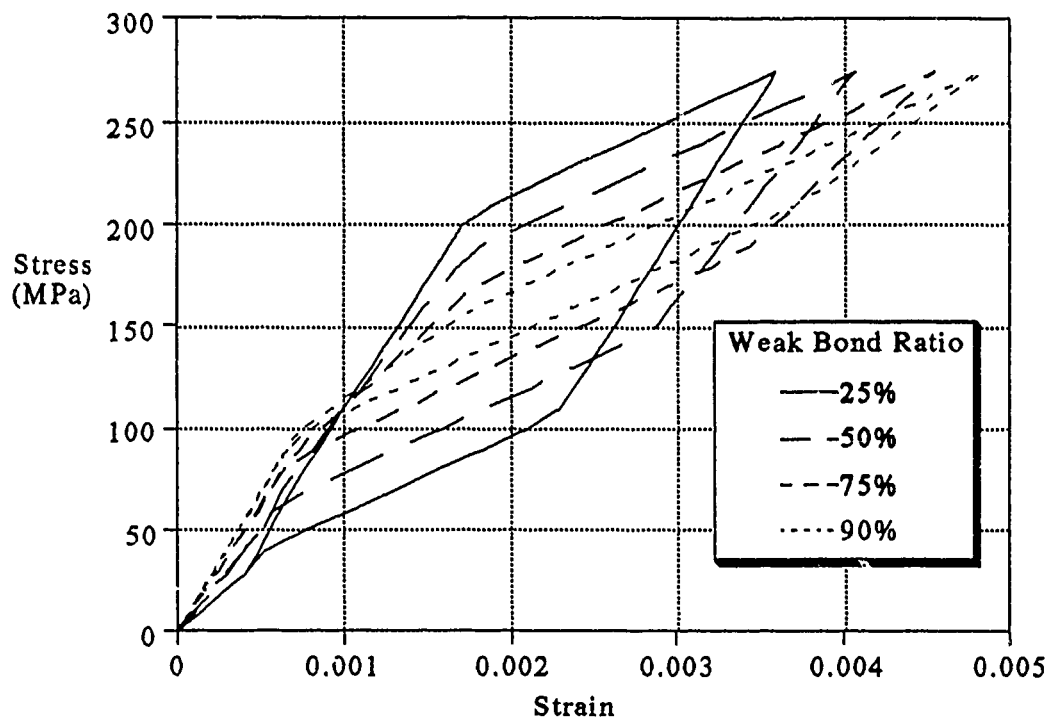
Figure 42. One-Dimensional Solutions of Combined Interphase Zone / Weak Bond for Various Weak Bond Ratios

small portion of the interface modeled as a third phase material.

Since the interphase zone yield stress had a pronounced effect on the one-dimensional model of section 4.2.1, its effect on the combined model was also examined. Figure 43 presents an interphase yield stress variation for a weak bond ratio of 50%. As expected, an increase in yield stress lengthens the portion of the curve between fiber/matrix separation and interphase yielding but shortens the one between interphase yield and maximum load. This observation is more difficult to make for a yield stress variation at a higher weak bond ratio as depicted in Figure 44. The same effect is occurring but it is manifesting itself in what seems to be a

91
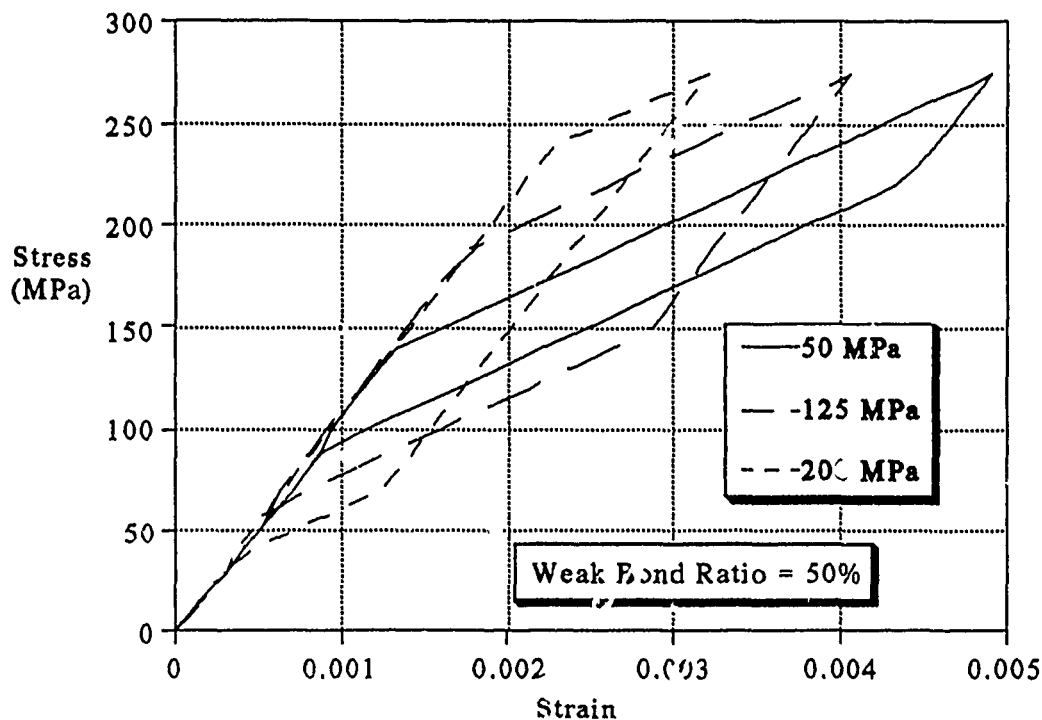
Figure 43. One-Dimensional Solutions of Combined Interphase Zone / Weak Bond With a Weak Bond Ratio of 0.50 for Various Interphase Zone Yield Stresses

change in slope of the upper portion of the curve.

The final investigation where a one-dimensional solution was employed involved the effect of interphase zone strain hardening for the combined model. This is shown in Figure 45, and as expected an increase in strain hardening results in increasing slope during the portion of loading where the interphase zone yields.

For a one-dimensional model the portions of the loading curve that are controlled by the various mechanisms described in Figure 41 are well defined, but for a two or three dimensional analysis where the fiber is circular rather than square this is not the case. Not all of the interphase zone
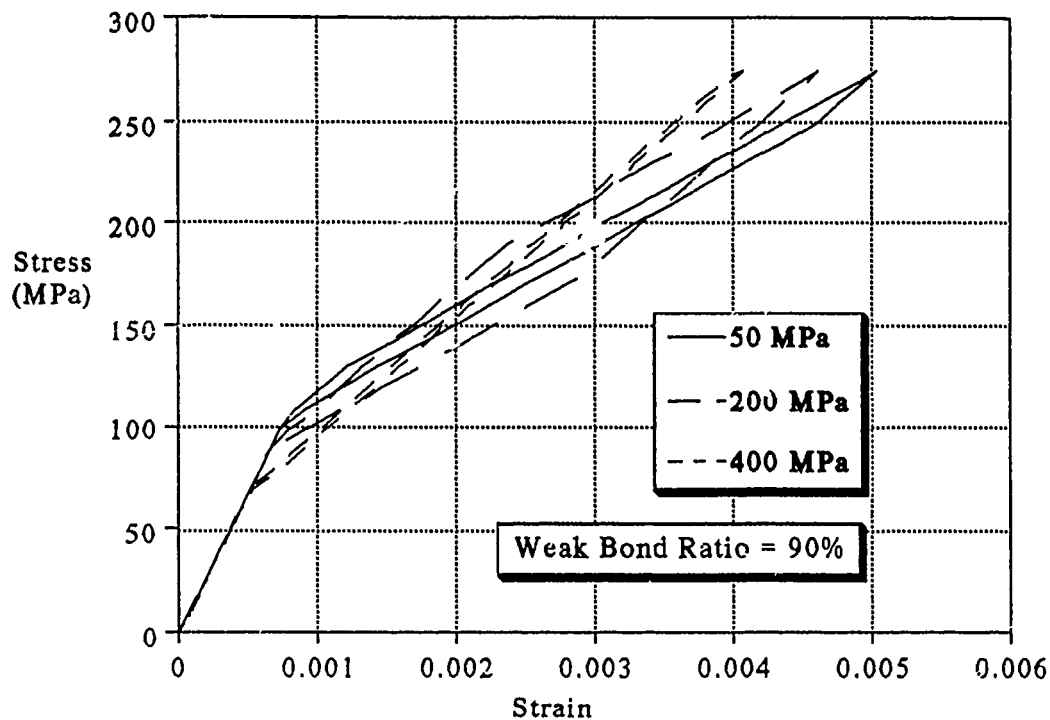
Figure 44. One-Dimensional Solutions of Combined Interphase Zone / Weak Bond With a Weak Bond Ratio of 0.90 for Various Interphase Zone Yield Stresses

yields at the same transverse load. After initial yield of a small area of the interphase any further load will cause a larger area to yield and so on until the entire region is plastic. In addition, a simplified one-dimensional model may provide a general understanding of how varying a specific parameter will induce trends in the data, but the calculations are far from an exact solution. Therefore, an investigation into a combined interphase zone / weak bond micromechanics model using more exact methods must be sought.

93
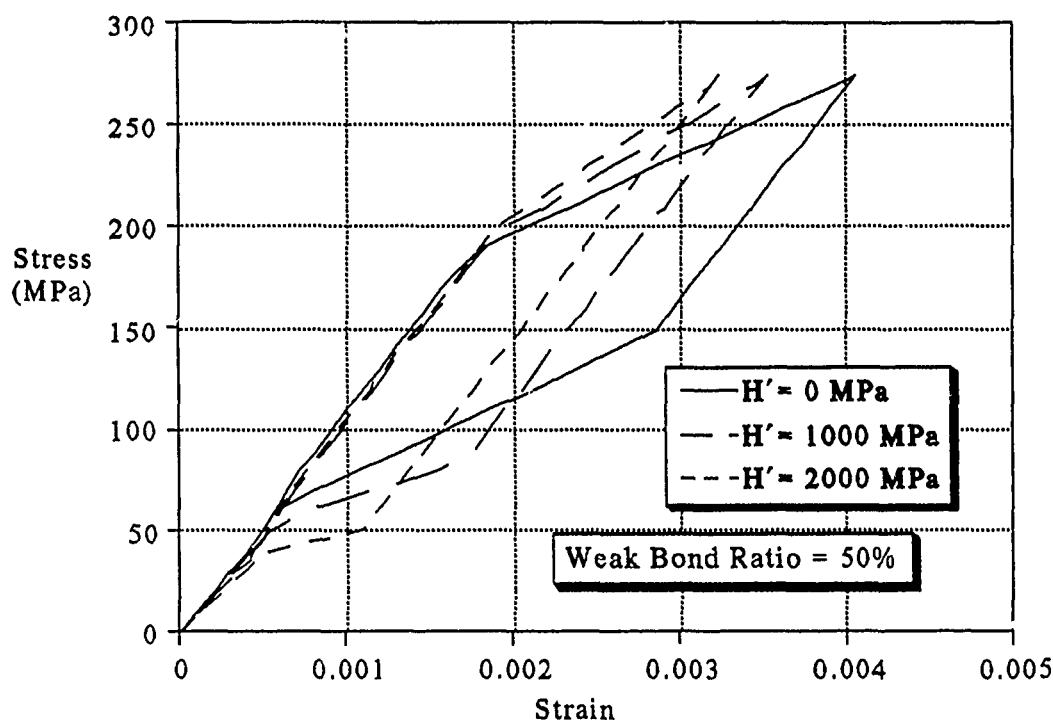
Figure 45. One-Dimensional Solutions of Combined Interphase Zone / Weak Bond for Various Strain Hardening Parameters

4.3.2 Finite Element Results of a Combined Interphase Zone / Weak Bond Model

A description of the finite element models used to analyze a combined interphase zone / weak bond interface between fiber and matrix is given in section 3.5. As mentioned in the development of the finite element models, a choice as to the positioning of the interphase zone along the fiber/matrix interface was necessary. A position was chosen such that the interphase zone was centered symmetrically about a 45°diagonal of the representative volume element(see Figure 10, page 43).

Furthermore, the weak bond ratio for the finite element calculations was defined to be the length along the interface modeled as perfectly

94

weak divided by the total interface length. The properties used were those listed in Table 5 on page 75, and both the weak bond ratio and interphase zone yield stress were varied to determine their effect on the overall composite characteristics. Also, the cooldown and loading sequence was identical to that used for the one-dimensional solutions.

Since several weak bond ratios were analyzed, the solutions are presented in separate figures to avoid excessive clutter. The results for weak bond ratios of 50% and higher are presented in Figure 46, and the results for weak bond ratios lower than 50% are given in Figure 47. One of the most noticeable characteristics is the tremendous difference in transverse response between the perfectly weak (100% weak bond ratio) and the 87% weak bond ratio. Even when a relatively small section between the fiber
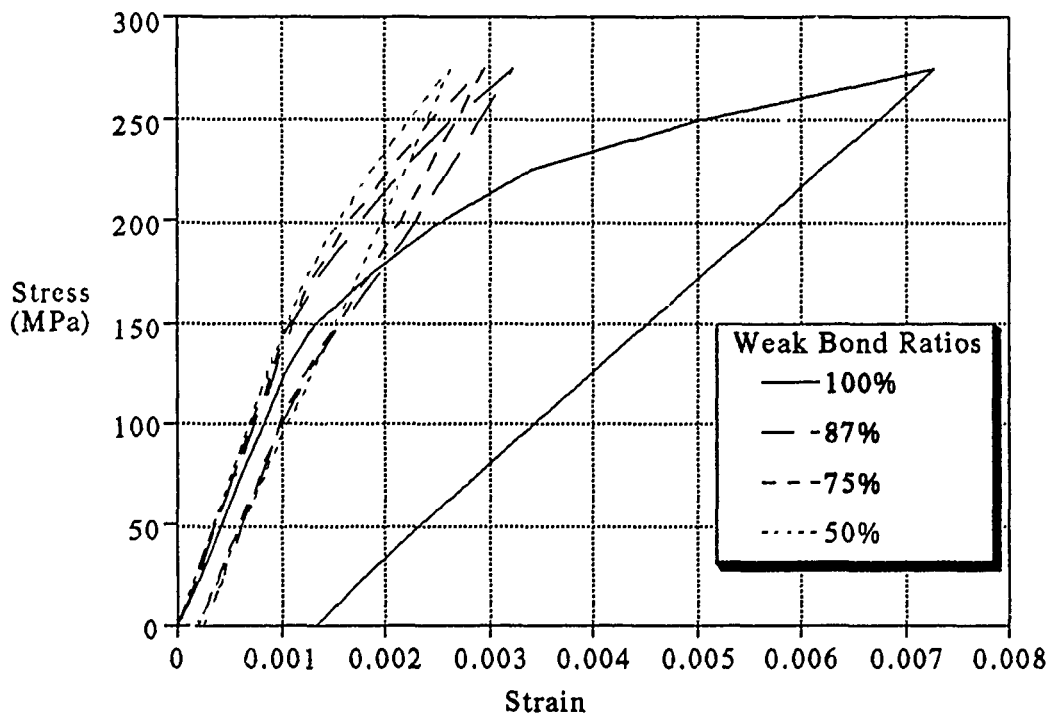
Figure 46. Finite Element Plane Stress Solutions of Combined Interphase Zone / Weak Bond Models for Various Weak Bond Ratios - High Range

95
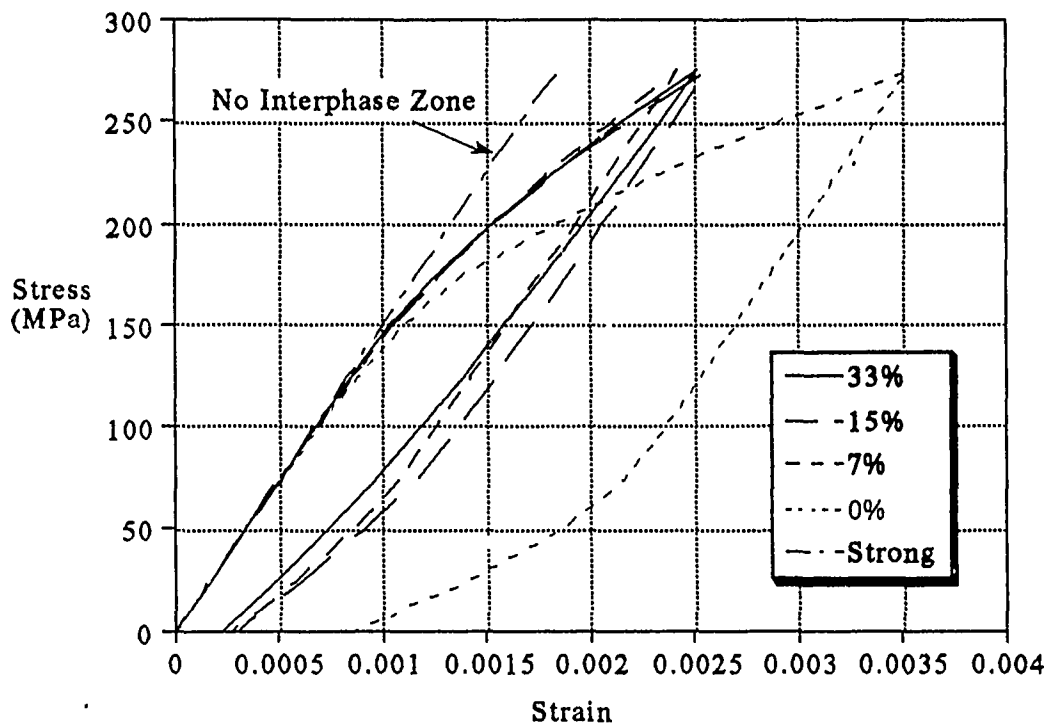
Figure 47. Finite Element Plane Stress Solutions of Combined Interphase Zone / Weak Bond Models for Various Weak Bond Ratios - Low Range

and matrix is modeled as an interphase zone, the structure becomes much

stiffer. The one-dimensional solutions presented a gradual change to a

perfectly weak bond as the weak bond ratio was varied. This discrepancy

in the one-dimensional solutions is possibly due to neglecting constraints

on the interphase zone from the surrounding material. In the finite ele

ment model the interphase zone is entirely encased in either matrix or

fiber mateiial. Therefore, any deformation of this zone will necessarily

deform the surrounding material, but the fiber and matrix are considerably

stronger and will resist it. Also, in the finite element solutions varying

the weak bond ratio does not effect the point of fiber/matrix separation or

96

the permanent strain existent after unloading. However, the general trend seen in the upper portion of the transverse response curve is very similar to the one-dimensional solutions since at the higher load levels a weakening of the structure occurs as the weak bond ratio is increased.

The low range of weak bond ratios (below 50%) also demonstrated surprising behavior when the weak bond ratio was changed from 0% to 7%. Again a jump in the results occurred as the model was changed from taking the entire interface as an interphase zone to a combined interphase zone / weak bond model. The same possible explanation applies here as was given for the 87% to 100% weak bond ratio jump. The combined interphase zone / weak bond models require the interphase to be completely surrounded by fiber and matrix material, creating a constraint on the interphase boundary. Hence, an interesting development has occurred. The combined model is stiffer than either of the two by themselves. Also, for all weak bond ratios greater than 0% relaxation of the thermal residual stresses during cooldown did not occur. As a final note on varying the weak bond ratio, very little effect is seen on the transverse response for weak bond ratios below 50%.

An examination into how varying the interphase zone yield stress effects the combined model is given in Figure 48 for a weak bond ratio of 87%. The results demonstrate how increasing the interphase yield stress stiffens the structure and decreases the energy dissipated per cycle. This same effect was observed in the one-dimensional solutions. As the yield stress was increased in the finite element solutions the curve approached nonlinear elastic behavior where the nonlinearity results from separation of the portion of the interface modeled as a weak bond.

97
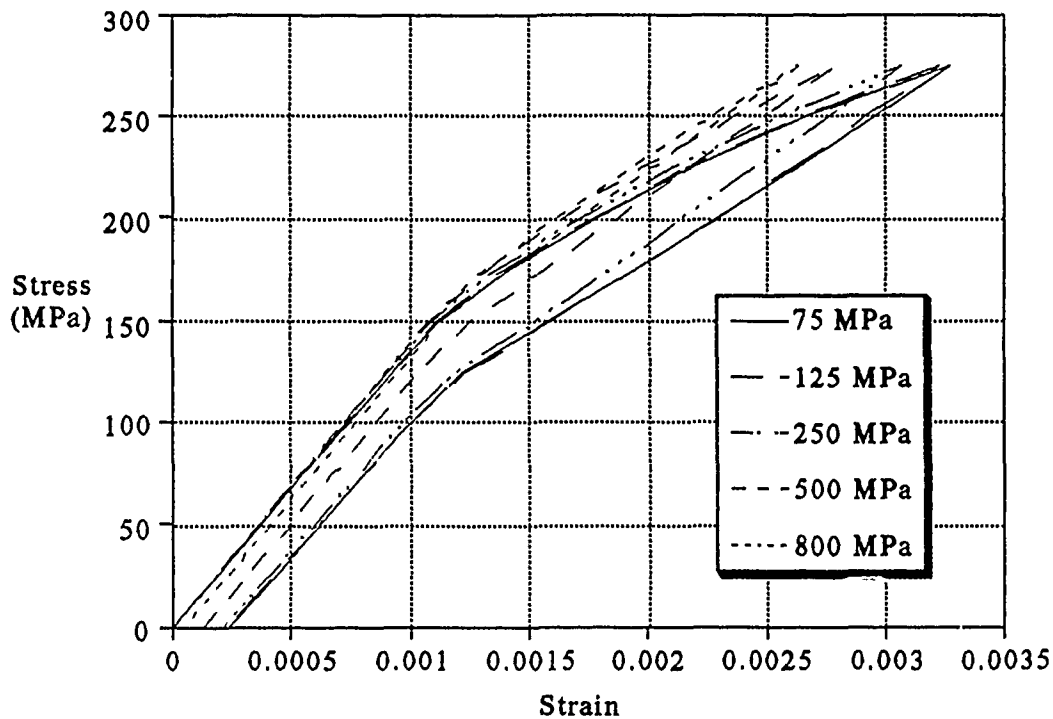
Figure 48. Finite Element Plane Stress Solutions of Combined Interphase Zone / Weak Bond With a Weak Bond Ratio of 87% for Various Interphase Zone Yield Stresses

Two solutions using the three-dimensional generalized plane strain model with a combined interphase zone / weak bond were obtained. They were at weak bond ratios of 7% and 87%. Figure 49 presents the 7% results as compared to the plane stress solution. Figure 50 presents the 87% results in the same manner. As in previous generalized plane strain solutions from earlier sections, the calculations result in a stiffer overall structure and decreased energy dissipation per cycle. However, in the linear elastic region before fiber/matrix separation the two types of analysis agree very well. Also, in the 87% weak bond ratio solution an increase in the point of fiber/matrix separation of approximately 50 MPa occurs for

98
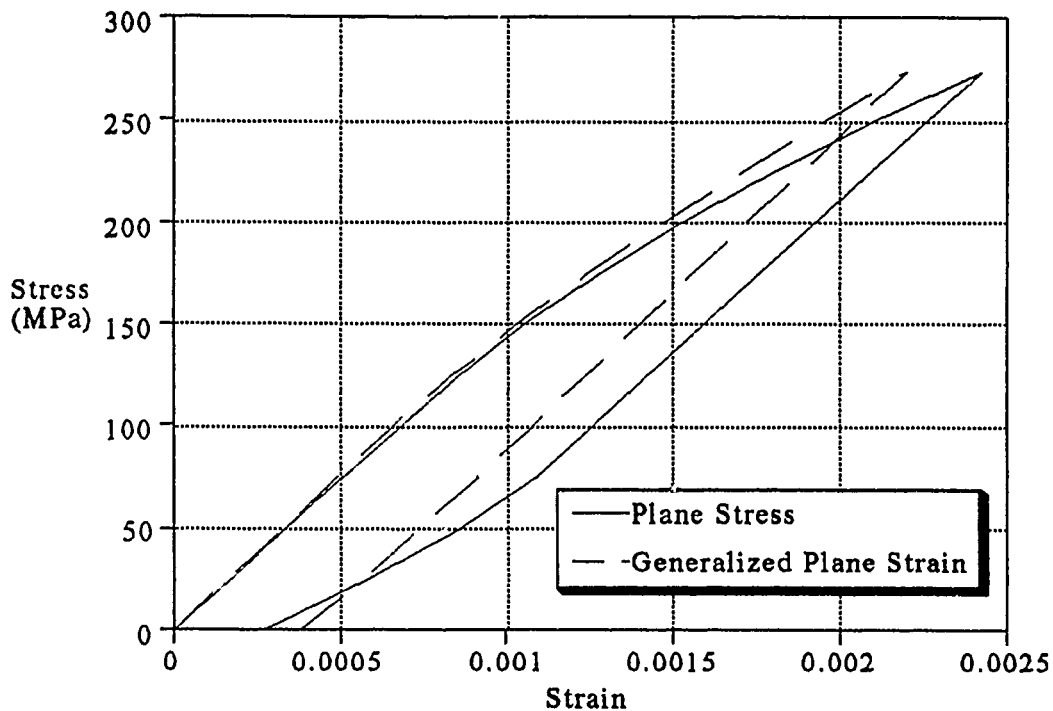
Figure 49. Finite Element Generalized Plane Strain Solution of Combined Interphase Zone / Weak Bond at 7% Weak Bond Ratio as Compared to Plane Stress Solution

the generalized plane strain analysis over the plane stress.

In summary, the combined interphase zone / weak bond models have demonstrated the ability to model energy dissipation at the interface, and at the same time prevent the relaxation of thermal residual stresses which was a drawback with the models that used only an interphase zone. However, the combined model offers little flexibility in the transverse behavior because it greatly stiffens the solutions over both the perfectly weak interface and all interphase zone models. Also, for all finite the element solutions, permanent strain still exists after unloading which has not been observed in experiment. Finally, the one-dimensional analysis deviated
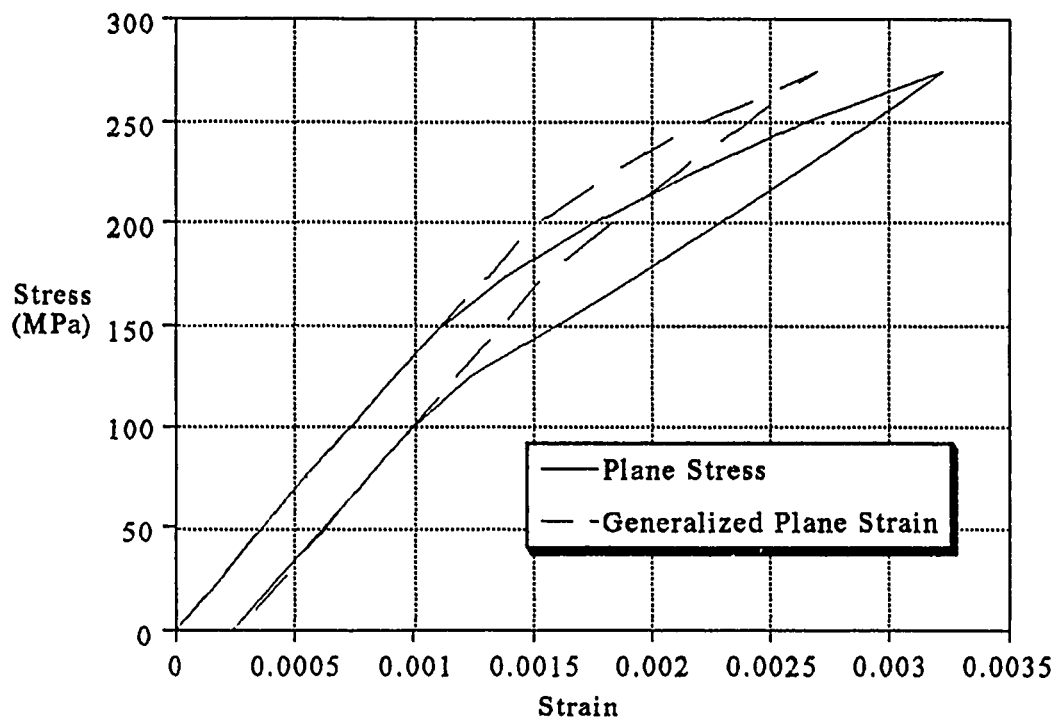
Figure 50. Finite Element Generalized Plane Strain Solution of Combined Interphase Zone / Weak Bond at 87% Weak Bond Ratio as Compared to Plane Stress Solution

more from the finite element solutions in this section than was observed in section 4.2. The simplifying assumptions of the one-dimensional analysis were not as capable of handling the more complex combined interphase zone / weak bond model of the interface.

V. Conclusions

The response of a micromechanical model is highly dependent on the fiber/matrix interface condition. An analyst must understand the proper interface conditions required for a particular composite before undertaking an investigation. This study has examined various interface conditions to determine their effect on the overall transverse normal characteristics using both a simplified one-dimensional analysis and the finite element method.

Traditionally, a perfectly strong interfacial bond is assumed for polymer or epoxy based composites. However, this assumption is erroneous for high temperature titanium based metal matrix composites. Experiments indicate that the interfacial bond for these composites fails early during initial transverse loading[33]. In addition, the metal matrix typically possesses a much higher thermal coefficient of expansion than the fiber. Therefore, relatively large thermal residual stresses are present in the composite after cooldown from the processing temperature, and finally, a reaction zone is present at the fiber/matrix interface where the fiber has penetrated into and reacted with the matrix forming a third phase material which is likely to possess its own unique properties.

Large thermal residual compressive stresses exist at the interface after cooldown in a high temperature metal matrix composite. These compressive stresses must be overcome before the matrix will separate from the fiber. Previous researchers have successfully modeled this phenomena by using a perfectly weak interface[2; 3]. However. difficulties arise from such models due to their lack of sufficient constraint at the interface.

101

Their overall transverse response cannot be modified to model a partial bonding at the interface. As a result, the weak bond solutions do not always agree with experiment(see Figure 2, page 16).

Hence, parametric studies into how various interface conditions effect the overall composite characteristics will provide insight into promising methods of modeling the complex fiber/matrix interface region. This study has examined both strong and weak bond models, investigating fiber/matrix separation and slip. In addition, an interphase zone between fiber and matrix has been added in an effort to model the energy dissipation mechanisms and additional constraints that cannot be modeled using a weak bond. Finally, a combined interphase zone / weak bond interface model was examined.

An important conclusion from the weak bond model is that not only fiber/matrix separation but also slip along the interface was found to have a pronounced effect on the overall characteristics. If friction is absent at the interface, then the initial modulus that occurs before fiber/matrix separation is considerably less than for a strong bond. This is due to interfacial slippage. When friction is added, slip is arrested and the initial modulus increases and approaches that of a strong bond. However, after fiber/matrix separation the added constraint from friction vanishes since the fiber and matrix are no longer in contact, and hence, the secondary slope after separation remains unchanged from an interface without friction(see Figure 17, page 54).

If the fracture surface between fiber and matrix is jagged in nature, then separation and slip will be independent. In other words, if the separation distance between fracture surfaces is small, slip will still not be al-

lowed. Adding such a constraint that prevents slip throughout the load range was found to greatly stiffen the structure. In fact, the added constraint stiffened the overall structure so much that the stresses in the matrix remained elastic, and therefore, a nonlinear elastic curve resulted. The transverse response with and without slip curves were shown to bound previously published experimental data(see Figure 24, page 64).

Modeling the nonlinearities at the interface by assuming an interphase zone possessing unique material properties allowed for excellent flexibility for including additional constraints not possible with the weak bond model. Also, the motivation for incorporating an interphase zone model is physically realistic in that it is based on experimental observations of a reaction zone between the fiber and matrix[39]. Cracks and other imperfections present in the reaction zone are modeled through the elastic-plastic properties of the interphase. The plastic properties (i.e. yield stress and strain hardening) of the interphase zone were found to have the greatest effect on the transverse characteristics of the composite. The zone size also had considerable impact on the results, but the elastic properties of the interphase such as Young's modulus and thermal coefficient of expansion exhibited only slight influence. In addition to possessing the capability for modeling a partially bonded interface, an advantage in using an interphase zone was that it allowed for significant energy dissipation during a loading and unloading sequence. Finally, the interphase zone models were found to produce a relaxation of the thermal residual stresses as the interphase exceeded its yield stress in compression during cooldown(see Figure 33 on page 79). However, for most materials the initial yield stress in compression is greater than in tension, but the

103

analysis methods used in this study did not have the capability to specify initial yield stresses that were different in compression and tension.

The combined interphase zone / weak bond interface was used for modeling a portion of the interface as if a perfectly weak bond existed and the remainder as if an interphase zone existed between fiber and matrix. It offered an advantage over the all interphase zone model in that it allowed for energy dissipation during a loading and unloading sequence while at the same time preventing a relaxation of the thermal residual stresses. A drawback of the combined interphase zone / weak bond interface was that for the finite element analysis it did not allow for flexibility in the transverse response characteristics. For instance, the combined model was in general substantially stiffer than either method used alone, and varying the parameters, such as the interphase material properties and the weak bond ratio, had little impact on the transverse response. This behavior is most likely due to the fact that the interphase is completely enclosed in either fiber or matrix, and hence, any deformation of its boundary will require equal deformation of the surrounding material which is considerably stronger. However, the one-dimensional solutions did not experience this difficulty since the simplifying assumptions removed all but a single displacement constraint. A summary of the various methods for modeling the interface and their characteristics are presented in Table 6.

In review of the analysis methods used in this study, both the finite element and simplified one-dimensional results are presented with a high degree of confidence. This confidence comes from agreement between the methods themselves and validation from a previous researcher's calcula-

Table 6. Summary of Interface Models and Their Characteristics

Interface Model	Characteristics
Strong	- Linear elastic to matrix yield - Sufficient for determining composite behavior before fiber/matrix separation
Weak	- Captures fiber/matrix separation. - Energy dissipation in the form of matrix plastic flow. Results in permanent strain after unloading. - Change in interfacial friction has little effect on secondary slope of transverse response curve
Weak with fiber/matrix slip constrained	- Captures fiber/matrix separation. - Greatly stiffens transverse response so that no matrix plastic flow occurs even under substantial loading. - Results in nonlinear elastic response.
Interphase Zone	- Simulates fiber/matrix separation in the form of interphase yielding. - Capable of modeling partial bonding by varying the interphase zone plastic properties. - Allows for energy dissipation in the form of both interphase and matix plastic flow. - Relaxation of thermal residual stresses occurs during cooldown. - Permanent strain exists after unloading, but not as significant as with the perfectly weak bond model.
Combined Interphase Zone / Weak Bond	- Finite element solutions produce stiffer transverse response than observed using either interphase zone or weak bond models alone, and parameter variations have little effect on it. - Energy dissipation in the form of both interphase and matrix plastic flow. - Prevents relaxation of thermal stresses that was experienced in the interphase zone model. - Permanent strain after unloading similar to interphase zone model.

tions(see Figure 18, page 55).

A surprising facet of the solution methods was that a plane stress rather than a plane strain analysis was found to more closely approximate a generalized plane strain analysis. This was concluded during the linear elastic portion of the study when using a strong interfacial bond. The explanation for this apparent anomaly is thought to be linked to the large thermal strains which are an order of magnitude greater than the mechanical strains. The plane strain analysis prevents any thermal contraction in the out-of-plane direction. On the other hand, both the plane stress and generalized plane strain analyses will allow out-of-plane thermal contraction.

The one-dimensional solutions were in general very good considering the simplifying assumptions. The one-dimensional results from the interphase zone model demonstrated excellent agreement with the finite element solutions. All trends due to a particular parameter variation were in accord, and for the most part, even the numerical values were close to the same. In fact, the level of sophistication in the one-dimensional model was greater than required. The interphase region above the fiber was found to have only a slight effect on the solutions, and could have been removed without greatly effecting the results.

The finite element code MSC/NASTRAN was exceptional in solving the nonlinear material problem. As mentioned earlier, the solutions demonstrated excellent agreement with previous calculations presented in the literature[2; 3]. Also, a converged solution at all load points was generally achieved after no more than three NASTRAN job submittals. Hence, the analysis methods used in this study were found to provide excellent in-

sight into micromechanical analysis problems that possess nonlinear ter-face conditions. As demonstrated 'n this study, the solution of such problems are essential when dealing with imperfect interfacial bonds in the presence of thermal residual stresses.

VI.   Recommendations and Suggestions

An interphase zone between the fiber and matrix was incorprated in an attempt to model a fiber/matrix bond other than perfectly strong or weak, in effect, a partial bond. Rather than modeling a partial bond in such a fashion, one might consider developing a new type of element similar to the gap element. However, it would need to possess additional constraint capabilities, such as transverse and longitudinal stiffness existing both before and after separation and a friction capability in the longitudinal direction. Developing such an element might be a formidable task, and the additional capabilities would have limited use for other types of applications, but nevertheless, such an element could be tailored to model any level of interfacial bonding from perfectly strong to perfectly weak.

Also, since the types of composites considered in this analysis are envisioned for high temperature applications, studies of the interfacial effects during thermomechanical loading cycles where both the temperature and applied load are changing simultaneously would be highly beneficial. The results presented in this paper are from applied transverse loading at constant temperature. An aircraft engine component such as a turbine blade will undergo extensive load and temperature variations from engine start up to shut down. The composite stress-strain history during such a thermomechanical cycle is instrumental in determining the useful life of the component. Therefore, it is imperative to understand how the integrity of the fiber/matrix interface effects a composite during such severe thermomechanical loading cycles.

Finally, a few suggestions are in order concerning the use of MSC/NASTRAN for solving the nonlinear problems presented in this study. For solutions involving the use of gap elements it is recommended to update the stiffness matrices after each iteration. The author found that incorrect results would occur if this recommendation was not followed. Also, when using the elastic-plastic interphase zone micromechanics model, it is recommended to set the values of Young's modulus and thermal coefficient of expansion of the interphase zone as close to those of the matrix properties as is practical. Otherwise, convergence may be difficult to achieve.

Bibliography

[1] Johnson, W. S., Lubowinski, S. J., and Highsmith, A. L. "Mechanical Characterization of Unnotched SCS6/Ti-15-3 Metal Matrix Composites at Room Temperature," Presented at the ASTM Symposium - Thermal and Mechanical Behavior of Ceramic and Metal Matrix Composites, Atlanta, GA, November, (1988).

[2] Nimmer, R. P. "Fiber-Matrix Interface Effects on the Presence of Thermally Induced Residual Stresses," Submitted for Publication in ASTM Journal of Composite Technology and Research, (1988).

[3] Nimmer, R. P., et al. "Micromechanical Modeling of Fiber/Matrix Interface Effects in SiC/Ti Metal Matrix Composites," Submitted for Publication in ASTM Journal of Composite Technology and Research, (1989).

[4] Chamis, C. C. and Sendeckyj, G. P. "Critique on Theories Predicting Thermoelastic Properties of Fibrous Composites," Journal of Composite Materials: 332-358 (July 1968).

[5] Jones, Robert M. Mechanics of Composite Materials, Hemisphere Publishing Corporation, ©1975.

[6] Hill, R. "Theory of Mechanical Properties of Fibre-Strengthened Materials III: Self-Consistent Model," Journal on the Mechanics and Physics of Solids, 13: 189-198 (No. 4, 1965).

[7] Sendeckyj, G. P. "Longitudinal Shear Deformation of Composites II, Stress Distribution," Journal of Composite Materials, 5: 82-93 (January 1971).

[8] Halpin, J. C., and Tsai, S. W. Effect of Environmental Factors on Composite Materials. Air Force Materials Laboratory, AFML-TR 67-423, June 1969.

[9] Adams, D. F., and Tsai, W. S. "The Influence of Random Filament Packing on the Transverse Stiffness of Unidirectional Composites," Journal of Composite Materials, 3: 368-380 (July 1969).

[10] Foye, R. L. "An Evaluation of Various Engineering Estimates of the Transverse Properties of Unidirectional Composites," Proceedings of the Tenth National SAMPE Symposium - Advanced Fibrous Reinforced Composites. (November 1966).

[11] Adams, D. F., and Doner, D. R. "Longitudinal Shear Loading of a Unidirectional Composite," Journal of Composite Materials, 1: 4-17 (1967).

[12] Adams, D. F., and Doner, D. R. "Transverse Normal Loading of a Unidirectional Composite," Journal of Composite Materials, 1: 152-164 (1967).

[13] Adams, D. F. "Inelastic Analysis of a Unidirectional Composite Subjected to Transverse Normal Loading," Journal of Composite Materials, 4: 310-328 (1970).

[14] Foye, R. L. "Theoretical Post-Yielding Behavior of Composite Laminates, Part I - Inelastic Micromechanics," Journal of Composite Materials, 7: 178-193 (April 1973).

[15] Crane, D. A., and Adams, D. F. Finite Element Micromechanical Analysis of a Unidirectional Composite Including Longitudinal Shear Loading, Final Report. Prepared for Army Materials and Mechanics Research Center, AMMRC TR 81-7, February 1981.

[16] Adams, D. F. "Elastoplastic Crack Propagation in a Transversely Loaded Unidirectional Composite," Journal of Composite Materials, 8: 38-54 (January 1974).

[17] Broutman, L. F., and Agarwal, B. D. "A theoretical Study of the Effect on an Interfacial Layer on the Properties of Composites," Polymer Engineering Science, 14: 581-588 (1974).

[18] Agarwal, B. D., and Bansal, R. K. "Effect of an Interfacial Layer on the Properties of Fibrous Composites: A Theoretical Analysis," Fibre Science and Technology, 12: 149-158 (1979).

[19] Owen, D. R. J., and Lyness, J. F. "Investigation of Bond Failure in Fibre-Reinforced Materials by the Finite Element Method," Fibre Science and Technology, 5: 129-141 (1972).

[20] Lene, F. and Leguillon, D. "Homogenized Constitutive Law for Partially Cohesive Composite Material," International Journal of Solids and Structures, 18: 443-458 (1982).

[21] Aboudi, J. "Damage in Composites - Modeling of Imperfect Bonding," Composites Science and Technology, 28: 103-128 (1987).

[22] Jones, J. P., and Whittier, J. S. "Waves at a Flexibly Bonded Interface," Journal of Applied Mechanics, 34: 905-909 (1967).

[23] Benveniste, Y. "On the Effect of Debonding on the Overall Behavior of Composite Materials," Mechanics of Materials, 3: 349+ (1984).

[24] Benveniste, Y. "The Effective Mechanical Behavior of Composite Materials With Imperfect Contact Between the Constituents," Mechanics of Materials, 4: 197-208 (1985).

[25] Steif, P. S., and Dollar, A. "longitudinal Shearing of a Weakly Bonded Fiber Composite, Jounal of Applied Mechanics, 55: 618+

[26] Benveniste, Y., and Aboudi, J. "A Continuum Model for Fiber Reinforced Materials With Debonding," International Journal of Solids and Structures, 20: 935-951 (1984).

[27] Mal, A. K., and Bose, S. K. "Dynamic Elastic Moduli of a Suspension of Imperfectly Bonded Spheres," Proceedings of the Cambridge Philosophical Society, 76, 587-600 (1974).

[28] Pagano, N. J., and Tandon, G. P. "Modeling of Imperfect Bonding in Fiber Reinforced Brittle Matrix Composites," to appear in Mechanics of Materials: (1989).

[29] Tandon, G. P., and Pagano, N. J. "On the Effective Transverse Shear Modulus of Debonding Composites," Submitted for Publication: (1989).

[30] Tandon, G. P., and Pagano. N. J. "On the Transverse Young's Modulus of Brittle Matrix Composites With Interfacial Debonding," Submitted for Publication: (1989).

[31] Pagano, N. J., and Tandon, G. P. "Elastic Response of Multi-directional Coated-Fiber Composites," Composites Science and Technology, 31: 273-293 (1988).

[32] Hopkins, D. A., and Chamis, C. C. "A Unique Set of Micromechanics Equations for High-Temperature Metal Matrix Composites," Testing Technology of Metal Matrix Composites, ASTM STP 964: 159-176 (1988).

[33] Naik, R. A., et al. "Effect of a High Temperature Cycle on the Mechanical Properties of Silicon Carbide/Titanium Metal Matrix Composites," Presented at the Symposium on High Temperature Composites, American Society for Composites: Dayton, OH (June 1989).

[34] Highsmith, A. L., and Naik, R. A. "Local Stresses in Metal Matrix Composites Subjected to Thermal and Mechanical Loading," Presented at the ASTM Symposium - Thermal and Mechanical Behavior of Ceramic and Metal Matrix Composites: Atlanta, GA (November 1988).

[35] Broek, D. Elementary Engineering Fracture Mechanics. Martinus Nijhoff Publishers, Dordecht, The Netherlands, ©1986.

[36] The MacNeal-Schwendler Corporation. MSC/NASTRAN Application Manual. 1989 Edition, Los Angeles, CA, ©1972.

[37] The MacNeal-Schwendler Corporation. MSC/NASTRAN User's Manual, Version 65C. Los Angeles, CA, ©1987.

[38] Structural Dynamics Research Corporation. <u>I-DEAS Supertab</u>
      <u>Pre/Post Processing Engineering Analysis User's Guide</u>. Milford,
      OH, ©1988.

[39] General Electric Aircraft Engines. <u>Titanium Aluminide Compos-</u>
      <u>ites. Intermim Report No. 4</u>. Prepared for Materials Laboratory,
      Wright Research and Development Center(AFSC), United States Air
      Force, Wright-Patterson AFB, OH under Contract F33657-86-C-
      2136, P00008. 15 June 1989.

Appendix A: Sample MSC/NASTRAN Data Deck

```
ID DROBERTS,TNOINTER
TIME 120
SOL 66
DIAG 50
ALTER 73 $
OUTPUT2 CSTM,GPL,GPDT,EPT,MPT//0/11 $
OUTPUT2 GEOM2,GEOM3,GEOM4,,//0/11 $
ALTER 1036 $
OUTPUT2 OUGV1,OES1,OSTR1,,//0/11 $
OUTPUT2 ,,,,//-9/11 $
CEND
TITLE = NO INTER, WEAK, PL STRESS
DISPLACEMENT = ALL
STRESS = ALL
   SEALL = ALL
   SUPER = ALL
      SPC =              1
      MPC =              5
SUBCASE         1
SUBTITLE =    TEMP 970
      TEMP(LOAD) = 1
      NLPARM =       1
SUBCASE         2
      TEMP(LOAD) = 10
      NLPARM =       2
SUBCASE         3
SUBTITLE =    C100+TEMP , 100+TEMP
      TEMP(LOAD) = 10
      LOAD =            2
      NLPARM =       3
SUBCASE         4
SUBTITLE =    C150+TEMP , 150+TEMP
      TEMP(LOAD) = 10
      LOAD =            3
      NLPARM =       3
SUBCASE         5
SUBTITLE =    C175+TEMP , 175+TEMP
      TEMP(LOAD) = 10
      LOAD =            4
      NLPARM =       3
SUBCASE         6
SUBTITLE =    C200+TEMP , 200+TEMP
      TEMP(LOAD) = 10
      LOAD =            5
      NLPARM =       3
SUBCASE         7
SUBTITLE =    C225+TEMP , 225+TEMP
      TEMP(LOAD) = 10
```

Executive Control Deck

Case Control Deck

114

```
              LOAD =           6
              NLPARM =    3
     SUBCASE          8
     SUBTITLE =    C250+TEMP , 250+TEMP
              TEMP(LOAD) = 10
              LOAD =           7
              NLPARM =    3
     BEGIN BULK
     NLPARM          1        1          ITER        1    -40      PW      NO
     NLPARM          2        8          ITER        1    -20      PW      NO
     NLPARM          3        5          ITER        1    -20      PW      NO
     GRID*[16 spaces] 291            0       .0148493        .0148493+GA  1
     *GA   1                 0.             0
     GRID*[16 spaces] 292            0       .0128879        .0165803+GA  2
     *GA   2                 0.             0
     GRID*[16 spaces] 293            0       .0108472        .017981702+GA  3
     *GA       3             0.             0
                          [grid points continued]
                                   |
                                   |
                                   |

     CQUAD4         545        1      291      300      301      292      0.
     CQUAD4         546        1      292      301      302      293      0.
     CQUAD4         547        1      293      302      303      294      0.
     CQUAD4         548        1      294      303      304      295      0.
     CQUAD4         549        1      295      304      305      296      0.
                       [quad4 elements continued]
                                   |
                                   |
                                   |

     CTRIA3         686        1      296      297      444      0.
     CTRIA3         687        1      297      298      444      0.
                       [tria3 elements continued]
                                   |
                                   |
                                   |

     CGAP           817        2      453      371                             1
     CGAP           818        2      452      370                             2
     CGAP           819        2      451      369                             3
                       [gap elements continued]
                                   |
                                   |
                                   |

     CORD2R*[16 spaces] 1            0    6.208301E-08       0.0699999+CO11
     *CO11 [17 spaces] 0.    6.208301E-08       0.0699999           0.01+CO12
     *CO12                   0.             0.             0.
     CORD2R*[16 spaces] 2            0    0.00490102       0.0698274+CO21
     *CO21 [17 spaces] 0.    0.00490102       0.0698274           0.01+CO22
     *CO22                   0.             0.             0.
                     [coordinate systems definitions continued]
                                   |
                                   |
```

```
                              |
MAT1[11 spaces]1 400000.153846.2      .37.82E-09  5.E-06    1000.        +MA 1
+MA 1         1500.   1500.    68.
MAT1[11 spaces]2 100000.38461.54      .37.82E-09  .00001    1000.        +MA 2
+MA 2         1500.   1500.    68.
PSHELL* [16 spaces]  1            1               .01               1+PA 1
*PA 1               1.               1           .8333333               0.
PSHELL* [16 spaces]  3            2               .01               2+PA 2
*PA 2               1.               2           .8333333               0.
PGAP          2      0.      0. 400000.  0.0000 150000.      .35     .35
SPC           1     291    3456     0.
SPC           1     292    3456     0.
SPC           1     293    3456     0.
SPC           1     294    3456     0.
                 [single point constraints continued]
                              |
                              |
                              |
MPC           5     525       2   -1.00     533      2    1.00
MPC           5     526       2   -1.00     533      2    1.00
MPC           5     527       2   -1.00     533      2    1.00
MPC           5     528       2   -1.00     533      2    1.00
                 [multipoint constraints continued]
                              |
                              |
                              |
TEMPD         1     970.
TEMPD        10      23.
FORCE         2     534       0     1.  .10486     (.      0.
FORCE         3     534       0    1.50  .10486    ᴗ.      0.
FORCE         4     534       0    1.75  .10486     0.     0.
FORCE         2     534       0    2.00  .10486     0.     0.
FORCE         2     534       0    2.25  .10486     0.     0.
FORCE         2     534       0    2.50  .10486     0.     0.
ENDDATA
```

Appendix B: Mathematica Program for a Simplified One-Dimensional Micromechanics Model With an Interphase Zone

This Mathematica notebook solves the constitutive equations for a nonlinear 1-dimensional transverse micromechanics model containing an elastic-plastic interphase zone between fiber and matrix.

Input Data and Clear Previous Run.

Model Parameters.
```
vf = .35;
fsiz = .07;
zonesiz = .05;
modF = 400000.;
modI = 100000.;
modM = 100000.;
aF = 5. 10^(-6);
aI = 10. 10^(-6);
aM = 10. 10^(-6);
t = 25.;
tp = 1000.;
sIys = 125.;
hp = 0.;
Clear[p1,p2,sa]
```

Load array.
```
load = {0, 10, 20, 30, 40, 50, 60, 70, 80, 90, 100,
110, 120, 130, 140, 150, 160, 170, 180, 190, 200,
210, 220, 230, 240, 250, 260, 270, 275, 270, 260,
250, 240, 230, 220, 210, 200, 190, 180, 170, 160,
150, 140, 130, 120, 110, 100, 90, 80, 70, 60, 50,
40, 30, 20, 10, 0};
nload = Length[load];
```

Define Constitutive Equations.

Calculate the constants a, b, and c used in the stress-strain and equilibrium equations.
```
a = fsiz;
b = zonesiz a;
c = 1/2 (-(2 a + 2 b) + Sqrt[(2 a + 2 b)^2 \
- 4 (a^2 (1 - 1/vf) + 2 a b + b^2)]);
```

Stress-Strain relations
```
eF = uF/a == sF/modF + aF (t - tp);
eI1 = (uI -uF)/b == sI1/modI + aI (t-tp) + ep1;
eM1 = (uM - uI)/c == sM1/modM + aM (t-tp);
eI2 = uF/a == sI2/modI + aI (t-tp) + ep2;
```

117

```
eM2 = uM/(a+b+c) == sM2/modM + aM (t-tp);
```

Equilibrium Equations

```
q1 = sF a + sI2 b == sI1 (a+b);
q2 = sI1 == sM1;
q3 = sM1 (a+b) + sM2 c == (a+b+c) sa;
```

Define equation set and independent variables.
Also, enter strain hardening equations.

```
eqnset = {eF,eI1,eM1,eI2,eM2,q1,q2,q3};
vars = {sF,sI1,sM1,sI2,sM2,uF,uI,uM,ep1,ep2};
sI1ys = sIys + hp Abs[p1];
sI2ys = sIys + hp Abs[p2];
```

Solve Constitutive Equations For All Possible Cases.

Case 1. |sI1| < sI1ys and |sI2| < sI2ys

```
solset1 = Solve[eqnset/.{ep1->p1,ep2->p2},vars];
f1={solset1[[1,1,2]],solset1[[1,2,2]],
solset1[[1,3,2]],solset1[[1,4,2]],solset1[[1,5,2]],
solset1[[1,6,2]],solset1[[1,7,2]],solset1[[1,8,2]],p1,p2};
```

Case 2. |sI1| > sI1ys and |sI2| < sI2ys

Subcase 2a. sI1 > sI1ys and |sI2| < sI2ys

```
solset2a = Solve[eqnset/.{sI1->sI1ys,ep2->p2},vars];
f2a={solset2a[[1,1,2]],sI1ys,
solset2a[[1,2,2]],solset2a[[1,3,2]],solset2a[[1,4,2]],
solset2a[[1,5,2]],solset2a[[1,6,2]],solset2a[[1,7,2]],
solset2a[[1,8,2]],p2};
```

Subcase 2b. sI1 < -sI1ys and |sI2| < sI2ys

```
solset2b = Solve[eqnset/.{sI1->-sI1ys,ep2->p2},vars];
f2b={solset2b[[1,1,2]],-sI1ys,
solset2b[[1,2,2]],solset2b[[1,3,2]],solset2b[[1,4,2]],
solset2b[[1,5,2]],solset2b[[1,6,2]],solset2b[[1,7,2]],
solset2b[[1,8,2]],p2};
```

Case 3. |sI1| < sI1ys and |sI2| > sI2ys

Subcase 3a. |sI1| < sI1ys and sI2 > sI2ys

```
solset3a = Solve[eqnset/.{ep1->p1,sI2->sI2ys},vars];
f3a={solset3a[[1,1,2]],solset3a[[1,2,2]],solset3a[[1,3,2]],
sI2ys,solset3a[[1,4,2]],solset3a[[1,5,2]],solset3a[[1,6,2]],
solset3a[[1,7,2]],p1,solset3a[[1,8,2]]};
```

Subcase 3b. |sI1| < sI1ys and sI2 < -sI2ys

```
solset3b = Solve[eqnset/.{ep1->p1,sI2->-sI2ys},vars];
f3b={solset3b[[1,1,2]],solset3b[[1,2,2]],solset3b[[1,3,2]],
-sI2ys,solset3b[[1,4,2]],solset3b[[1,5,2]],solset3b[[1,6,2]],
solset3b[[1,7,2]],p1,solset3b[[1,8,2]]};
```

Case 4. |sI1| > sI1ys and |sI2| > sI2ys

Subcase 4a.   sI1 > sI1ys and sI2 > sI2ys
```
solset4a = Solve[eqnset/.{sI1->sI1ys,sI2->sI2ys},vars];
f4a={solset4a[[1,1,2]],sI1ys,solset4a[[1,2,2]],sI2ys,
solset4a[[1,3,2]],solset4a[[1,4,2]],solset4a[[1,5,2]],
solset4a[[1,6,2]],solset4a[[1,7,2]],solset4a[[1,8,2]]};
```

Subcase 4b.   sI1 < -sI1ys and sI2 > sI2ys
```
solset4b = Solve[eqnset/.{sI1->-sI1ys,sI2->sI2ys},vars];
f4b={solset4b[[1,1,2]],-sI1ys,solset4b[[1,2,2]],sI2ys,
solset4b[[1,3,2]],solset4b[[1,4,2]],solset4b[[1,5,2]],
solset4b[[1,6,2]],solset4b[[1,7,2]],solset4b[[1,8,2]]};
```

Subcase 4c.   sI1 > sI1ys and sI2 < -sI2ys
```
solset4c = Solve[eqnset/.{sI1->sI1ys,sI2->-sI2ys},vars];
f4c={solset4c[[1,1,2]],sI1ys,solset4c[[1,2,2]],-sI2ys,
solset4c[[1,3,2]],solset4c[[1,4,2]],solset4c[[1,5,2]],
solset4c[[1,6,2]],solset4c[[1,7,2]],solset4c[[1,8,2]]};
```

Subcase 4d.   sI1 < -sI1ys and sI2 < -sI2ys
```
solset4d = Solve[eqnset/.{sI1->-sI1ys,sI2->-sI2ys},vars];
f4d={solset4d[[1,1,2]],-sI1ys,solset4d[[1,2,2]],-sI2ys,
solset4d[[1,3,2]],solset4d[[1,4,2]],solset4d[[1,5,2]],
solset4d[[1,6,2]],solset4d[[1,7,2]],solset4d[[1,8,2]]};
```

Apply Load History and Plot Results.

Determine solution arrays. Two solution arrays are computed,
alvar and totdis. The alvar array contains the complete
solution set of all variables at each load step. A
single element of alvar is of the form: {{sF, sI1, sM1, sI2,
sM2, uF, uI, uM, ep1, ep2}, sA}. Totdis contains only the
overall displacement of the structure. A single
element of totdis contains {uM, sA}.

```
p1=0.;
p2=0.;
n=1;
While[n <= nload, sa = load[[n]];
 vp = {0.,0.,0.,0.,0.,0.,0.,0.,0.,0.};
 v = f1;
 While[Chop[v-vp]!={0,0,0,0,0,0,0,0,0,0},
 vp = v;
 v = Which[Abs[vp[[2]]]<=sI1ys && Abs[vp[[4]]]<=sI2ys,f1,
    vp[[2]] > sI1ys && Abs[vp[[4]]] <= sI2ys, f2a,
    vp[[2]] < -sI1ys && Abs[vp[[4]]] <= sI2ys, f2b,
    Abs[vp[[2]]] <= sI1ys && vp[[4]] > sI2ys, f3a,
    Abs[vp[[2]]] <= sI1ys && vp[[4]] < -sI2ys, f3b,
    vp[[2]] > sI1ys && vp[[4]] > sI2ys, f4a,
    vp[[2]] < -sI1ys && vp[[4]] > sI2ys, f4b,
```

119

```
       vp[[2]] > sI1ys && vp[[4]] < -sI2ys, f4c,
       vp[[2]] < -sI1ys && vp[[4]] < -sI2ys, f4d];
   p1 = v[[9]]; p2 = v[[10]]];
  alvar[n]={v,sa};
  totdis[n]={v[[8]],sa};
  na = n+1; n=na];
```

Modify the total displacement array, totdis, to contain
average strain after cooldown instead of total displacement.
Create new array, es, that contains the total average strain
and applied stress.

```
length = a+b+c;
es = Table[{(totdis[i][[1]] - totdis[1][[1]])/length,
 totdis[i][[2]]}, {i,nload}]
```

Plot the Result.

```
ListPlot[es, PlotJoined->True]
```

Appendix C: Mathematica Program for a Simplified One-Dimensional Micromechanics Model With a Combined Interphase Zone / Weak Bond

This Mathematica notebook solves the constitutive equations for a nonlinear 1-dimensional transverse micromechanics model which models a portion of the fiber/matrix interface as if a perfectly weak bond exists and the remainder as if an elastic-plastic interphase zone exists between fiber and matrix.

Input Data and Clear Previous Run.

Model Parameters.
```
doasiz = 1.0
vf = .35;
fsiz = .07;
zonesiz = .05;
modF = 400000.;
modI = 100000.;
modM = 100000.;
aF = 5. 10^(-6);
aI = 10. 10^(-6);
aM = 10. 10^(-6);
t = 25.;
tp = 1000.;
sIys = 125.;
hp = 0.;
Clear[p1,p2,sa]
```

Load array.
```
load = {0, 10, 20, 30, 40, 50, 60, 70, 80, 90, 100,
110, 120, 130, 140, 150, 160, 170, 180, 190, 200,
210, 220, 230, 240, 250, 260, 270, 275, 270, 260,
250, 240, 230, 220, 210, 200, 190, 180, 170, 160,
150, 140, 130, 120, 110, 100, 90, 80, 70, 60, 50,
40, 30, 20, 10, 0};
nload = Length[load];
```

Define Constitutive Equations.

Calculate the constants a, b, c, and d used in the stress-strain and equilibrium equations.
```
a = fsiz;
b = zonesiz a;
c = 1/2 (-(2 a + 2 b) + Sqrt[(2 a + 2 b)^2 \
- 4 (a^2 (1 - 1/vf) + 2 a b + b^2)]);
d = doasiz a;
```

121

<u>Stress-Strain relations</u>
```
eF = uF/a == sF/modF + aF (t - tp);
eI1 = (uI -uF)/b == sI1/modI + aI (t-tp) + ep1;
eM1 = (uM - uG)/(b+c) == sM1/modM + aM (t-tp);
eI2 = uF/a == sI2/modI + aI (t-tp) + ep2;
eM2 = (uM - uI)/c == sM2/modM + aM (t-tp);
eM3 = uM/(a+b+c) == sM3/modM + aM (t-tp);
```

<u>Equilibrium Equations</u>
```
q1 = sF a + sI2 b == sM1 d + sI1 (a+b-d);
q2 = sI1 == sM2;
q3 = sM1 d + sM2 (a+b-d) + sM3 c == (a+b+c) sa;
```

<u>Define equation set and independent variables.</u>
<u>Also, enter strain hardening equations.</u>
```
eqnset = {eF,eI1,eM1,eI2,eM2,eM3,q1,q2,q3};
vars = {sF,sI1,sM1,sI2,sM2,sM3,uF,uI,uM,uG,ep1,ep2};
sI1ys = sIys + hp Abs[p1];
sI2ys = sIys + hp Abs[p2];
```

<u>Solve Constitutive Equations For All Possible Cases.</u>

<u>Case 1. |sI1| < sI1ys and |sI2| < sI2ys</u>

<u>• Situation 1_1.   sM1 < 0. or uG - uF < 0.</u>
```
solset1s1 = Solve[eqnset/.{uG->uF,
ep1->p1,ep2->p2},vars];
f1s1={solset1s1[[1,1,2]],solset1s1[[1,2,2]],
solset1s1[[1,3,2]],solset1s1[[1,4,2]],solset1s1[[1,5,2]],
solset1s1[[1,6,2]],solset1s1[[1,7,2]],
solset1s1[[1,8,2]],solset1s1[[1,9,2]],
solset1s1[[1,7,2]],p1,p2};
```

<u>• Situation 1_2.   sM1 > 0. or uG - uF > 0.</u>
```
solset1s2 = Solve[eqnset/.{sM1->0.,
ep1->p1,ep2->p2},vars];
f1s2={solset1s2[[1,1,2]],solset1s2[[1,2,2]],0.,
solset1s2[[1,3,2]],solset1s2[[1,4,2]],solset1s2[[1,5,2]],
solset1s2[[1,6,2]],solset1s2[[1,7,2]],
solset1s2[[1,8,2]],solset1s2[[1,9,2]],p1,p2};
```

<u>Case 2. |sI1| > sI1ys and |sI2| < sI2ys</u>

<u>Subcase 2a. sI1 > sI1ys and |sI2| < sI2ys</u>

<u>• Situation 2a_1.   sM1 < 0. or uG - uF < 0.</u>
```
solset2as1 = Solve[eqnset/.{uG->uF,
sI1->sI1ys,ep2->p2},vars];
f2as1={solset2as1[[1,1,2]],sI1ys,
solset2as1[[1,2,2]],solset2as1[[1,3,2]],
solset2as1[[1,4,2]],solset2as1[[1,5,2]],
solset2as1[[1,6,2]],solset2as1[[1,7,2]],
```

```
solset2as1[[1,8,2]],solset2as1[[1,6,2]],
solset2as1[[1,9,2]],p2};
```

• Situation 2a_2. sM1 > 0. or uG - uF > 0.
```
solset2as2 = Solve[eqnset/.{sM1->0.,
sI1->sI1ys,ep2->p2},vars];
f2as2={solset2as2[[1,1,2]],sI1ys,0.,
solset2as2[[1,2,2]],solset2as2[[1,3,2]],
solset2as2[[1,4,2]],solset2as2[[1,5,2]],
solset2as2[[1,6,2]],solset2as2[[1,7,2]],
solset2as2[[1,8,2]],solset2as2[[1,9,2]],p2};
```

Subcase 2b. sI1 < -sI1ys and |sI2| < sI2ys

• Situation 2b_1. sM1 < 0. or uG - uF < 0.
```
solset2bs1 = Solve[eqnset/.{uG->uF,
sI1->-sI1ys,ep2->p2},vars];
f2bs1={solset2bs1[[1,1,2]],-sI1ys,
solset2bs1[[1,2,2]],solset2bs1[[1,3,2]],
solset2bs1[[1,4,2]],solset2bs1[[1,5,2]],
solset2bs1[[1,6,2]],solset2bs1[[1,7,2]],
solset2bs1[[1,8,2]],solset2bs1[[1,6,2]],
solset2bs1[[1,9,2]],p2};
```

• Situation 2b_2. sM1 > 0. or uG - uF > 0.
```
solset2bs2 = Solve[eqnset/.{sM1->0.,
sI1->-sI1ys,ep2->p2},vars];
f2bs2={solset2bs2[[1,1,2]],-sI1ys,0.,
solset2bs2[[1,2,2]],solset2bs2[[1,3,2]],
solset2bs2[[1,4,2]],solset2bs2[[1,5,2]],
solset2bs2[[1,6,2]],solset2bs2[[1,7,2]],
solset2bs2[[1,8,2]],solset2bs2[[1,9,2]],p2};
```

Case 3. |sI1| < sI1ys and |sI2| > sI2ys

Subcase 3a. |sI1| < sI1ys and sI2 > sI2ys

• Situation 3a_1. sM1 < 0. or uG - uF < 0.
```
solset3as1 = Solve[eqnset/.{uG->uF,
ep1->p1,sI2->sI2ys},vars];
f3as1={solset3as1[[1,1,2]],solset3as1[[1,2,2]],
solset3as1[[1,3,2]],sI2ys,solset3as1[[1,4,2]],
solset3as1[[1,5,2]],solset3as1[[1,6,2]],
solset3as1[[1,7,2]],solset3as1[[1,8,2]],
solset3as1[[1,6,2]],p1,solset3as1[[1,9,2]]};
```

• Situation 3a_2. sM1 > 0. or uG - uF > 0.
```
solset3as2 = Solve[eqnset/.{sM1->0.,
ep1->p1,sI2->sI2ys},vars];
f3as2={solset3as2[[1,1,2]],solset3as2[[1,2,2]],0.,
solset3as2[[1,3,2]],sI2ys,solset3as2[[1,4,2]],
solset3as2[[1,5,2]],solset3as2[[1,6,2]],
```

123

```
solset3as2[[1,7,2]],solset3as2[[1,8,2]],
p1,solset3as2[[1,9,2]]]};
```

Subcase 3b. |sI1| < sI1ys and sI2 < -sI2ys

• Situation 3b_1. sM1 < 0, or uG - uF < 0.
```
solset3bs1 = Solve[eqnset/.{uG->uF,
ep1->p1,sI2->-sI2ys},vars];
f3bs1={solset3bs1[[1,1,2]],solset3bs1[[1,2,2]],
solset3bs1[[1,3,2]],-sI2ys,solset3bs1[[1,4,2]],
solset3bs1[[1,5,2]],solset3bs1[[1,6,2]],
solset3bs1[[1,7,2]],solset3bs1[[1,8,2]],
solset3bs1[[1,6,2]],p1,solset3bs1[[1,9,2]]]};
```

• Situation 3b_2. sM1 > 0, or uG - uF > 0.
```
solset3bs2 = Solve[eqnset/.{sM1->0.,
ep1->p1,sI2->-sI2ys},vars];
f3bs2={solset3bs2[[1,1,2]],solset3bs2[[1,2,2]],0.,
solset3bs2[[1,3,2]],-sI2ys,solset3bs2[[1,4,2]],
solset3bs2[[1,5,2]],solset3bs2[[1,6,2]],
solset3bs2[[1,7,2]],solset3bs2[[1,8,2]],
p1,solset3bs2[[1,9,2]]]};
```

Case 4. |sI1| > sI1ys and |sI2| > sI2ys

Subcase 4a. sI1 > sI1ys and sI2 > sI2ys

• Situation 4a_1. sM1 < 0, or uG - uF < 0.
```
solset4as1=Solve[eqnset/.{uG->uF,
sI1->sI1ys,sI2->sI2ys},vars];
f4as1={solset4as1[[1,1,2]],sI1ys,solset4as1[[1,2,2]],
sI2ys,solset4as1[[1,3,2]],solset4as1[[1,4,2]],
solset4as1[[1,5,2]],solset4as1[[1,6,2]],
solset4as1[[1,7,2]],solset4as1[[1,5,2]],
solset4as1[[1,8,2]],solset4as1[[1,9,2]]]};
```

• Situation 4a_2. sM1 > 0, or uG - uF > 0.
```
solset4as2=Solve[eqnset/.{sM1->0.,
sI1->sI1ys,sI2->sI2ys},vars];
f4as2={solset4as2[[1,1,2]],sI1ys,0.,solset4as2[[1,2,2]],
sI2ys,solset4as2[[1,3,2]],solset4as2[[1,4,2]],
solset4as2[[1,5,2]],solset4as2['[1,6,2]],
solset4as2[[1,7,2]],solset4as2[[1,8,2]],
solset4as2[[1,9,2]]]};
```

Subcase 4b. sI1 < -sI1ys and sI2 > sI2ys

• Situation 4b_1. sM1 < 0, or uG - uF < 0.
```
solset4bs1=Solve[eqnset/.{uG->uF,
sI1->-sI1ys,sI2->sI2ys},vars];
f4bs1={solset4bs1[[1,1,2]],-sI1ys,solset4bs1[[1,2,2]],
sI2ys,solset4bs1[[1,3,2]],solset4bs1[[1,4,2]],
```

124

```
solset4bs1[[1,5,2]],solset4bs1[[1,6,2]],
solset4bs1[[1,7,2]],solset4bs1[[1,5,2]],
solset4bs1[[1,8,2]],solset4bs1[[1,9,2]]};
```

· Situation 4b_2.   sM1 > 0. or uG - uF > 0.
```
solset4bs2=Solve[eqnset/.{sM1->0.,
sI1->-sI1ys,sI2->sI2ys},vars];
f4bs2={solset4bs2[[1,1,2]],-sI1ys,0.,solset4bs2[[1,2,2]],
sI2ys,solset4bs2[[1,3,2]],solset4bs2[[1,4,2]],
solset4bs2[[1,5,2]],solset4bs2[[1,6,2]],
solset4bs2[[1,7,2]],solset4bs2[[1,8,2]],
solset4bs2[[1,9,2]]};
```

Subcase 4c.   sI1 > sI1ys and sI2 < -sI2ys

· Situation 4c_1.   sM1 < 0. or uG - uF < 0.
```
solset4cs1 = Solve[eqnset/.{uG->uF,
sI1->sI1ys,sI2->-sI2ys},vars];
f4cs1={solset4cs1[[1,1,2]],sI1ys,solset4cs1[[1,2,2]],
-sI2ys,solset4cs1[[1,3,2]],solset4cs1[[1,4,2]],
solset4cs1[[1,5,2]],solset4cs1[[1,6,2]],
solset4cs1[[1,7,2]],solset4cs1[[1,5,2]],
solset4cs1[[1,8,2]],solset4cs1[[1,9,2]]};
```

· Situation 4c_2.   sM1 > 0. or uG - uF > 0.
```
solset4cs2 = Solve[eqnset/.{sM1->0.,
sI1->sI1ys,sI2->-sI2ys},vars];
f4cs2={solset4cs2[[1,1,2]],sI1ys,0.,solset4cs2[[1,2,2]],
-sI2ys,solset4cs2[[1,3,2]],solset4cs2[[1,4,2]],
solset4cs2[[1,5,2]],solset4cs2[[1,6,2]],
solset4cs2[[1,7,2]],solset4cs2[[1,8,2]],
solset4cs2[[1,9,2]]};
```

Subcase 4d.   sI1 < -sI1ys and sI2 < -sI2ys

· Situation 4d_1.   sM1 < 0. or uG - uF < 0.
```
solset4ds1 = Solve[eqnset/.{uG->uF,
sI1->-sI1ys,sI2->-sI2ys},vars];
f4ds1={solset4ds1[[1,1,2]],-sI1ys,solset4ds1[[1,2,2]],
-sI2ys,solset4ds1[[1,3,2]],solset4ds1[[1,4,2]],
solset4ds1[[1,5,2]],solset4ds1[[1,6,2]],
solset4ds1[[1,7,2]],solset4ds1[[1,5,2]],
solset4ds1[[1,8,2]],solset4ds1[[1,9,2]]};
```

· Situation 4d_2.   sM1 > 0. or uG - uF > 0.
```
solset4ds2 = Solve[eqnset/.{sM1->0.,
sI1->-sI1ys,sI2->-sI2ys},vars];
f4ds2={solset4ds2[[1,1,2]],-sI1ys,0.,solset4ds2[[1,2,2]],
-sI2ys,solset4ds2[[1,3,2]],solset4ds2[[1,4,2]],
solset4ds2[[1,5,2]],solset4ds2[[1,6,2]],
solset4ds2[[1,7,2]],solset4ds2[[1,8,2]],
solset4ds2[[1,9,2]]};
```

Apply Load History and Plot Results.

Determine solution arrays. Two solution arrays are computed,
alvar and totdis. The alvar array contains the complete
solution set of all variables at each load step. A single
element of alvar is of the form: {{sF, sI1, sM1, sI2, sM2,
uF, uI, uM, ep1, ep2}, sA}. Totdis contains only the overall
displacement of the structure. A single element of totdis
contains {uM, sA}.

```
p1=0.;
p2=0.;
n=1;
While[n <= nload, sa = load[[n]];
 vp = {0.,0.,0.,0.,0.,0.,0.,0.,0.,0.,0.,0.};
 v = f1s2;
 While[Chop[v-vp]!={0,0,0,0,0,0,0,0,0,0,0,0},
 vp = v;
 uGF = vp[[10]]-vp[[7]];
 v = Which[Abs[vp[[2]]]<=sI1ys && Abs[vp[[4]]]<=sI2ys
    && (vp[[3]]<0. || uGF<0), f1s1,
    Abs[vp[[2]]] <= sI1ys && Abs[vp[[4]]] <= sI2ys
    && (vp[[3]]>0. || uGF>0), f1s2,
    vp[[2]] > sI1ys && Abs[vp[[4]]] <= sI2ys
    && (vp[[3]]<0. || uGF<0),f2as1,
    vp[[2]] > sI1ys && Abs[vp[[4]]] <= sI2ys
    && (vp[[3]]>0. || uGF>0),f2as2,
    vp[[2]] < -sI1ys && Abs[vp[[4]]] <= sI2ys
    && (vp[[3]]<0. || uGF<0), f2bs1,
    vp[[2]] < -sI1ys && Abs[vp[[4]]] <= sI2ys
    && (vp[[3]]>0. || uGF>0), f2bs2,
    Abs[vp[[2]]] <= sI1ys && vp[[4]] > sI2ys
    && (vp[[3]]<0. || uGF<0), f3as1,
    Abs[vp[[2]]] <= sI1ys && vp[[4]] > sI2ys
    && (vp[[3]]>0. || uGF>0), f3as2,
    Abs[vp[[2]]] <= sI1ys && vp[[4]] < -sI2ys
    && (vp[[3]]<0. || uGF<0), f3bs1,
    Abs[vp[[2]]] <= sI1ys && vp[[4]] < -sI2ys
    && (vp[[3]]>0. || uGF>0), f3bs2,
    vp[[2]] > sI1ys && vp[[4]] > sI2ys
    && (vp[[3]]<0. || uGF<0), f4as1,
    vp[[2]] > sI1ys && vp[[4]] > sI2ys
    && (vp[[3]]>0. || uGF>0), f4as2,
    vp[[2]] < -sI1ys && vp[[4]] > sI2ys
    && (vp[[3]]<0. || uGF<0), f4bs1,
    vp[[2]] < -sI1ys && vp[[4]] > sI2ys
    && (vp[[3]]>0. || uGF>0), f4bs2,
    vp[[2]] > sI1ys && vp[[4]] < -sI2ys
    && (vp[[3]]<0. || uGF<0), f4cs1,
    vp[[2]] > sI1ys && vp[[4]] < -sI2ys
    && (vp[[3]]>0. || uGF>0), f4cs2,
    vp[[2]] < -sI1ys && vp[[4]] < -sI2ys
```

```
       && (vp[[3]]<0. || uGF<0), f4ds1,
       vp[[2]] < -sI1ys && vp[[4]] < -sI2ys
       && (vp[[3]]>0. || uGF>0), f4ds2];
  p1 = v[[11]]; p2 = v[[12]]];
 alvar[n]={v,sa};
 totdis[n]={v[[9]],sa};
 na = n+1; n=na];
```

Modify the total displacement array, totdis, to contain
average strain after cooldown instead of total displacement.
Create new array, es, that contains the total average strain
and applied stress.

```
length = a+b+c;
es = Table[{(totdis[i][[1]] - totdis[1][[1]])/length,
 totdis[i][[2]]}, {i,nload}]
```

Plot the Result.

```
ListPlot[es, PlotJoined->True]
```

127

1. AD	2. CODE									INDEXER	CATALOGER	EDITOR
A230529	FLD											
	GRP											
	SUB-GRP									REVIEWER	REVIEWER	VERIFIER

6. U-TITLE	11. DATE	16. PROJECT
7. C-TITLE	REGRADE DATE	17. TASK
8. T-CLASS	12. PP	18. M-ACRONYM
9. DESC. NOTE	14. OA-SERIES	19. N-SERIES
10. AUTHOR	15. CONTRACT	20. R-CLASS

21. SUPPLEMENTARY NOTE

22. DISTRIBUTION/AVAILABILITY STATEMENTS

23. DESCRIPTORS

*

	24. DESCRIPTOR CLASSIFICATION	U CRD	C CFRD	S SRD	R SFRD

25. IDENTIFIERS AND/OR OPEN-ENDED TERMS

	26. IDENT. & O. E. TERMS CLASSIFICATION	U CRD	C CFRD	S SRD	R SFRD

27. ABSTRACT ☐ DTIC ☐ AUTHOR ☐ MOD. ☐ NO ABST. ☐ SEE BACK COPY FROM PAGE(S) _XIII_	28. ABSTRACT CLASSIFICATION U CRD C CFRD S SRD R SFRD	29. INVENTORY 1

30. INDEX ANNOTATION (MUST BE UNCLASSIFIED)

31. SPEC CODE	32. REGRADE CODE	33. DISTRIBUTION/ AVAILABILITY CODES		34. SERIAL NUMBER	36. DOCUMENT LOCATION
A X Y Z	A B C D E F G	DIST.	AVAIL. /SPECIAL	35. SOURCE CODE 012285	1 NTIS 2 DTIC
37. CLASS BY				38. DECLASS. ON	39. CONF. ON

REPORT DOCUMENTATION PAGE

Public reporting burden for this collection of information is estimated to average 1 hour per response, including the time for reviewing instructions, searching existing data sources, gathering and maintaining the data needed, and completing and reviewing the collection of information. Send comments regarding this burden estimate or any other aspect of this collection of information, including suggestions for reducing this burden, to Washington Headquarters Services, Directorate for Information Operations and Reports, 1215 Jefferson Davis Highway, Suite 1204, Arlington, VA 22202-4302, and to the Office of Management and Budget, Paperwork Reduction Project (0704-0188), Washington, DC 20503

1. AGENCY USE ONLY (Leave blank)	2. REPORT DATE	3. REPORT TYPE AND DATES COVERED
	December 1990	Master's Thesis

4. TITLE AND SUBTITLE
MICROMECHANICAL MODELING OF THE FIBER/MATRIX INTERFACE REGION IN A METAL MATRIX COMPOSITE

5. FUNDING NUMBERS

6. AUTHOR(S)

David D. Robertson, Capt, USAF

7. PERFORMING ORGANIZATION NAME(S) AND ADDRESS(ES)

Air Force Institute of Technology
Wright-Patterson AFB OH 45433-6583

8. PERFORMING ORGANIZATION REPORT NUMBER

AFIT/GAE/ENY/90D-22

9. SPONSORING / MONITORING AGENCY NAME(S) AND ADDRESS(ES)

Ted Fecke
WRDC/POTC
Wright-Patterson AFB OH 45433

10. SPONSORING / MONITORING AGENCY REPORT NUMBER

11.

12a DISTRIBUTION AVAILABILITY STATEMENT

Approved for public release; distribution unlimited

12b. DISTRIBUTION CODE

13. ABSTRACT (Maximum 200 words)

The effects of various fiber/matrix interface conditions on the transverse normal response of a high temperature titanium based metal matrix composite were examined. Analysis methods included both a simplified one-dimensional mathematical model and a finite element analysis using MSC/NASTRAN. Results from a weak fiber/matrix bond indicate that interfacial separation and slip have a major impact on the transverse response, overly weakening the structure and resulting in substantial matrix plastic flow. An elastic-plastic interphase zone between the fiber and matrix was then incorporated in an effort to model possible additional constraints. By varying the plastic properties of the interphase zone it was possible to model any level of bonding from strong to weak.

14. SUBJECT TERMS
Composite Materials, Micromechanical Modeling, Metal Matrix Composites, High Temperature Composite, Fiber/Matrix Interface

15. NUMBER OF PAGES
142

16. PRICE CODE

17. SECURITY CLASSIFICATION OF REPORT	18. SECURITY CLASSIFICATION OF THIS PAGE	19. SECURITY CLASSIFICATION OF ABSTRACT	20. LIMITATION OF ABSTRACT
Unclassified	Unclassified	Unclassified	UL

NSN 7540-01-280-5500

Standard Form 298 (Rev 2-89)
Prescribed by ANSI Std Z39-18
298-102